18 Seismicity and seismotectonics of the Swiss Alps

N. Pavoni, H. R. Maurer, Ph. Roth, & N. Deichmann

Contents

18.1 Introduction

The results of detailed microearthquake and seismotectonic surveys performed 1986–1991 in the frame of NRP 20 in the Swiss Alps are reported. The aim of the project was a systematic investigation of the local seismic activity and its relationship to local tectonics in the seismoactive regions of the eastern traverse and the western traverse of NRP 20 by use of an array of portable seismic stations. A valuable contribution to our knowledge of recent tectonic movements, the present deformation and stress state of the crust, the velocity structure, the location and extent of seismoactive structural features was expected to be obtained from these studies.
The investigations in the eastern Swiss Alps are part of the thesis work of Philippe Roth (Roth 1990), the investigations in the Valais (western Swiss Alps) form part of the thesis work of Hansruedi Maurer (Maurer 1993), both performed at the ETH Zürich. The presentation and discussion of these investigations form the main part of this report.
A brief presentation of the seismicity in Switzerland as well as an overview of microearthquake and seismotectonic investigations performed in Switzerland prior to the beginning of NRP 20 shall serve as an intruduction to the NRP 20 studies. A synthesis is presented in the final section.

18.2 Seismicity in Switzerland

Switzerland is part of the Alpine orogenic belt. This fold-and-thrust belt represents a zone of pronounced Cenozoic crustal deformation and tectonothermal mobilization. It represents a zone of lithospheric convergence and shearing located between the Eurasian plate and the African plate. Tectonic deformation has continued into the present time. This is clearly documented by the seismic activity.

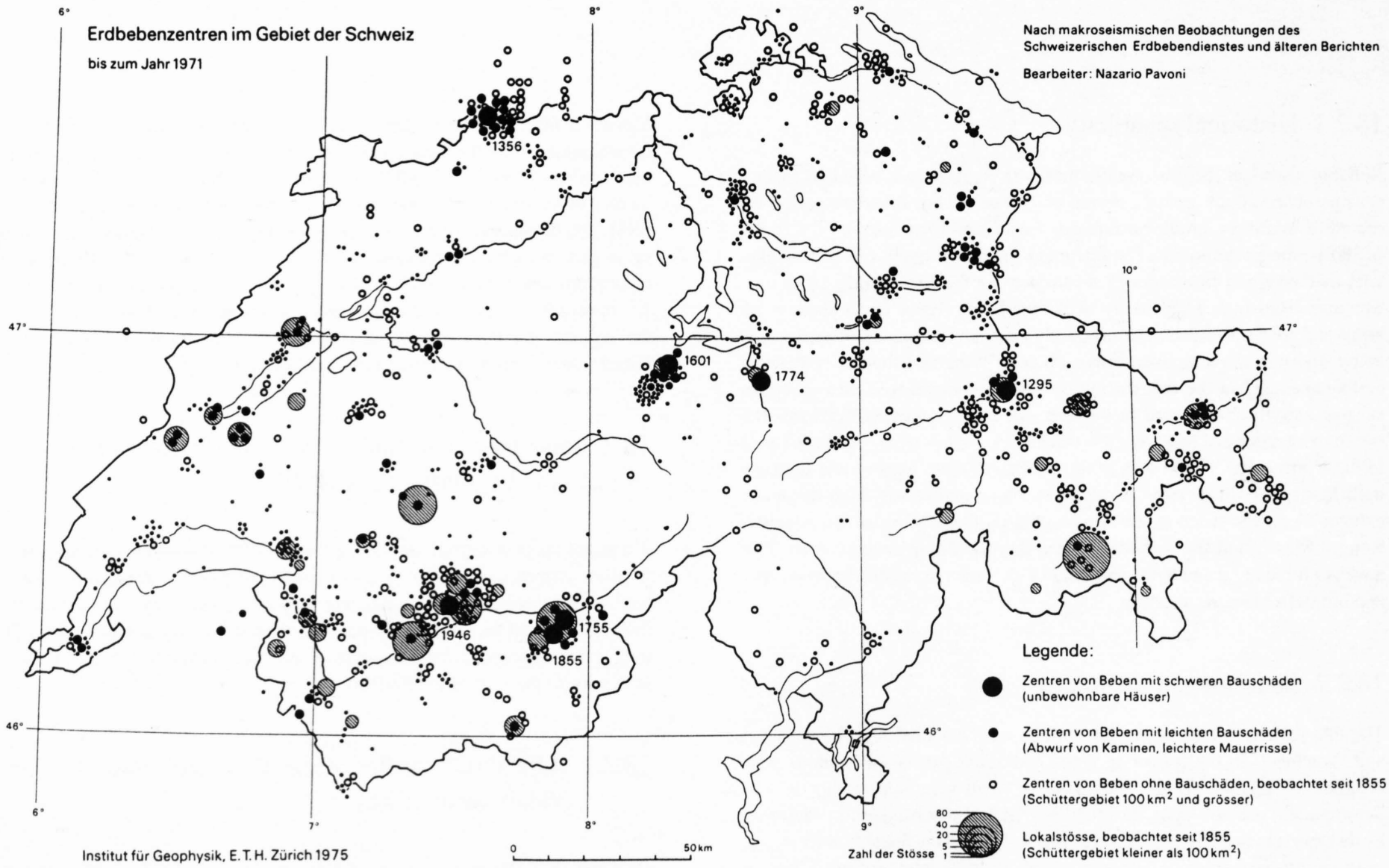

Figure 18-1
Historical seismicity of Switzerland, based on macroseismic observations. Period 1295–1971. After Pavoni (1977). Full circles: Historical earthquakes with severe damage to buildings ($I_o \geq$ VIII, year indicated) or light damage to buidlings (VI $\leq I_o <$ VIII); period 1295–1971. Open circles: Historical earthquakes with epicentral intensities IV $\leq I_o <$ VI; period 1855–1971. Small dots or hatched areas: Local shocks; period 1855–1971.

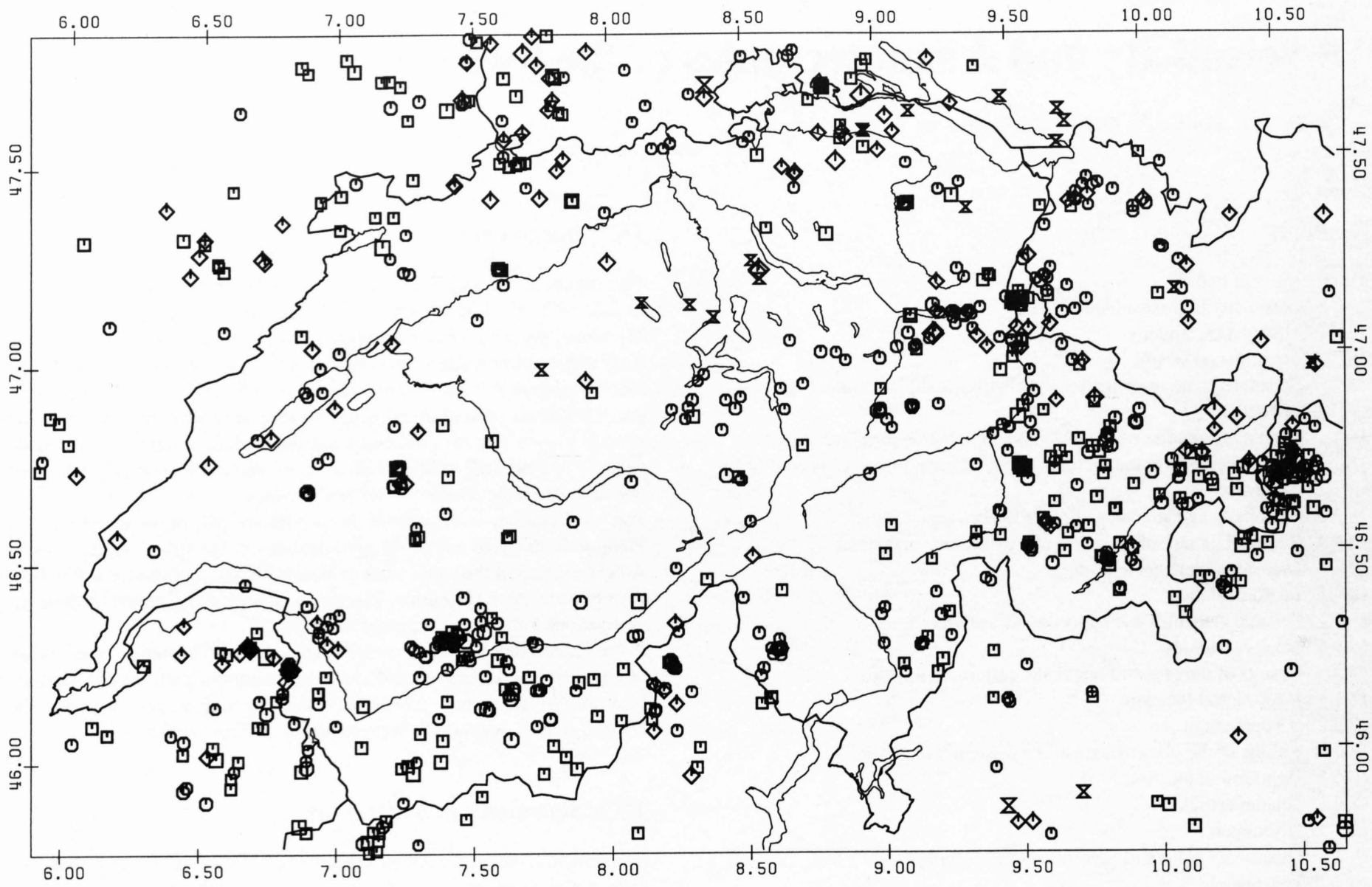

M_L \ Z	≥0	≥6	≥13	≥25
≥1				
≥2				
≥3				
≥4				
≥5				

Figure 18-2
Seismicity of Switzerland 1983–1992. Magnitudes ML > 2.0. Earthquakes selected from the catalogue of the Swiss Seismological Service. Epicenter symbols: size according to magnitude; type of symbol according to focal depth range.

18.2.1 Historical seismicity

Reliable historical records of earthquakes in Switzerland, based on macroseismic observations, cover a period of 700 years. For this time period the record of relatively strong earthquakes (epicentral intensities VI ≤ I_o ≤ IX, MSK) is almost complete. The historical record of small, felt earthquakes with no damage to constructions is complete for the period since 1855.
The map of historical seismicity of Switzerland (Figure 18-1) displays regions and zones of differing seismic activity. A similar pattern of seismically active and less active regions shows up both in the distribution of stronger earthquakes and in the distribution of weak local events. Zones of higher seismic activity are located in western and northeastern Switzerland. Between them, a zone of relatively low seismicity extends from the Black Forest in the North to the Ticino area in the South. All these zones trend orthogonally to the strike of the Alps. An additional zone of relatively high seismicity extends along the strike of the Alps on the northern boder of the Aiguilles Rouges Massif and the Aar Massif into the Vorarlberg seismic zone. This zone is probably related to the important Cenozoic hinge zone between Alps and northern Molasse foredeep.

18.2.2 Instrumental seismicity

The first permanent seismological stations were installed in 1911 at Zurich and Neuchâtel. In the following years additional permanent stations were installed at Basel, Chur and Brig. Four of them were later equipped with 3-component seismographs, the so called "Universalseismograph", designed by de Quervain and Piccard: A heavy mass of 21 tons is floated on springs so as to record mechanically two components of horizontal motion as well as the vertical motion. Since 1970 the network of permanent seismological stations of the Swiss Seismological Service (SSS) has been systematically modernized and enlarged. At present it consists of 26 permanent stations, with additional local temporary networks.

More than 6000 microearthquakes have been recorded since 1973. The magnitude threshold for the location of earthquakes within the network of permanent stations of the SSS is ML = 1.8. Routinely, about 100 earthquakes are located every year within Switzerland (see Monthly Seismic Bulletins of the SSS). The distribution of microearthquakes (Figure 18-2) displays nearly the same pattern as the distribution of historical earthquakes. The historically more active seismic regions display a higher rate of microearthquake activity. It is concluded that, in a country of moderate seismicity, such as Switzerland, the regions of relatively high microearthquake activity represent the preferred source regions of further large earthquakes.

18.3 Seismotectonic studies in Switzerland prior to the beginning of NRP 20

The installation of seismic stations in Switzerland allowed the detection and location of microearthquakes. It also allowed insights into the velocity structure and the mechanism of faulting. Here we would like to mention some earlier studies about the relationship between local seismicity and tectonics, and to give a brief account about the state of seismotectonic research in Switzerland prior to the start of the NRP 20.

18.3.1 Aftershock studies of the 1924 and 1946 Valais earthquakes

On April 15, 1924, an earthquake of epicental intensity RF I_o = VIII occured near Visp in the Valais. It was felt in the whole of Switzerland. Based on the experience of the strong 1855 Visp earthquake, aftershocks were expected to occur. Therefore, it was decided to install a portable, 3-component seismograph, a small version of the Univeralseismograph de Quervain-Piccard, in

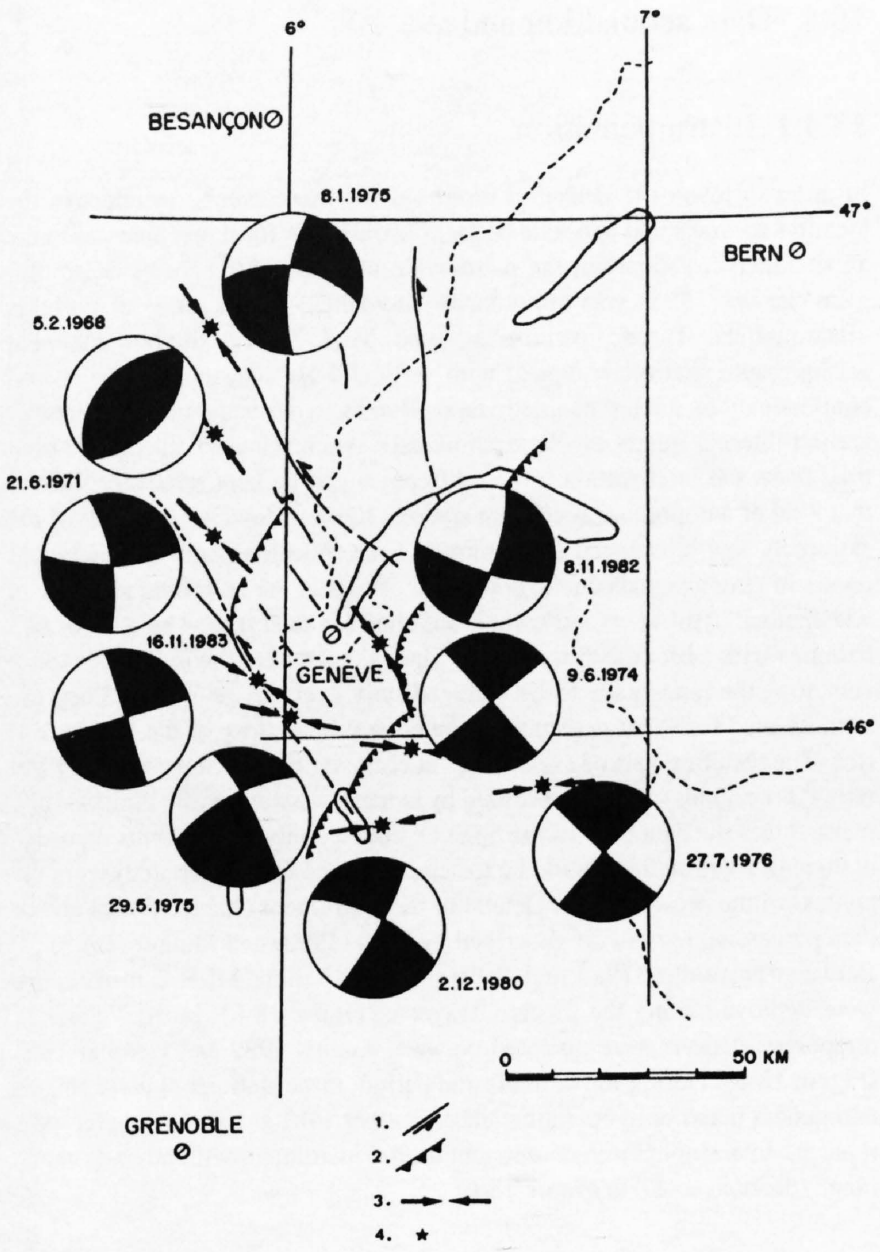

Figure 18-3
Fault-plane solutions and major faults bordering the Geneva basin. After Sambeth and Pavoni (1988). Equal area projection, lower hemisphere. Compressional quadrants black. Date of the earthquake is indicated. Legend: 1 – Strike-slip fault, 2 – Reverse fault, 3 – Orientation of P-axis, 4 – Epicenter.

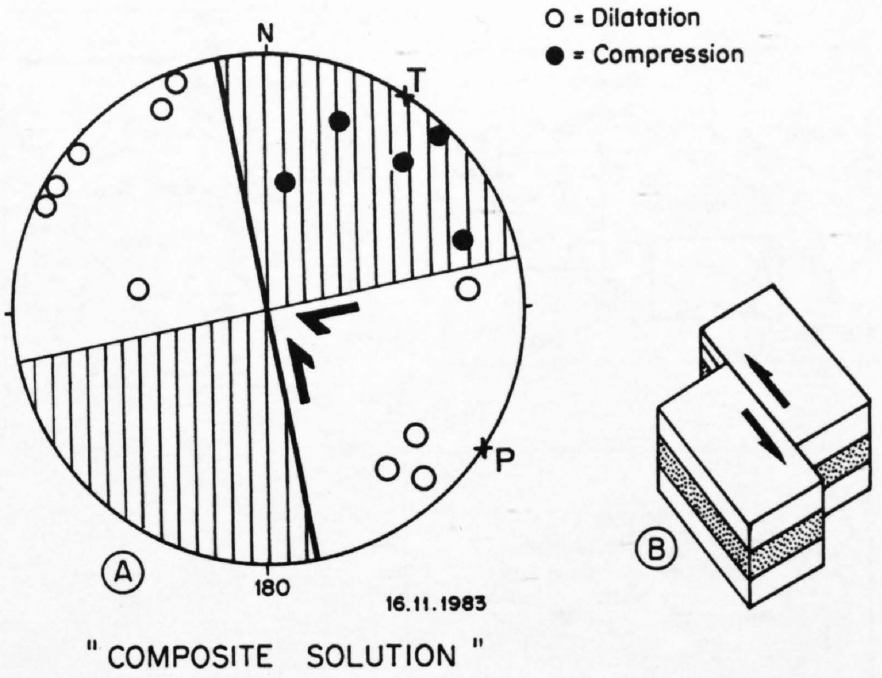

Figure 18-4
a) Composite fault-plane solution of the two events of November 16, 1983 (see Figure 18-3), located on the Vuache strike-slip fault (after Sambeth, 1984). Lower hemisphere, equal area projection. Hatched: Compressional quadrants. The strike and dip of the NNW–SSE trending nodal plane, and the left-lateral sense of displacement along this plane correspond to the trend and type of the Vuache fault
b) Block diagram of the seismoactive Vuache fault.

the epicentral area. The instrument was installed in the basement of the Lonza factory in Visp. A telephone line had then just been installed in this factory. By phone it was possible to have an excellent time control and correlation of the intrumental chronometers in Visp and Zurich to a few tens of a second. Only a few hours after the final installation of the instrument in Visp a strong aftershock occured which was also registered in Zurich. For the first time it was possible to measure the travel times of P- and S-waves between Visp and Zurich with great accuracy and to determine the crustal P- and S-wave velocities in the Central Alps (De Quervain, 1926). This was worldwide the first experiment to investigate aftershocks by use of a portable seismograph installed in the epicentral area.

A large number of aftershocks were recorded in the Valais region following the 1946 Valais earthquake (Magnitude ML = 5.7), the strongest earthquake in Switzerland during this century. Their epicentral distribution and focal depths were investigated by Wanner and Grütter (1949) and Wanner (1955). The zone of aftershocks, the so called Wildhorn seismic zone, trends WSW–ENE along the northern slope of the Rhone Valley between Sanetsch-Pass and Mt. Bonvin. Up to the present day it remains the seismically most active zone in Switzerland.

18.3.2 Active tectonics in the northern Alpine foreland (Jura Mountains, Swiss Plateau)

In a discussion and evaluation of the various tectonic hypotheses about the origin of the folds within the Jura Mountains it was shown by Pavoni (1967) that the hypocenters of several larger earthquakes in this region were clearly located within the basement, i. e. below the folded sedimentary cover. The focal depths were derived from the intensity distributions. Later investigations confirmed these results and showed that seismicity is distributed within the sedimentary cover as well as within the basement underneath the Jura and the Molasse basin down to 30 km (Jimenez and Pavoni, 1984; Mayer-Rosa and Garcia, 1986; Deichmann 1987a; Deichmann and Baer, 1990). Fault-plane solutions of earthquakes (Pavoni and Peterschmitt, 1974; Pavoni, 1977, 1980a, 1984; Deichmann, 1987a), station diagrams (Pavoni, 1984; Roth, 1986), and precise relative locations of microearthquakes (Deichmann, 1990) reveal a NW–SE shortening and NE–SW extension along N–S trending sinistral and complementary E–W trending dextral strike-sklip faults in the basement underneath the central Jura Mountains and the central Molasse Basin.

In the case of the Folded Jura further seismological investigations confirmed the existence and pattern of active strike-slip fault zones in the basement as postulated by a kinematic analysis of the folds and faults observed at the surface (Pavoni, 1961). Seismically active faults are also observed in the folded sedimentary cover. The Vuache fault SE of Geneva, e. g., is a well defined seismoactive fault (Blondel et al.,; Sambeth, 1984; Sambeth & Pavoni, 1988; see Figures 18-3, 18-4). From a seismological point of view an involvement of the basement in the folding process of the Jura Mountains seems reasonable.

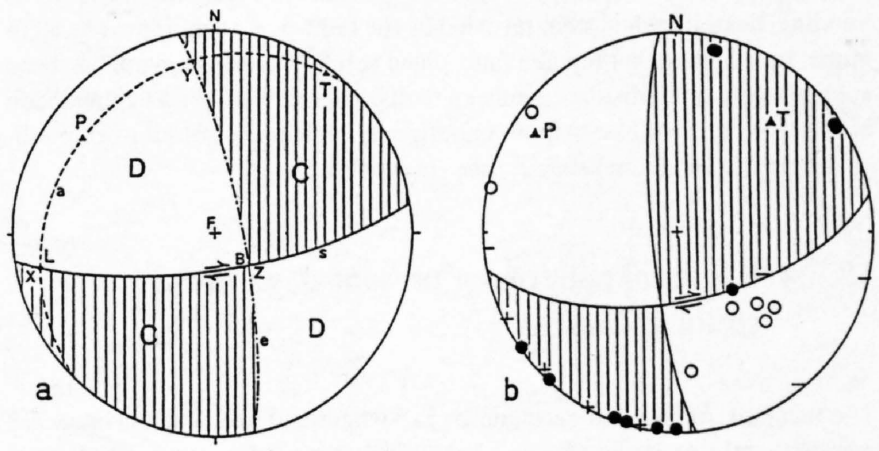

Figure 18-5
Comparison of observed type of faulting and fault-plane solutions of earthquakes in the Wildhorn seismic zone.
a) Fault diagram, lower hemisphere, equal area projection (after Pavoni 1980b). Locality: Six du Samarin, road near point 1592. Ultrahelvetic upper Jurassic limestone. Fault plane s: Strike N82E, dip 74S. Slickensides: Trend N260E, plunge 11, sense of displacement dextral. Dash-point line: Trace of auxiliary plane, normal to the fault plane. P: Axis of maximum shortheing 306/20 (trend/plunge). T: Axis of maximum lengthening 36/03. Hatched: "C"-quadrants.
b) Fault-plane solution of the earthquake of October 9, 1986. Epicenter located at 46N19.3Lat./7E29,0 Long. (near Swiss coordinates Km 603/130). Magnitude ML: 3.4. Focal depth: 5 km. Nodal plane 1: 79/61 SE (strike/dip), sense of displacement dextral. Nodal plane 2: 175/79 SW, sense of displacement sinistral. P-axis: 304/12 (trend/plunge). T-axis: 41/28. Hatched: C-quadrants. Nodal plane 1 corresponds in its orientation and sense of displacement very nearly to the observed fault plane (Figure 18-5a).

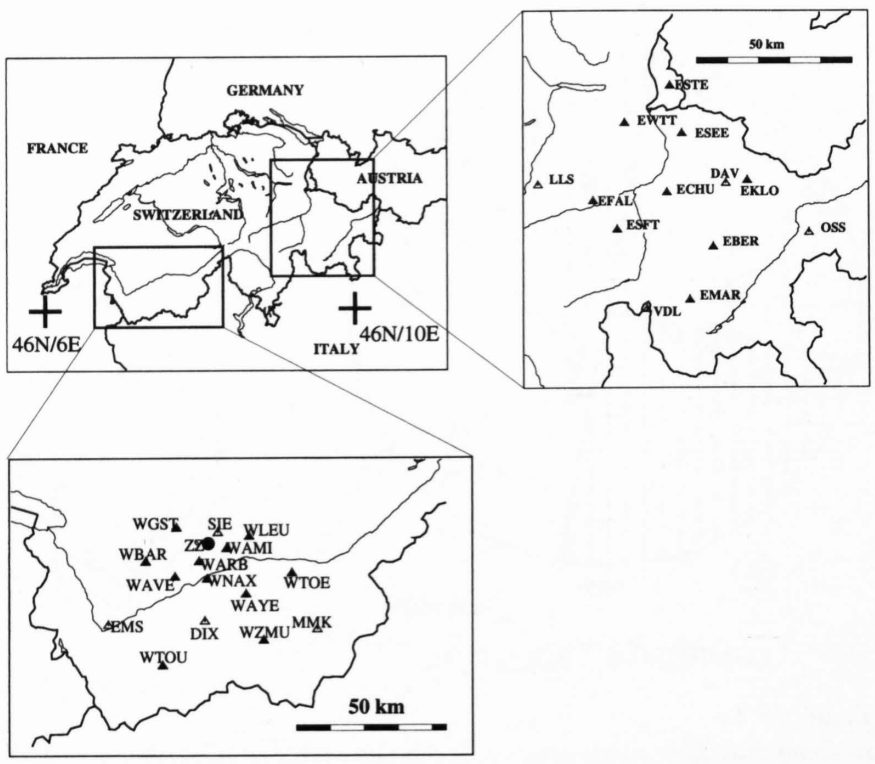

Figure 18-6
Overview of the investigation areas. Open triangles: Permanent SSS stations. Solid triangles: Temporary MLR-2 stations. Solid dot: Zeuzier network (ZZ).

18.3.3 Seismicity and tectonics of the Wildhorn seismic zone

The region is part of the aftershock zone of the 1946 Valais earthquake. Microearthquake surveys were conducted for several weeks in 1975, 1976 and 1977 on the northern slope of the Rhone Valley between Wildstrubel and Sanetsch-Pass, using a network of five portable MEQ-800 seismic stations (Pavoni 1977b, 1980b; Perraudin 1981). The foci of the earthquakes within the Wildhorn seismic zone are situated either in the Helvetic nappes or in the sedimentary cover and the crystalline basement of the Aar massif. Of special interest is a system of WSW–ENE trending faults which can be traced in the Wildhorn seismic zone from Le Serac in the west over Chable Court and Sex Rouge into the Vallon des Andins. It crosses the Lienne valley south of Vatseret. The faults cut through the nappe structures of the Wildhorn nappe. They dip steeply to SSE. They represent the surface expression of the W-E trending, dextral fault system revealed by the fault-plane solutions. The technique, by which an earthquake fault-plane solution is represented, has been applied to observed displacements on faults. This allows a direct comparison of observed type of Neo-Alpine faulting and fault-plane solutions of earthquakes in the Wildhorn seismic zone (Figure 18-5).

18.3.4 Regional patterns of present-day crustal strain and stress

The focal mechanisms of earthquakes in Switzerland and adjacent areas are predominantly of strike-slip or normal fault type (Mayer-Rosa & Pavoni 1977). An early attempt to illustrate the relationship between neotectonic deformation and fault-plane solutions of earthquakes in a seismotectonic map was presented by Pavoni & Mayer-Rosa (1977, 1978). A longterm, systematic seismotectonic investigation encompassing the whole of northern Switzerland was initiated in 1982 on behalf of the Neotectonics Study Group of NAGRA. On this occasion the construction and interpretation of „station diagrams“ was introduced by Pavoni (1984). Station diagrams provide information about the local or regional crustal deformation state acting in the region surrounding a seismological station. They complete the information provided by fault-plane solutions (see Section 18.4.3).
The orientations of P-axes were found to display a regular counterclockwise rotation from NNW–SSE in eastern Switzerland to NW–SE and WNW–ESE in western Switzerland and W–E in the Haute Savoie region, indicating a regular, fan-like pattern of maximum horizontal compressive stresses in the crust, roughly perpendicular to the strike of the Alps and Jura Mountains. Maximum horizontal extension, as indicated by the orientation of T-axes, trends parallel to the strike of the Alps (Pavoni 1975, 1977a, 1980a).

18.4. Data acquisition and analysis

18.4.1 Instrumentation

In order to lower the detection threshold for weak events, to improve the location accuracy and to obtain better constraints on focal mechanisms in the areas under investigation, the nationwide network of the Swiss Seismological Service (SSS) was temporarily augmented by an array of portable seismographs. These instruments (type MLR-2) are single-component seismographs that are equipped with vertical 1-Hz sensors and that record continuously on analog magnetic tape. Thanks to a broadband time receiver and an internal quartz clock, continuously synchronized with the external time code, the inter-station timing difference can be kept relatively low for that kind of autonomous recording station (10 ms). However, because of the extremely low tape speed (0.33 mm/s), head misalignments and emergent onsets of strong signals due to non-linear effects of the recording system can add another 20 ms of error. Power is supplied for each station by a set of five batteries with a lifetime of two years. Since the speed of the magnetic tape is very low, the tapes have to be changed only every three weeks. They are initially read for event detection in the central laboratory of the SSS in Zurich. The resulting lists of event-times at each station are then correlated and only those signals of events recorded by at least two stations are digitized and merged into the data base of the SSS. Of course, only those events recorded at three or more stations could be located and used for further analysis in the context of the present study. Details of the instrument characteristics and of data processing system are described by Roth (1990) and Maurer (1993).
Between November 1986 and September 1988, nine MLR-2 instruments were deployed along the Eastern Traverse (Figure 18-6). In the Valais, 11 temporary stations were operated between August 1989 and October 1991 (Figure 18-6). During the second time period, three stations of a six single-component network in operation since October 1981 at Lac de Zeuzier were replaced by a single three-component digital instrument with large dynamic range (denoted as ZZ in Figure 18-6).

18.4.2 Seismic velocities and hypocenter locations

Reliable hypocenter locations are an essential prerequisite for any seismotectonic study. Normally, the information on the seismic velocities of the Earth's crust and mantle necessary for the earthquake location procedure are derived from seismic refraction studies. Given a sufficient number of earthquakes in a particular region as well as a dense station coverage, it is possible to solve simultaneously for both the hypocentral locations and an average velocity model with station corrections (e. g. Lee and Stewart, 1981).

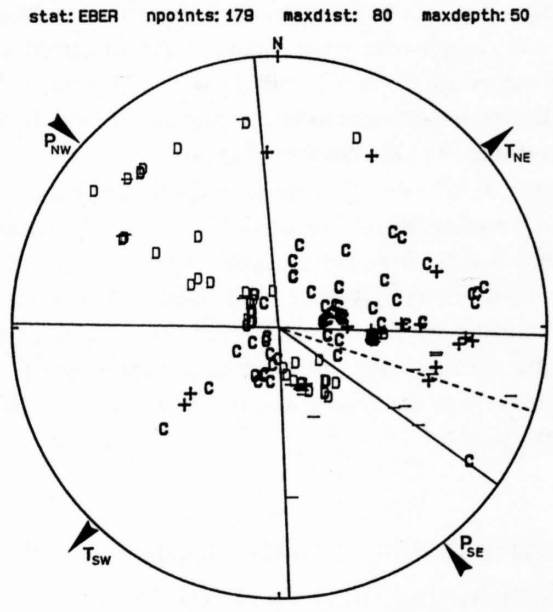

Figure 18-7
Example of a station diagram for the station EBER (see Figure 18-11). The station is situated in the center of the circle; radius of this map: 80 km. Each earthquake epicenter is represented by the polarity of the first arrival recorded at the station EBER. Period of observation: November 1986 to September 1988. The straight lines separate sectors containing predominantly compression (C or +) from sectors containing predominantly dilatation (D or –). A sector with mixed polarity is also present. P_{NW}, P_{SE}, T_{NE} and T_{SW} are the bisectors of each polarity domain (the dashed bisector of the mixed sector being considered as the border between the C and D domain) and are indicative of the main horizontal compressive stress axes.

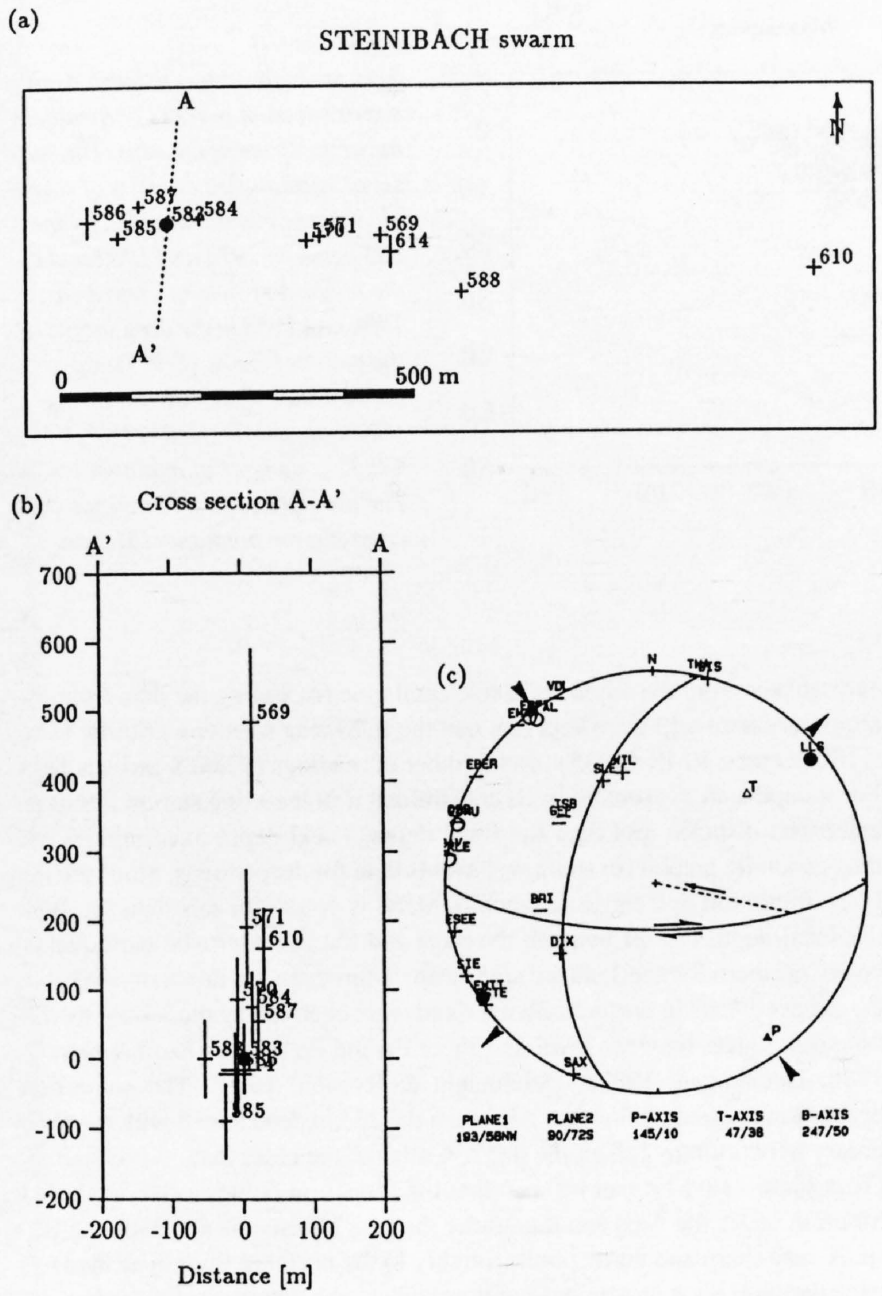

Figure 18-8
Example of relative locations. Steinibach swarm: July 1987. ML ranges between 1.5 and 2.4, geographical coordinates of master event (black point): 46.908N, 9.123E, Swiss Km-coord. 728.2/196.5. Size of crosses gives computed standard deviation. Events are numbered in chronological order. (a) Map view. (b) cross-section A-A'. (c) Composite fault-plane solution of two members of the series, Full circles and + = compression. Void circles and – = dilatation; equal area lower hemisphere projection. The east-west striking plane is the active rupture plane. Slip vector indicated by a dashed line and an arrow.

By complementing velocity information from other sources with information partaining specifically to the area under investigation and by allowing for local deviations from an average velocity model through station corrections, this technique improves the consistency of the hypocentral locations. Details of the procedure as well as the resulting velocity-depth functions can be found in Roth (1990), Maurer (1993) and in Maurer & Kradolfer (1995). The resulting epicenter maps and focal-depth cross-sections are presented in the following sections for the eastern and western region separately.
The focal-depth distribution is indicative of the rheology of the Earth's crust and is therefore of particular interest. Unfortunately, focal depths of local earthquakes determined from direct arrivals are often poorly constrained. In the following depth-cross-sections we have therefore included only those events for which the hypocentral locations are considered to be sufficiently reliable. Selection criteria used include locations based on at least nine observations, an RMS (root mean square of the travel-time residuals) not larger than 0.35 s and a GAP (largest angle spanned by two neighboring lines between epicenter and stations) not greater than 180 degrees (this last criterion ensures that the epicenter lies within the station network).

18.4.3 Seismotectonics

The relationship between seismicity and local tectonic deformation was investigated with focal mechanisms, station diagrams, and precise relative locations of earthquake clusters.
First, focal mechanisms based on the distribution of first-motion polarities of the P-waves were determined from fault-plane solutions (e. g. Aki &

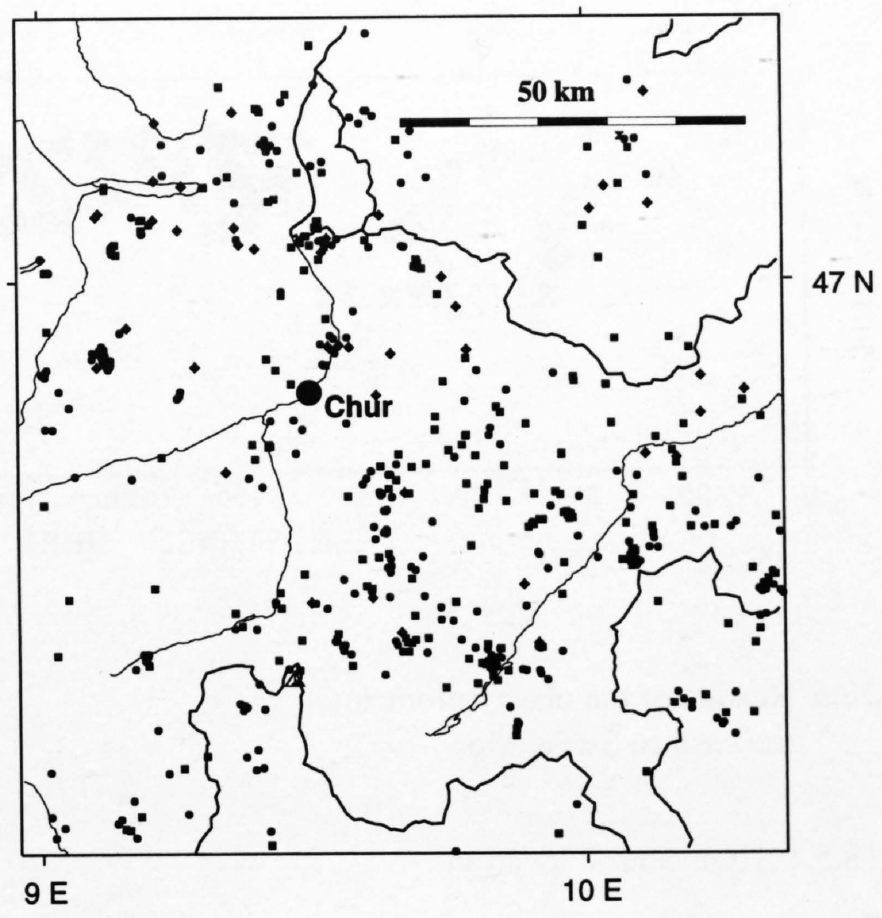

Figure 18-9
Epicenter map of the eastern Swiss Alps for the period 1984–1990 (563 events). Symbols represent different focal depths (see Figure 18-2).

Richards, 1980). The procedure was applied to all those events that were strong enough to be recorded by a sufficient number of stations with good azimuthal coverage.
The second type of investigation is the construction of so-called station diagrams (Pavoni, 1984; Roth, 1986). Station diagrams are circular maps of the area surrounding a seismic station in which the epicenters are represented by the polarity of the first arrival recorded at this station. Particularly in regions of strike-slip tectonics, these station diagrams can be used to obtain quickly and accurately the orientation of the horizontal stress components. If the stress field in the region covered by the diagram is roughly homogeneous, some azimuthal distribution of compressions (C) and dilatations (D) should become apparent.
Indeed, as the example of Figure 18-7 shows, sectors can be separated containing predominantly C or D. Sectors of mixed polarity are sometimes also present. The greatest and least horizontal compressive components of the present deformation field can be approximated by the bisectors of the compression and dilatation domains, respectively, where the mixed sectors can be either considered or ignored. One advantage of the method is that also weak earthquakes with only few well developed first arrival polarities can be used.
The third method we applied is the precise relative relocation of earthquake swarms. If earthquakes occurring in the same small focal volume show the same signal character, one can assume that they possess the same focal mechanism. If an accurate relocation of the different earthquakes can be achieved, the foci are usually found to lie on a plane, which coincides with one of the nodal planes of the fault-plane solution. This plane can be viewed as the plane of failure with separate or possibly overlapping patches on which slip occurred as a series of individual events. A cross-correlation technique in the frequency- or in the time-domain allows a very accurate determination of the arrival-time differences and the hypocenters are then relocated relative to a chosen master event. In the present study we used the time-domain method. The time delays are obtained directly from the maximum of the cross-correlation of P- and S-phases (Plantet & Cansi, 1988; Deichmann & Garcia-Fernandez, 1992). For the permanent stations of the SSS-network, these time delays can be determined with an accuracy of 3 to 5 ms for both P- and S-waves. For the portable, autonomously recording MLR-2 stations, only S-P differences were used for the master event relocation, as these stations do not share the same time base. The standard deviations of the relative hypocentral locations, as calculated from the matrix inversion used in the location algorithm or as derived from Monte-Carlo simulations, amounts to a few tens of meters. As an example, Figure 18-8 shows the results of this procedure applied to the Steinibach swarm, which occurred near the twon of Elm (Kanton Glarus) in July 1987. In this case, the hypocenter distribution coincides with the E–W striking nodal plane, which is thus clearly identified as the active fault plane.

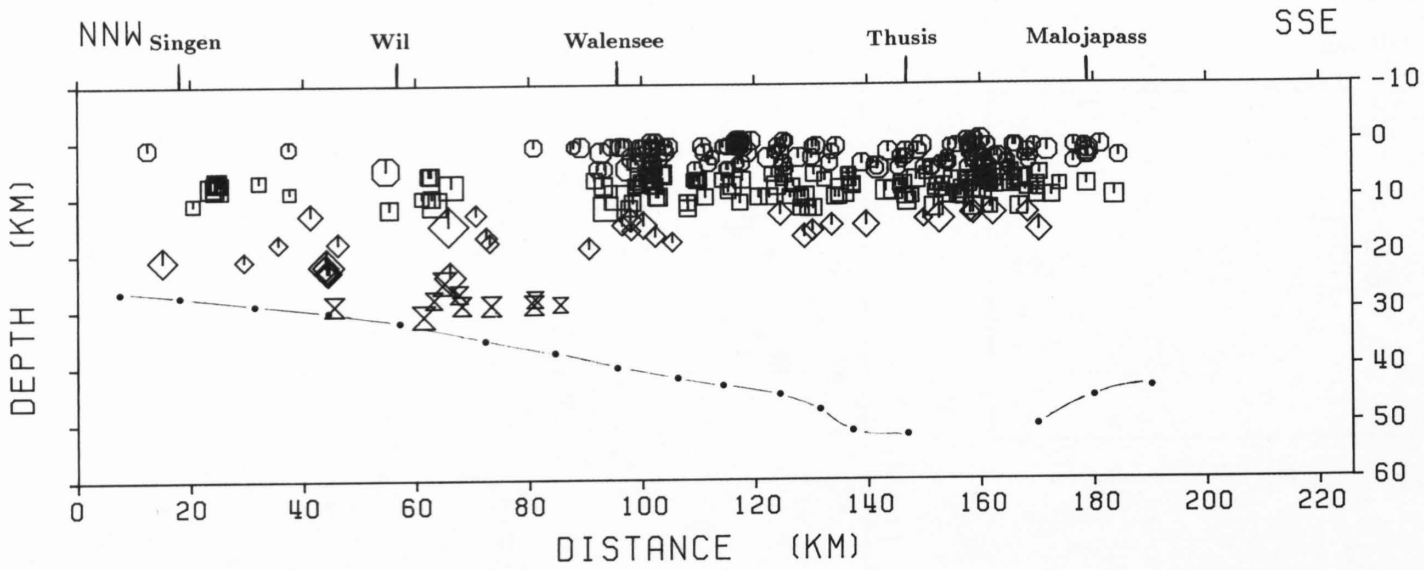

Figure 18-10
Selected hypocenters projected onto a cross-section roughly perpendicular to the strike of the Alps. The subset of earthquakes consists of reliably located events recorded by the SSS between 1972 and 1989 and by the temporary network between 1986 and 1988 in the area shown by the map in Figure 18-9. These earthquakes satisfy the following selection criteria: GAP≤ 180°, RMS ≤ 0.35 s, number of readings ≥ 9. The dot-dashed line represents the crust-mantle boundary (Moho).

18.5 Results of the observations in the eastern Swiss Alps

18.5.1 Hypocentral locations

During the period between November 1986 and September 1988, while the temporary MLR-2 stations were in operation, more than 300 local earthquakes were located in the region shown in the epicenter map in Figure 18-9. The magnitudes ML range from 0.5 to 4.2.
One of the most striking features revealed by this study is the restricted vertical extension of the seismogenic zone in this area. All the earthquakes located by the temporary network are confined to the upper 13 km of the crust. Between 13 km and the Moho, which in this region reaches depths of more than 50 km, the crust seems to be aseismic. The cut-off of seismic activity at about 13 ± 1 km is independent of the various velocity models that were tried.
Figure 18-10 shows a selection of reliably located hypocenters projected onto a vertical cross-section roughly perpendicular to the strike of the Alps. The data set for this figure consists of earthquakes recorded by the SSS between 1972 and 1989 in the eastern part of Switzerland. To consider events with a reasonably well constrained focal-depth determination, only those earthquakes from the whole available catalogue (including the data from the temporary network) were kept that met the following selection criteria: GAP ≤ 180 degrees, RMS ≤ 0.35 s, and number of readings (P and S-arrivals) ≥ 9. Focal depths are reasonably well constrained if at least one station lies at an epicentral distance less than the focal depth. Focal-depth uncertainties are thus generally greater for shallower events than for deeper ones. Since the average minimum epicentral distance (DMIN) is 16 km for this data set, both the focal-depth cut-off beneath the Alps and the lower-crustal earthquakes below northern Switzerland are significant. Moreover, the depth of several of the deeper events in northern Switzerland were checked by modelling travel-time differences between PMP and Pg or Pg and Pn (Mayer-Rosa & Garcia, 1986; Deichmann, 1987a; Deichmann & Rybach, 1989). The somewhat deeper lower bound below the Alps than the 13 km determined with the temporary network may reflect the larger scatter of the older data.
From Figure 18-10 it can be seen that the transition between the depth distribution under the Alps and that under the Jura Mountains and Molasse Basin is very sharp and corresponds roughly to the northern margin of the Helvetic domain. Such an obvious contrast can also be determined if earthquake data from the whole country are selected (Deichmann & Baer, 1990). This contrast can propably not be explained in terms of temperature, since from the lower heat flow values measured in the Alps one would expect a deeper lower limit of the seismogenic zone there. However, the temperature distribution is complicated by the Alpine orogeny, as well as by regional hydrothermal circulation.

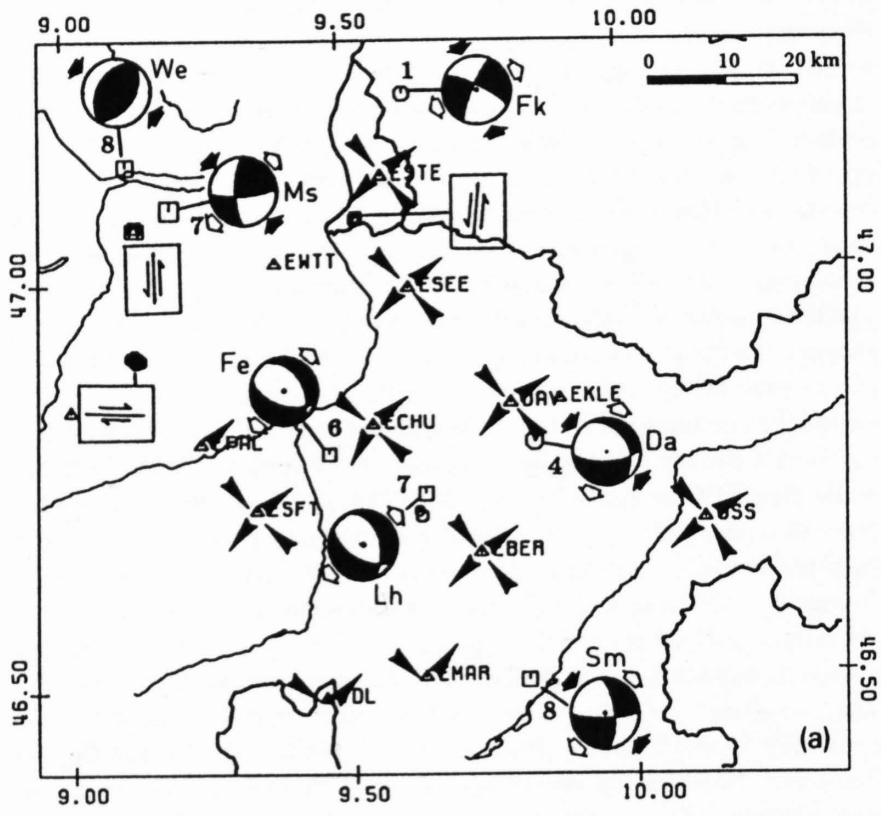

Figure 18-11
Map view of the investigated area in the eastern Swiss Alps. Circles indicate fault-plane solutions, equal area lower hemisphere projections, compressional quadrants black. Numbers next to focal mechanisms denote focal depths in km. Arrows surrounding stations represent the station diagram axes, indicative of greatest and least horizontal compressive stress (see text). The three arrow pairs enclosed in a box represent east-west dextral and north-south sinistral strike-slip movements on steep planes, as evidenced by accurate relative locations of earthquake swarms. The westernmost one corresponds to the Steinibach fault (Figure 18-8).

18.5.2 Seismotectonics

The events and corresponding parameters for which fault-plane solutions could be constructed are summarized in Table 18-1. The stereographic plot with the first-motion polarities of the Steinibach events is shown in Figure 18-8; the others can be found in Roth et al. (1992). Figure 18-11 reveals that all three principal fault types (strike-slip, normal and reverse) are present. The fault-plane solutions have a simple collective relation: the P axes are confined to a near vertical plane striking northwest-southeast, while the T axes are confined to a near vertical plane striking northeast-southwest.
In Figure 18-11, arrows at the stations represent an average orientation of the the horizontal component of least and greatest stress obtained from the station diagrams described in the previous section. Although the underlying information for each diagram is independent from that of the neighbouring station (one polarity for each earthquake-station pair), the orientation of these axes change very little from station to station. It furthermore coincides with the horizontal traces of the P and T axes of the fault plane solutions.

No.	Location	Date	Time	Depth [km]	P-Axis Az.	P-Axis Dip	T-Axis Az.	T-Axis Dip
Sm	St. Moritz	1987.04.29	20:41	8	312	24	219	08
St	Steinibach	1987.07.26	10:56	1	145	10	047	38
Ms	Mürtschenstock	1987.10.28	23:49	7	132	05	040	23
Fk	Feldkirch	1987.11.01	10:16	1	159	16	249	01
Fe	Feldis	1988.04.17	03:41	6	320	69	216	06
Lh	Lenzerheide	1988.05.23	21:56	7	325	85	231	05
We	Weesen	1989.04.02	06:58	8	303	05	212	88
Da	Davos	1990.03.18	09:54	4	317	56	201	17

Table 18-1
Focal mechanism parameters, eastern Swiss Alps

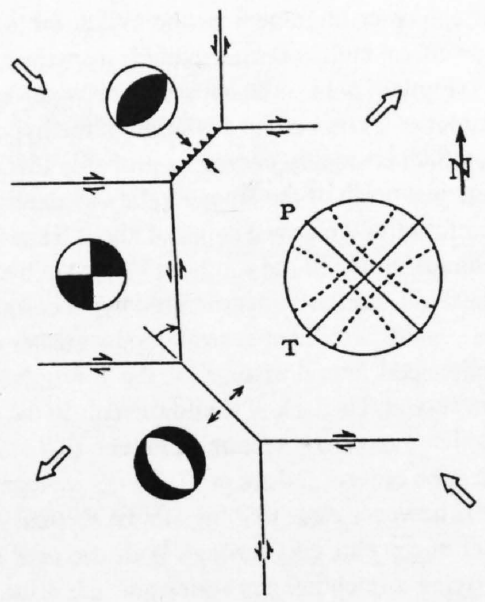

Figure 18-12
Schematic block geometry idealizing the present deformation pattern of the eastern Swiss Alps represented in Figure 18-11. Large arrows denote increment of northwest-southeast compression and northeast-southwest extension; small arrows indicate response (relative displacements) of blocks. Stereo-plot on the right side shows orientations of planes that contain P- and T-axes. Dashed lines give ± 20° deviation from these planes. Modified after Hill (1982).

The focal mechanism of the Steinibach series, which was presented as an example in the previous section, is shown in Figure 18-11 by the trace of its rupture planes together with a pair of slip vectors drawn inside a rectangular box. Such rupture planes with corresponding slip direction could be determined for a total of three earthquake clusters (see Section 18.7.4). The N–S striking, seismoactive Spanegg fault, e. g., is in good agreement with the N–S fault systems observed in the region Murgseefurggel, Mürtschenfurggel and Spanegg, and further north in the region of Obstalden and Filzbach, from where slikensides with horizontal striations are reported (Oberholzer, 1933, p. 79).
Thus, these three different types of investigation, summarized in Figure 18-11, give a consistent general picture of the studied area. An idealized sketch of the overall deformation mechanism is shown in Figure 18-12. The maximum horizontal shortening is oriented NW–SE, the maximum horizontal extension NE–SW. This overall deformation is accommodated by (1) right-lateral and left-lateral slip on vertical E–W and N–S striking planes, respectively, (2) reverse slip on NW and SE dipping planes, and (3) normal slip on NE and SW dipping planes. Under this idealized geometry, the fault plane solutions have a simple collective relation to the regional deformation field: the P axes are confined to a vertical plane striking in the direction of maximum horizontal regional compression, and the T axes are confined to a vertical plane striking in the direction of maximum horizontal regional extension. Local deviations in the orientation of preexisting faults from the idealized geometry of Figure 18-12 will result in deviations of the P and T axes of fault plane solutions from the regional orientation of these orthogonal planes. On the stereo net of Figure 18-12, an arbitrary scatter of up to 20 degrees in P and T axis orientations with respect to the idealized northwest and northeast striking planes is indicated by a dashed band.

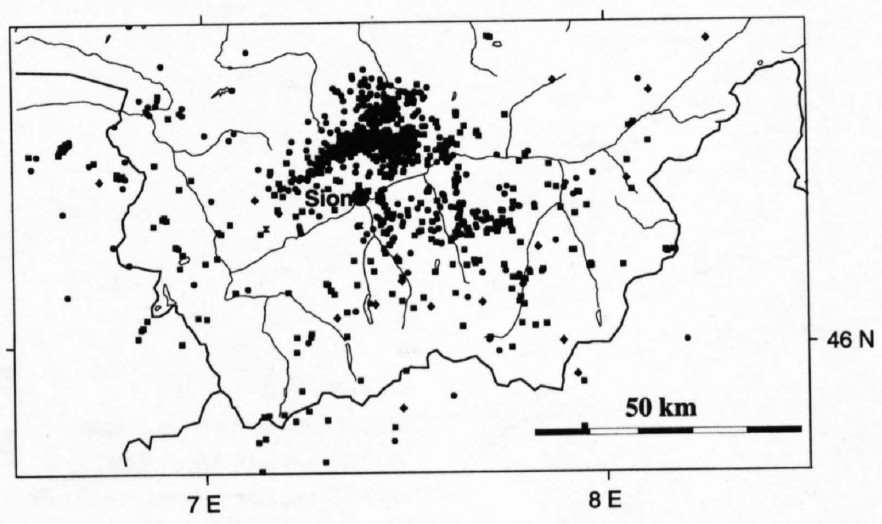

Figure 18-13
Epicenter map of the western Swiss Alps for the period 1983–1992 (1497 events). Symbols represent different focal depths (see Figure 18-2).

18.6 Results of the observations in the western Swiss Alps

18.6.1 Hypocentral locations

The compiled data set that consists of all locatable earthquakes in the Valais and surrounding areas between January 1983 and October 1992 comprises 1497 events. As shown in Figure 18-13, the epicentral distribution in the northern Valais is more structured than in the south. A conspicuous earthquake cluster is located in the zone of the Helvetic nappes, in the area of the Rawil depression. It corresponds roughly to the aftershock region of the 1946 Wildhorn event. The region east of Leukerbad including the Lötschental, where the Aar massif reaches the surface, was almost completely aseismic during the last 10 years. The epicentral distribution south of the Rhone Valley is rather diffuse and thus more difficult to characterize. It is, however, remarkable that only few earthquakes have been detected in the southwestern part of the Valais.
As already discussed previously, for an appraisal of the focal- depth distribution the data set was restricted to those events the locations of which are sufficiently reliable. The following selection criteria were adopted in this case: GAP ≤ 180 degrees, the total number of observations for each event ≥ 10 and ALE ≤ 2.0. ALE stands for Average Logarithmic Eigenvalue, a parameter of the location algorithm that characterizes the hypocenter-station geometry (Kradolfer 1989). Only 295 events satisfy these criteria. A relatively small number of shallow events is selected. The ALE threshold often rejects such events because of their unfavorable location geometry (large epicentral-distance / focal-depth ratio). Figure 18-14 shows an epicenter map of the selected data set and a projection of the hypocenters onto a structural model of the crust derived from the NRP 20 reflection profiles.

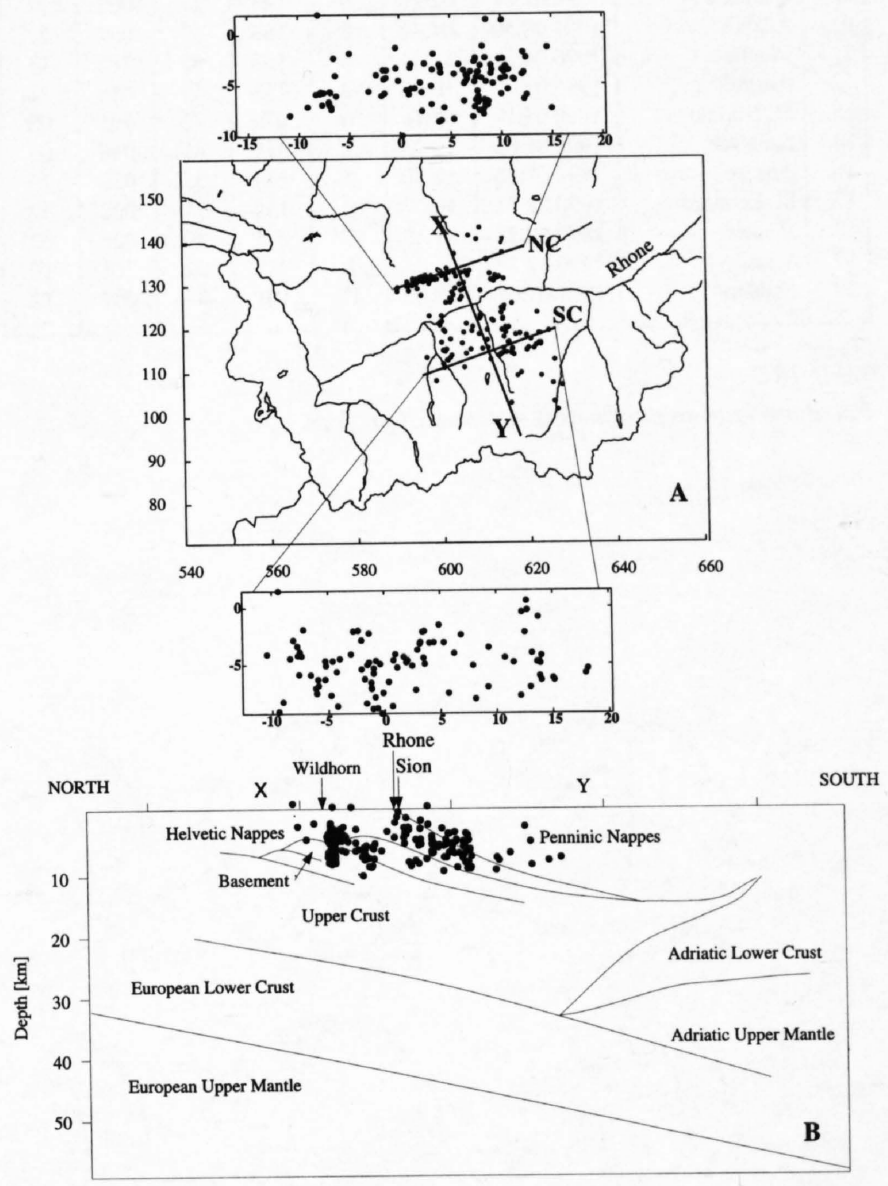

Figure 18-14
A) Epicenter map of events with reliable focal depths. The selection criteria are GAP ≤ 180° and at least 10 observations per event. Only those events situated less than 15 km from the traverse XY (shown in Figure 18-14B) are displayed. The cross sections perpendicular to XY show the depth distribution of the seismicity north (NC) and south (SC) of the Rhone River. The map comprises 219 events.
B) Vertical cross section of the seismicity pattern shown in A superimposed on a crustal model (XY) obtained from reflection seismology data (adapted from Valasek, 1992).

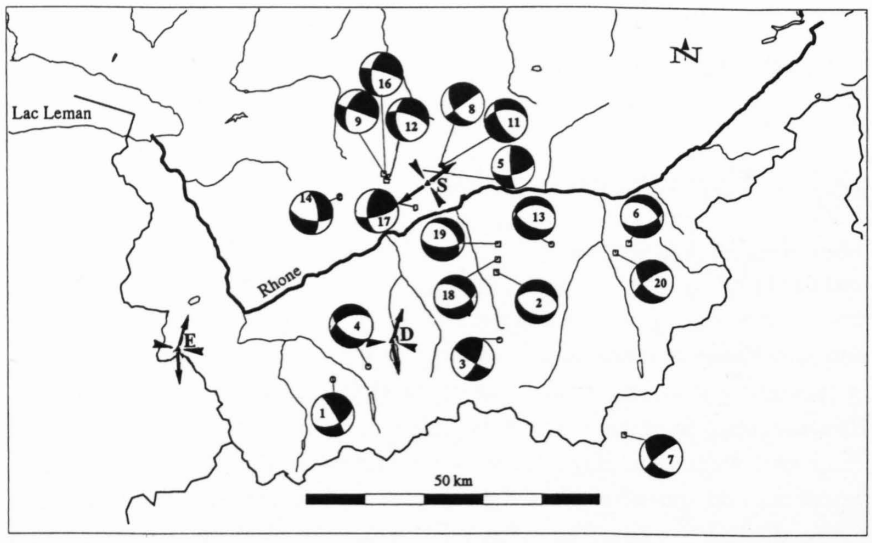

Figure 18-15
Location of the focal mechanisms in the western Swiss Alps. The number plotted in each focal mechanism corresponds to the numbers in Table 18-2. In addition, station diagrams, adapted from Roth (1986), are shown.
Stations: E = Emosson, D = Dixence, S = Sion.
See Figures 18-11 and 18-7 for further explanations.

No.	Location	Date	Time	Depth	P-Axis		T-Axis	
				[km]	Az.	Dip	Az.	Dip
1.	Mauvoisin	1985.01.04	16:57	10	279	33	023	21
2.	Vissoie	1986.01.19	06:54	6	143	82	013	05
3.	Zermatt	1986.02.15	01:43	5	252	07	345	21
4.	Dixence	1986.02.26	13:07	7	094	58	188	02
5.	Zeuzier	1986.10.09	10:08	5	304	12	041	28
6.	Stalden	1987.03.22	01:36	10	286	58	192	02
7.	M. Rosa	1987.05.30	19:45	9	101	33	357	21
8.	Montana	1989.01.07	02:29	6	108	27	002	27
9.	Anzere	1989.09.30	04:41	8	163	27	057	27
11.	Montana	1990.04.28	22:24	4	108	52	212	11
12.	Anzere	1990.05.07	16:06	7	153	49	046	14
13.	St. Niklaus	1990.05.11	08:16	6	076	72	191	08
14.	Sanetsch	1990.06.03	19:23	2	315	41	048	03
16.	Anzere	1990.07.26	12:30	6	154	35	050	19
17.	St. Leonard	1990.08.31	10:57	9	132	11	032	42
18.	Vissoie	1990.09.25	05:19	8	273	60	007	02
19.	Vissoie	1990.12.17	23:34	8	311	62	201	10
20.	Stalden	1991.09.07	18:09	11	101	37	002	12

Table 18-2
Focal mechanism parameters, western Swiss Alps.

The conspicuous epicenter alignment in the Wildhorn zone, south of the Rawil, delineate a vertical fault zone that extends from the near surface down to a depth of 8 km (Figure 18-14). The apparent horizontal scatter in this projection is on the order of 2 km, but the deviation of the hypocenters from the actual fault zone, which is slightly curved, is probably less. The two smaller earthquake clusters just north of the Rhone Valley evidently belong to separate zones of seismic activity below a depth of about 5 km. The diffuse seismicity in the Penninic domain of the southern Valais visible on the epicenter map is reflected also in a similarly unstructured hypocentral distribution.
There are only few events with hypocentral depths greater than 10 km. Furthermore, no pronounced lateral change of the lower bound of the seismogenic layer is observed. The lack of shallow events in the southermost part of the profile, visible on the cross section in Figure 18-14, is a consequence of the adopted selection criteria and are probably not representative of the actual seismicity. It is however clear that the almost vertical alignment of hypocenters in the northern part cuts through both the near-surface Helvetic nappes, the underlying autochthonous series and the crystalline basement. South of the Rhone Valley the seismic activity is observed only in the Penninic nappes that form the uppermost structural units in that region.

18.6.2 Seismotectonics

The available well-constrained fault-plane solutions are shown in Figure 18-15 and the corresponding parameters are summarized in Table 18-2. The stereographic projections of the first-motion polarities, which have been published either only in the Ph.D. thesis of Maurer (1993) or not at all in this form, are reproduced in Figure 18-16. The remaining fault-plane solutions are taken from Pastore et al. (1992). In addition, we have included in Figure 18-3 three station diagrams constructed by Roth (1986).
A striking feature of Figure 18-15 is the difference between the solutions of the northern- and the southern Valais. In the north, strike-slip mechanisms with a normal fault component are predominant. The P-axis orientations are mostly NW-SE. In contrast to this, the fault plane solutions in the south show mainly normal faulting with N-S oriented T-axes. The new focal mechanisms in the northern Valais agree well with earlier studies (Pavoni, 1980b) and the solutions in the southern Valais confirm the results of Eva (1991) and Pastore (1993). Moreover, the same change in orientation of the P- and T-axes across the Rhone Valley can also be seen as a change in orientation of the maximum and minimum average directions of horizontal compressive stress derived from the station diagrams (Roth, 1986). Thus, the different seismicity pattern between the southern and northern Valais, discussed previously, is evidently also reflected in different styles of tectonic deformation.
It is also noteworthy that the strike of faults mapped at the surface by Pavoni (1980b) is parallel to the conspicuous WSW–ENE alignment of the epicenters in the Wildhorn seismic zone. The slip on these faults also agrees very well with one of the focal mechanisms in the same locality (number 5 in Table 18-2, and Figures 18-4, 18-15 and 18-16). On the other hand, the fault planes identified from the relative hypocenter locations of the two earthquake clusters near Anzère (focal mechanisms number 9 and 16) strike WNW–ESE. This direction, which is oblique to the main trend of the epicenters, coincides with the strike of recent faults in the area as mapped by Burkhard (1988a).

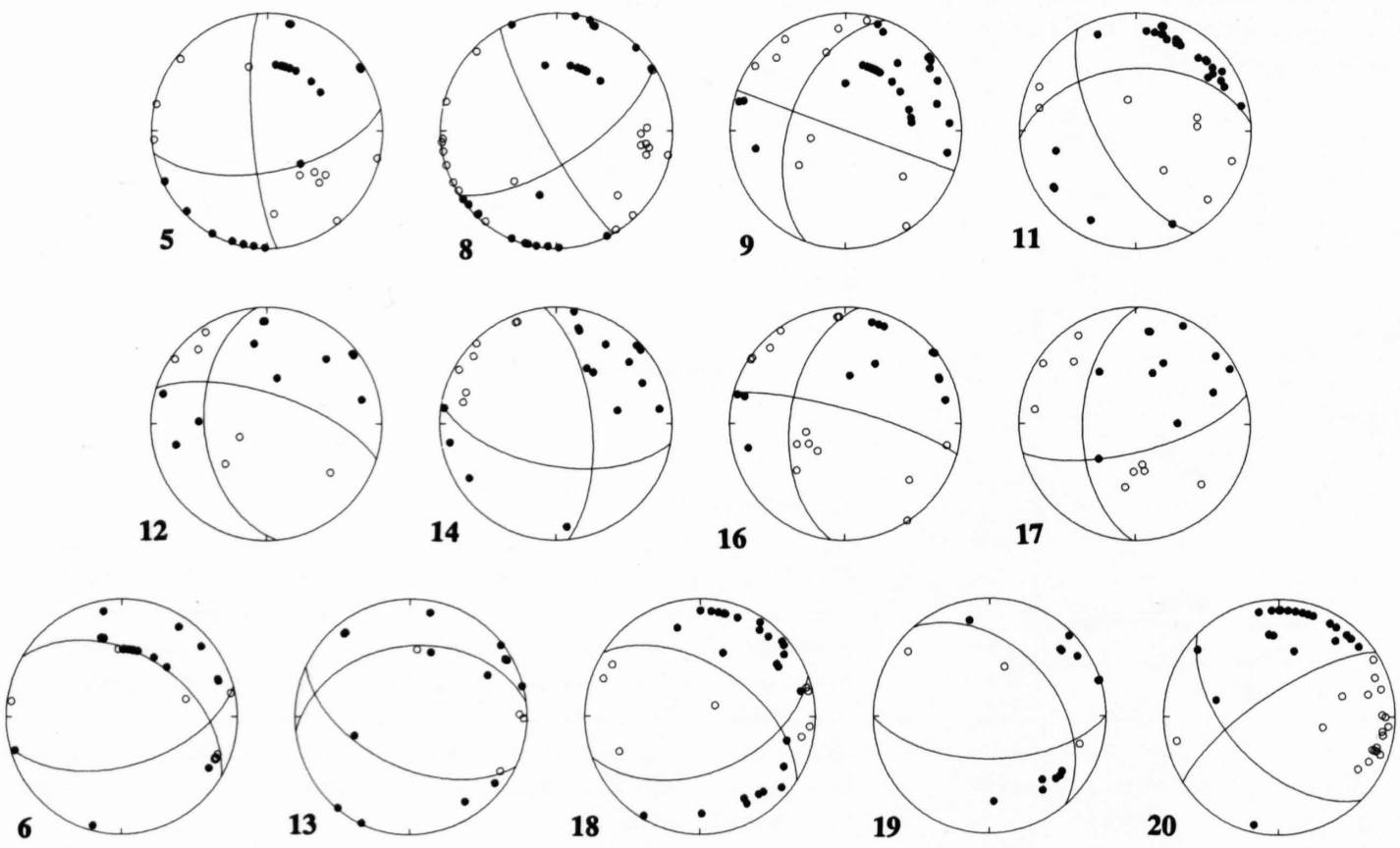

Figure 18-16
Focal mechanisms and data points, western Swiss Alps. The numbering corresponds to the listing in Table 18-2. Full circles = compression. Void circles = dilatation. Lower hemisphere, equal area projections.

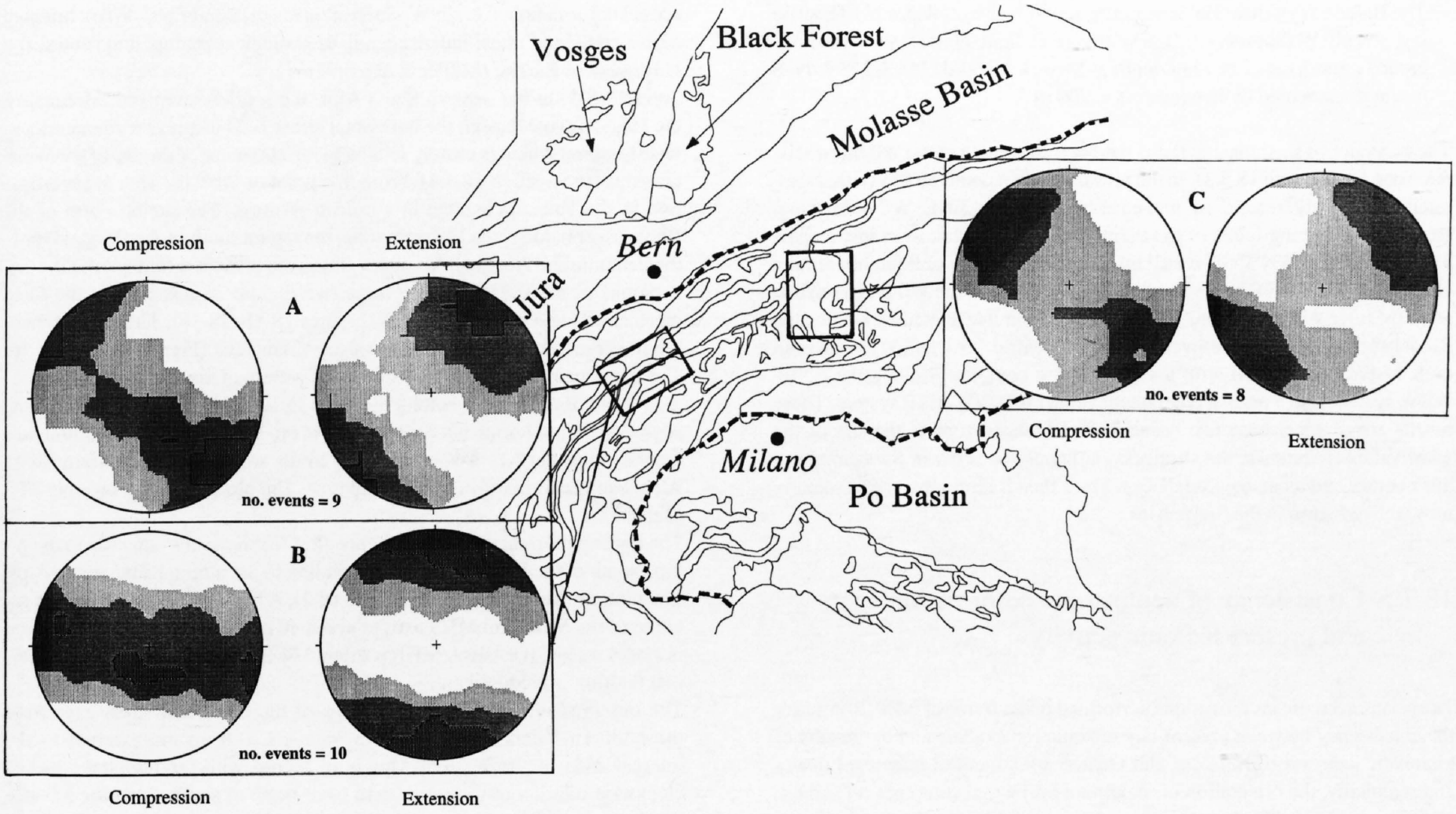

Figure 18-17
Dihedra plots to represent regional stress orientations (Angelier and Mechler, 1977). The degree of shading indicates the compatiblility of compressional resp. dilatational quadrant of fault-plane solutions within the areas delimited by the small rectangular frames (see also Figure 18-6). The darkest shading indicates maximum compatibility of the events used. The directions in the stereo plots with the highest degree of compatibility (darkest shading) indicate roughly the orientation of the main stress axes. A: northern Valais; B: southern Valais; C: eastern Swiss Alps;

18.7 Discussion

18.7.1 Distributed pattern of present tectonic activity

The observed seismicity clearly documents the distributed occurrence of present-day tectonic activity in the Swiss Alps and adjacent regions. A similar pattern of seismically active or less active regions shows up both in the distribution of stronger earthquakes and in the distribution of local shocks and microearthquakes in Switzerland. Inspite of the tectonic nature of the earthquakes, it is difficult to find a correlation between the distribution of epicenters and the conventional tectonic zoning in the Alps. The regions in which the present investigations have been performed, the Grisons and the central Valais, represent the seismically most active regions in the Swiss Alps. They correlate with axial depressions of the Alpine edifice. Furthermore, they correlate with the location of the minima of isostatic anomalies (Klingelé,1979), and the regions of maximum uplift rates in the Alps (Gubler, 1991; see Chapter 19).

18.7.2 Focal depths

There is a remarkable dichotomy with regard to the distribution of focal depths in northern Switzerland (Mayer-Rosa & Garcia, 1986; Deichmann, 1987a; Roth, 1990; Roth et al., 1992). Within the Alps the foci are located in the upper crust down to 15 km, whereas in the northern foreland (Swiss Plateau, Jura Mountains) the foci are distributed throughout the entire depth range of the crust, down to the Moho. Fluids at high pressures are considered to be a possible cause for the greater depth of brittle deformation in the crust of the foreland (Deichmann and Rybach, 1989).

18.7.3 Focal mechanisms, precise relative location of earthquakes

The reliability and significance of well constrained fault-plane solutions (FPS), including the ones of small earthquakes, has been demonstrated in many detailed seismotectonic investigations performed in Switzerland prior to and within the frame of NRP 20. The type of faulting to produce an earthquake is reliably represented by the nodal planes of the FPS. The application of a very precise relative location technique to the earthquakes of a particular cluster, combined with the well-constrainend FPS of the master event enables the mapping of the active fault. These modern seismological techniques allow a direct comparison with local and regional tectonics.

18.7.4 Seismoactive faults and Systems

Our understanding of seismoactive faults and fault zones in the Swiss Alps has been greatly increased by the present investigations. A fault, fault zone or fault system is considered to be seismoactive if one or several of the following criteria are satisfied (Pavoni, 1992):

(1) Direct observation of faulting in connection with an earthquake.
(2) Occurrence of well-located earthquakes or microearthquake activity close to a known fault. In addition, a well-constrained fault-plane solution with one nodal plane showing the same orientation and sense of displacement as the fault is requested.
(3) Close correspondence between orientation of nodal planes and senses of displacement of well-constrained fault-plane solutions with the type and orientation of young faults or fault zones observed in the epicentral region.
(4) Mapping of hypocenters by high-precision relative location of individual events of a local cluster of earthquakes displaying almost identical signal forms. Control by well-constrained fault-plane solution(s).

In the eastern Swiss Alps the following seismoactive faults have been identified:

- The Steinibach fault (Upper Sernft Valley, W of Elm, Canton Glarus), an E–W striking, steeply south dipping, dextral strike-slip seismogenic fault (Figure 18-8). Hypocenter of the reference event (black point in Figure 18-8) located in two kilometers depth below the surface at Swiss km-coord. 728.2/196.5. Horizontal extent documented by the distribution of hypocenters of 1 km, vertical extent of 500 m.
- The Spanegg fault (near Spaneggsee, Canton Glarus), a N–S striking, sinistral strike-slip seismogenic fault. Hypocenter of the reference event located in 6 km depth at Swiss km-coord. 727.9/214.0. N-S horizontal extent of 800 m documented by the distribution of hypocenters (see Section 18.5.2).

– The Balzers fault (near Balzers, Fürstentum Liechtenstein), a N 10 E striking, steeply W-dipping, sinistral seismogenic fault. Hypocenter of the reference event located in 7 km depth at Swiss km-coord. 758.4/215.7. N–S extent documented by hypocenters is 200 m.

The existence of seismogenic faults has been confirmed in the Wildhorn seismic zone (see section 18.3.3). In the present study it could be shown that seismicity is mainly related to movements along the ENE–WSW striking, steeply SSE dipping faults of the main shear zone as well as to movements along associated WNW–ESE striking faults. Due to the oblique orientation of these WNW–ESE faults with respect to the trend of the Wildhorn seismic zone (Maurer & Deichmann, 1995), they may be interpreted as reactivated Riedel shears. The actual movements are of dextral, strike-slip type on both fault systems, combined with a slight reverse component along the ENE–WSW system, and a normal component along the WNW–ESE system. These results are of special interest because the Wildhorn zone is the site of the 1946 Valais earthquake, the strongest earthquake to occur in Switzerland in this century and its many aftershocks. Since then it represents the seimically most active region in the Swiss Alps.

18.7.5 Consistency of neotectonic deformation and present tectonic activity

The seismotectonic investigations performed in the frame of NRP 20 confirm the consistency between present-day tectonic movements and the results of kinematic analyses of Neogene and Quaternary structural features. Locally and regionally, the orientation of maximum horizontal compression and extension, as indicated by the orienation of P-axes and T-axes, corresponds well with the orientation of maximum horizontal crustal shortening and extension derived from tectonic investigations. Evidently the stress field which causes the present seismicity is very similar in its orientation to the stress field of the last 5 to 10 million years which produced the neotectonic deformation.

18.7.6 Regional pattern of the present deformation and stress state of the crust in the Swiss Alps

In addition to detailed insights into the relationship between seismicity and tectonics on a very local scale, the microearthquake studies confirm the regular, regional pattern of the present tectonic stress field acting within the upper crust of the eastern and western Swiss Alps. Strike-slip and normal faulting characterize the dominant deformation process at present.
In the eastern Swiss Alps (Figure 18-11) maximum horizontal crustal extension (MHE) is oriented NE–SW, maximum horizontal crustal shortening (MHS) is oriented NW–SE. This general pattern of present crustal deformation is well illustrated by the two dihedra plots in Figure 18-17c. In the eastern part of the Swiss plateau a slight rotation of MHS into a NNW–SSE orientation, as shown by the orientation of P-axes, and a corresponding ENE–WSW orientation of MHE, as shown by the orientation of T-axes, are indicated (Pavoni, 1980a, 1984; Deichmann, 1987b, 1990). This slight difference in P- and T-axes orientations, in the northern foreland relative to the Alps, produces a slight curvature of the corresponding P- and T-trajectories. A similar slight curvature of P-and T-axes is observed in the transition from the central Swiss Alps to the central Swiss Plateau. Whether this slight stress deviation is significant and to what extent it is related to some differential, lateral dextral movements between the Swiss Alps and their foreland, remains an open question. To the north of Switzerland the same pattern of crustal deformation, i. e. NNW–SSE oriented MHS and ENE–WSW oriented MHE, continues, quasi-independently of geological zoning, into central and northwestern Europe (Müller et al., 1992).
Towards SW, in the western Swiss Alps, the southwestern Jura Mountains, the Haute Savoie region, the horizontal stress field displays a counterclockwise rotation, which is closely related to the curvature of the arc of the Western Alps (see Section 18.3.4). From this point of view the area of investigation in the Valais is located in a crucial position. The region north of the Rhone river belongs the Helvetic zone, the region south of the Rhone river to the Penninic and Austroalpine zones. There are distinct differences in the orientations of the stress fields in these two regions as revealed by the focal mechanisms and station diagrams (Figures 18-15, 18-16). These differences are illustrated in the dihedra plots of the Valais area (Figure 18-17a and b). The upper pair (Figure 18-17a) shows the pattern of the stress field in the region north of the Rhone, belonging to the Helvetic, i. e. external zone of the Alps. Maximum horizontal compression is oriented NW–SE, maximum horizontal extension NE–SW, comparable to the situation in the eastern Swiss Alps. Faulting is mainly of strike-slip type. The plots are based on eight FPS (Table 18-2).
The lower pair of dihedra plots (Figure 18-17b) shows the situation in the region south of the Rhone river, corresponding to the internal zone of the Alps. The plots are based on ten FPS (Table 18-2). A distinct counterclockwise rotation of the MHE and MHS axes of about 40 degrees, as compared with the northern region, is evident. MHE is orientd N–S, MHS is trending E–W. Normal faulting is predominant.
The observed difference of orientations of the horizontal stress axes from the northern Valais to the southern Valais, i. e. from the external to the internal zone of the Western Alps is in accord with the regional counterclockwise rotation of the stress field from north to south along the arc as a whole.
The question whether there is a very sharp or a more gradual transition from the northern to the southern stress regime in the Valais cannot be answered yet. Further systematic microearthquake investigations are necessary. The predominance of normal faulting along E–W striking planes is a very remarkable observation. A possible explanation, based on the results of two-dimensional geodynamic modeling, is given by Werner & Gudmundsson (1992).
Of great importance for the understanding of the present tectonic regime in the central Valais are the dextral shearing movements along the Rhone valley fault system which were first identified in the Wildhorn seismic zone in the seventies and since then have been confirmed and investigated in great detail by the studies performed in the frame of NRP 20. These movements are part of the large-scale crustal indentation and twisting between the European, Adriatic and Ligurian lithospheres, of which so much has been learned by the combined national and international research efforts during the last decade.

Acknowledgements

Apart from the substancial financial support of the Swiss National Science Foundation we gratefully acknowledge the contribution of M. Baer with his software for the acquisition and analysis of seismic data at the Swiss Seismological Service. We gratefully acknowledge the help of C. Baerlocher, M. Dietiker, P. Zweifel, M. Grieder and R. Turi with installation and maintenance of recording instruments. We thank J. D. Rouiller and his colleagues of the Centre de Recherches Scientifiques Fondamentales et Appliequées, Sion, for logistic support in running the temporary stations in the Valais. M. Burkhard, D. Mayer-Rosa, U. Kradolfer and St. Mueller contributed with fruitful discussions and active support in the course of this study. Contribution number 884 of the Institute of Geophysics, ETH Zürich.

19 Recent crustal movements, geoid and density distribution: Contribution from integrated satellite and terrestrial measurements

H.-G. Kahle, A. Geiger, B. Bürki, E. Gubler, U. Marti, B. Wirth, M. Rothacher, W. Gurtner, G. Beutler, I. Bauersima, & O. A. Pfiffner

Contents

19.1 Introduction

In the near future space geodetic techniques will provide most valuable information on the kinematics and dynamics of the earth's lithosphere. Already plate motions have been determined by using worldwide VLBI (Very Long Baseline Interferometry) data (Robaudo et al., 1993; Ryan et al., 1993), SLR (Satellite Laser Ranging) (Smith et al., 1994) and GPS (Global Positioning System) (Blewitt, 1993). In the last few years numerous measurements have been made at European stations using these techniques. A new European geodetic reference system is being established by using GPS (Gubler & Hornik, 1993). Establishment of a GPS based reference system is also in progresss in Switzerland (Gubler, 1992, 1993; Schneider, 1989, 1993). Within a few more years, repeated measurements will provide a basis for the assessment of horizontal and vertical movements. Since there were no previous satellite data available at the time of the NRP 20 project, mainly terrestrial techniques were used for determining uplift rates. The Geodesy Group of NRP 20 comprises the Swiss Federal Office of Topography, Berne (L+T), the Astronomical Institute of the University of Berne (AIUB) and the Geodesy and Geodynamics Laboratory (GGL) of the Institute of Geodesy and Photogrammetry (IGP) of the ETH Zurich (ETHZ) (Kahle et al., 1987, 1989). Their activities for determining density parameters and recent crustal movements in the years between 1985 and 1990 are summarized in the following paper.

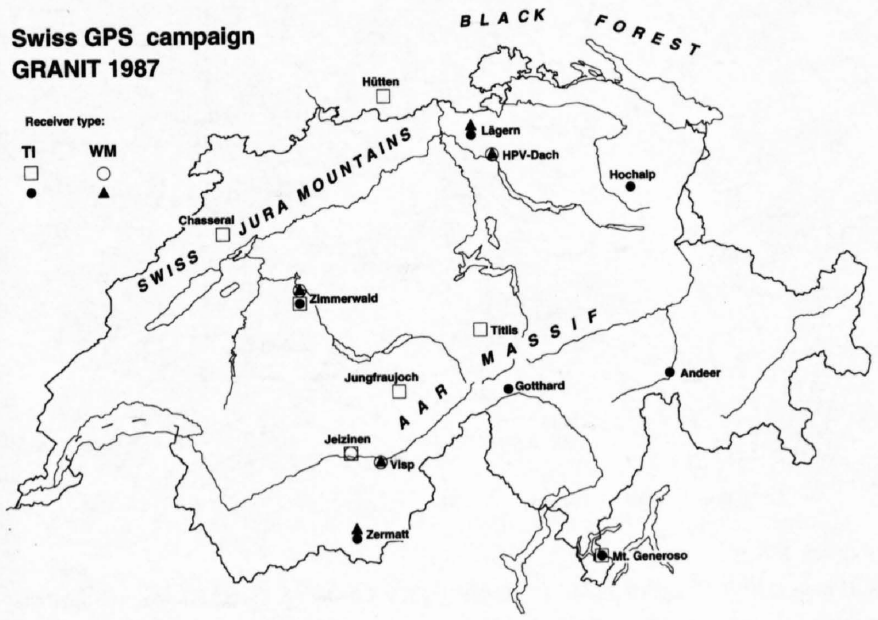

Figure 19-1
Stations of the GPS campaign GRANIT 1987. Two symbols for each receiver type indicate two different sessions.

The geodesy group of NRP 20 pursued two principal goals. The first was the determination of recent crustal movements (RCM) in the Alps. These are mainly detected by means of spaceborne surveying systems (particularly the Global Positioning System (GPS)) and by classical leveling techniques. Both methods were employed during NRP 20 . Two leveling lines in the cantons of Ticino and Valais were re-measured with high precision leveling instruments and annual uplift rates were calculated. Two GPS campaigns were conducted for RCM purposes. The first one, GRANIT, connects the three seismic traverses and ties the satellite station in Zimmerwald to the Swiss Jura mountains and the Alps in order to assess the relative stability of this Satellite Laser Ranging (SLR) site. The second GPS campaign was performed along the leveling line from Visp to Zermatt.
The second goal of the geodetic part of NRP 20 was to contribute to density modelling of the geologic depth structures along the three traverses. For this purpose more than 80 deflections of the vertical were observed with the zenith camera. In addition, gravity measurements and GPS data formed the input for our modelling.

19.2 The GPS campaign GRANIT

In 1987 the Geodesy Group of NRP 20 established a precise connection between the Western and Eastern Traverse by means of GPS measurements (Beutler et al., 1989). The 14 selected stations (Figure 19-1) will form a basic network for the detection of recent crustal movements in Switzerland. The connection of this GRANIT network (Geodätische Rückversicherung der Astrostation Zimmerwald und Nullmessungen in den Traversen) with the permanent SLR station in Zimmerwald made possible the determination of WGS 84 coordinates with an accuracy of a few centimeters (Rothacher et al., 1988). Zimmerwald is located in the Swiss Molasse Basin, a sedimentary basin filled with detrital Alpine material. Its connection with stations in the Aar massif, the Swiss Jura Mountains and the Black Forest, Germany, is of importance in assessing future local movements of the SLR reference site in Zimmerwald. Together with the two stations Jungfraujoch and Monte Generoso, Zimmerwald forms the first high-accuracy baseline parallel to the main compression direction of the Alps. It was measured for the first time in 1985 by means of SLR and GPS (Rothacher et al., 1986, Bürki et al., 1987). Besides connecting the traverses, the GRANIT network can be used as an initial source for investigation of the relative movements of the main tectonic structures in Switzerland. Since the coordinates of all stations are known with respect to the Swiss reference system, GRANIT can also be used to connect the coordinate system of the Swiss triangulation network with the International Terrestrial Reference Frame (ITRF) used for GPS orbit determinations by the International Geodynamic GPS Service (IGS) (Beutler et al., 1994). In the meantime the L + T is in the process of establishing a new national GPS network (LV 95) comprising 104 stations with an expected horizontal accuracy of 1cm (Wiget et al., 1994). This network should be completed in 1995.

19.2.1 The measurements

GRANIT was the first GPS campaign in Switzerland which covered the entire country. Seven TI-4100 receivers were provided by the following 6 organisations: Alfred Wegener Institut, Bremerhaven (AWI), Geodätisches Institut, Hannover (GIH), Hochschule der Bundeswehr, Neubiberg (HSBW); Institut für Erdmessung, Hannover (IEMH), Observatorium Lustbüel, Graz (OLU), Technische Universität München (TUM). At the same time the ETHZ measured with their WM GPS receivers. Coordination was performed jointly by the L + T, the AIUB and the GGL of IGP-ETH. The necessary local ties were measured and evaluated by the L + T. Satellite coverage at that time allowed data to be taken for 4 h per day (for a total of 3 days).

Figure 19-2
Recent vertical movements and their double standard deviation computed for selected first order leveling benchmarks relative to a reference benchmark at Aarburg (after Gubler, 1991).

19.2.2 The processing of the GPS campaign

The processing was performed at the AIUB by means of the Bernese GPS Software version 3.2 (Rothacher et al., 1990a). Since no other European VLBI or SLR sites (apart from Zimmerwald) were occupied during the observations, it was not possible to determine orbit parameters by means of fiducial points. Therefore, two orbit parameters (along track error and semi-major axis of the orbit ellipse) were estimated for each satellite in order to reduce the influence of systematic errors caused by the broadcast satellite orbits. The influence of the ionosphere was eliminated by making use of the ionosphere-free linear combination L3 of the L1/L2 measurements. In addition to the standard troposphere model one troposphere parameter was estimated for each baseline (Rothacher et al., 1990b, 1992). The original 3-second data was decimated to an interval of 30 seconds. All ambiguities were resolved. This resulted in an improvement of quality by a factor of 4 compared to the coordinates without ambiguity resolution.

19.2.3 Results

The quality of the results were compared in three different ways:

Formal mean errors of the coordinates
The formal mean errors of the complete solution relative to Zimmerwald are 1 to 2 mm in a north-south and 1 mm in an east-west direction, between 7 and 14 mm in height and about 1 mm in baseline length. These values are certainly too optimistic because systematic errors often cannot be revealed by statistical methods alone.

Repeatability
During the first two days the same sites were occupied. The differences between the two daily solutions (after a translation) are in the range of 7 to 8 mm in position and about 35 mm in height.

Comparison with the results of the 1985 GPS campaign
The baselines between the stations Zimmerwald, Jungfraujoch and Monte Generoso were observed in 1985 with 2 TI-4100 receivers. A comparison between the results of 1985 and 1987 showed very good agreement. The largest residuals are on the baseline from Monte Generoso to Jungfraujoch with a difference of 15 mm. The other two baselines differ by only 3 and 1 mm respectively.

19.3 Leveling and recent vertical crustal movements

GPS is a suitable method for obtaining accurate coordinates in a relatively short time period. With classical methods much more time is necessary to obtain similar results and to assess recent crustal movements (RCM). In the recent past, mainly national geodetic surveys have been used for large-scale

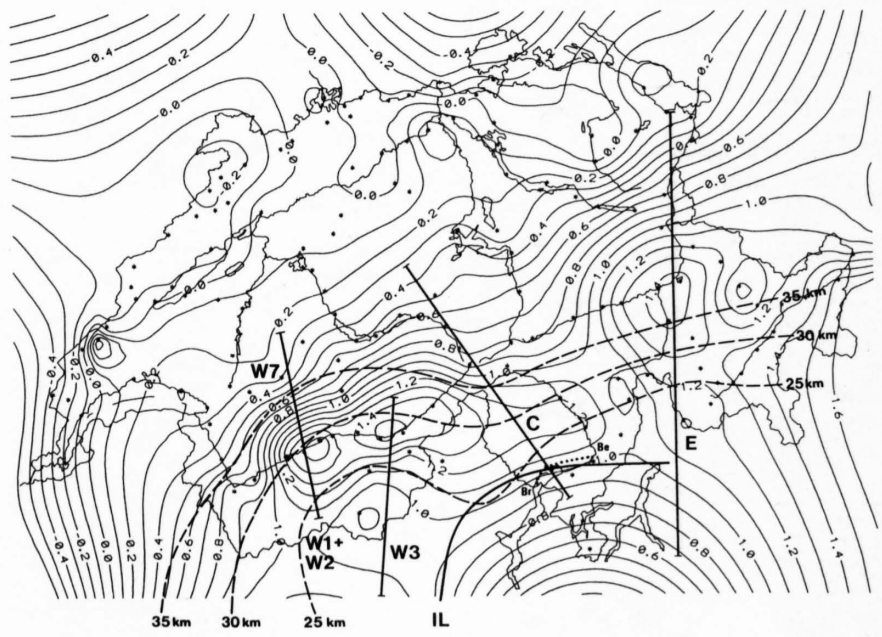

Figure 19-3
Contour map of uplift rates in mm/a [after Gubler]. Dashed lines: Contour map of Conrad discontinuity [after Valasek & St. Mueller, Chapter 23]. W7+W1+W2, W3, C and E: Location of uplift and geologic profiles shown in Figures 19-4a, b, c and d. Br-Be = Leveling line Brissago-Bellinzona. IL = Insubric Line.

investigations of RCM, namely higher-order triangulation networks (Reilly & Gubler, 1990) and higher-order leveling networks (Gubler et al, 1992). These have been re-measured after a long time interval and with adequate accuracy. In most cases, however, existing triangulation networks are either not accurate enough to determine horizontal displacements or re-measurements have not yet been carried out. So far, significant results have been reported for limited areas only. For the scope of NRP 20, the investigations were concentrated on the vertical component of RCM, leveling being at least one order of magnitude more accurate than triangulation.

19.3.1 The Swiss first-order leveling net

The L+T established a first-order leveling net covering the entire area of Switzerland and forming 18 loops with a total of 3000 km of leveling lines (see Figure 19-2). The first measurement cycle was carried out between 1905 and 1927. The second one was begun in 1943 and finished in 1990. The standard deviations computed from the adjustments are 1.4 and 0.8 mm per square root of 1 km. These measurements allow the determination of significant relative movements between the Swiss Jura Mountains (Jeanrichard, 1990), the Alpine foreland and the Alps. From early interpretations of leveling, gravity and seismic data it was concluded that besides isostatic rebound effects also horizontal compression contributes to the ongoing uplift of the Alps (Kahle et al., 1980). In this project new detailed data sets are considered and analyzed:
In a first step the raw leveling data was adjusted according to a specially-designed least squares adjustment where the heights of the benchmarks are computed together with their relative vertical velocities. These computations yield a variance-covariance matrix of the heights and the velocities as well. The procedures used for this investigation are described in detail by Gubler et. al. (1984). Figure 19-2 shows a selection of the calculated uplift rates together with an indication of their level of significance (after Gubler, 1991). The two heavy lines on both sides of the columns give the error bars: two times the standard deviation. As a rule of thumb, a vertical rate is significant on a 95% level if it is larger than the error bars. Since no connections of high precision for coastal areas are available yet, all calculations refer to an arbitrary benchmark in Aarburg in the Swiss Molasse Basin. The movements relative to this station exceed their standard deviation by a factor of four in the Alpine part of Switzerland and can be regarded as highly significant.
In Figure 19-3 the uplift rates are shown as contours at an interval of 0.1 mm/a. Superimposed on these isolines of uplift are the contours of the top of the lower crust of the southern Alps, often referred to as the "Adriatic" Conrad discontinuity (compare Valasek & Mueller, Chapter 23). It is interesting to note that the shift of maximum uplift rates from the central crystalline massifs towards the south correlates with the indenting Adriatic wedge. It may, therefore, be concluded that part of the uplift of the Southern Alps is caused by continuing penetration of the Adriatic wedge into the European lithosphere.

19.3.2 Dedicated measurements for NRP 20

Two leveling lines were specially measured for NRP 20, namely Visp–Zermatt and Bellinzona–Brissago (Gubler, 1988). The latter forms part of the Swiss first-order leveling net and was measured in 1919 as part of a loop connecting the Simplon line with the Gotthard line (location see Figure 19-3). This line was chosen because it crosses the Insubric line. The question was whether this line had been active between 1920 and 1987. The evaluation showed no significant relative movements between the benchmarks along the line Bellinzona – Brissago. The detected uplifts are of the same order as their standard deviation. The Insubric line can, therefore, be considered as relatively stable.
The leveling line from Visp to Zermatt was studied because it is located close to the seismic profiles. It was measured for the first time in 1930 according to second-order standards only. This line was re-measured in 1987 according to first-order standards. The evaluation of the measurements showed a significant decrease of uplift rates between Visp and Zermatt in the order of 0.7 mm/a (compare also Figure 19-4b). This is more than three times the standard deviation. Leveling results in the Simplon area, one line over the Simplon pass and the other one through the Simplon railway tunnel, have shown a similar gradient from north to south.

19.3.3 Profiles

In addition to the results presented in Figures 19-2 and 19-3, profiles were compiled to show uplift rates together with the geological structures. Four profiles were selected (Figures 19-4a, b, c and d) the locations of which are shown in Figure 19-3. The RCM profiles were calculated with the PC software SURFER/GRAPHER from Golden Software Inc.

The profile of Figure 19-4a follows the seismic lines W7, W1 and W2. The steep gradient of the uplift profiles in the N correlates with the northern flank of the underlying external basement uplift. Exhumation of this basement uplift was particularly rapid in the last ca. 5 Ma. It occurred in conjunction with a deep-seated detachment linked to the basal thrust of the Adriatic wedge (see Steck et al., Chapter 12, Pfiffner et al., Chapter 13.1 and Escher et al., Chapter 16). The recent uplift maximum (near Sierre) correlates with the pronounced seismic activity observed in this area (see Pavoni et al. Chapter 17).

The profile of Figure 19-4b follows seismic line W3 rather closely. The maximum uplift rate at the northern end corresponds to a maximum of seismic activity observed in the area around Visp-Brig. This uplift maximum is located to the south of the external basement uplift. The elongated area of maximum uplift between Sierre and Brig runs somewhat oblique to the southern steep limit of the external basement uplift ("back folds" of the Aar massif; see Figures 12-4 and 12-6). On the other hand the maximum straddles the Rhone segment of the Simplon-Rhone fault. This fault, although it is a normal fault moving the hanging wall block down to the WSW, has a strike-slip component along the Rhone valley. From the movement direction one would expect it to be of transtensive rather than transpressive nature along this segment, rendering it an unlikely explanation for the observed recent uplift pattern.
If recent uplift is explained by ongoing horizontal compression, slip on the basal thrust of the rigid Adriatic wedge could cause internal deformation of the Alpine nappe pile ahead of it (including the latest formed, i.e. the external basement uplift) and could in fact produce the uplift pattern observed today. The elongated uplift maximum would be due to local vertical escape above the southern limit of the external basement uplift.

The profile of Figure 19-4c straddles the three segments C1, C2 and C3 of the Central Traverse. The maximum uplift is located in a more southerly position compared to the adjacent profiles to the west and east. If related to active horizontal compression, uplift would be distributed across a wide zone between Mio/Pliocene thrusting, north-directed in the north (Aar massif – Jura Mountains) and south directed in the south (Southern Alps – Milan Fold belt).

The profile of Figure 19-4d is parallel to the seismic line E1 but extended southwards across the Insubric line. Maximum uplift rates coincide with an area of pronounced seismic activity (Chur). The steep gradient in the north (Chur-St. Gallen) could be explained by ongoing exhumation of the external basement uplift (Aar massif) linked to a deep seated thrust fault at the base of the Adriatic wedge, similar to the situation discussed for the profile of Figure 19-4a. The fact that the uplift maximum and its northern gradient are situated farther north along the Eastern as compared to the Western Traverse also mirrors the shape of the northern tip of the Adriatic wedge. The latter extends as far north as Thusis in the Eastern Traverse and consists of lower crust, the wedge having a shallow N-dipping top surface. In the Western Traverse the tip of the indenter is located beneath Zermatt. The wedge itself consists of mantle rocks, bounded by a steeply N-dipping top surface.
In summary, an explanation for the observed uplift patterns could be ongoing crustal compression ahead of the Adriatic wedge including local vertical escape.

19.3.4 Conclusions

It is concluded that the new results are consistent with a general wedge-shaped pattern of Alpine uplift. In addition it was shown that the maximum of strain energy calculated from the uplift rates is in good coincidence with the major seismicity zone in Switzerland (Geiger et al., 1986, 1993). It has to be pointed out, however, that two epoch measurements alone do not allow the detection of variations in the vertical velocities but give the average rates for the time period only. From nodal benchmarks, where lines with different time periods meet, there is evidence, however, that the uplift rates are uniform in time for the periods considered.

19.4 GPS profile Visp–Zermatt

Besides the leveling measurements, 12 GPS stations were established along the leveling line from Visp to Zermatt with the aim of generating a first network for investigating horizontal movements in this area as well as to provide the basis for a local geoid calculation. Due to visibility problems in the terrestrial network the total number of stations had to be increased to 20. The whole network is shown in Figure 19-5.

a)

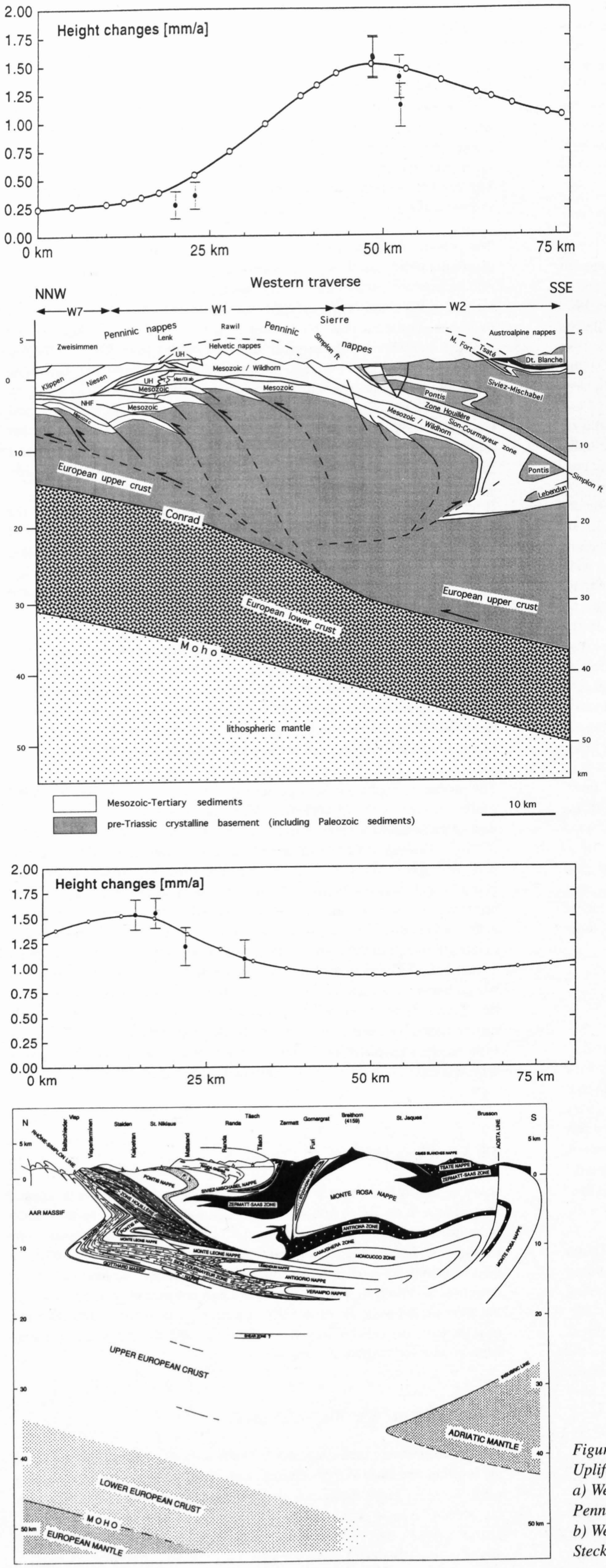

b)

Figure 19-4
Uplift and geologic profiles along various traverses of NRP 20.
a) Western Traverse (seismic lines W7, W1 and W2). Geologic structure of Penninic nappes in W2 partly after Steck et al., Chapter 12.
b) Western traverse, southern part (seismic line W3). Geologic profile from Steck et al., Chapter 12.

c)

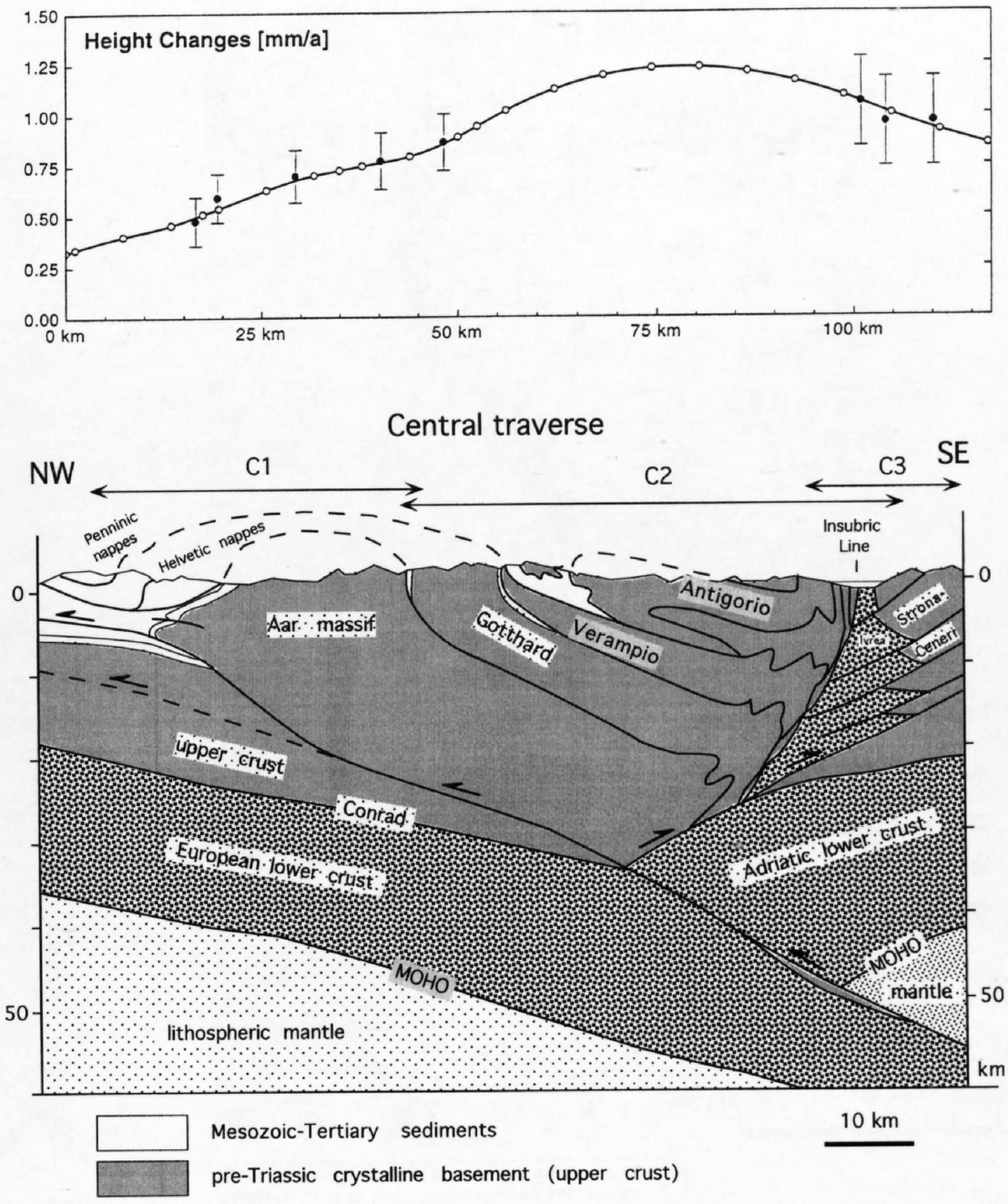

d)

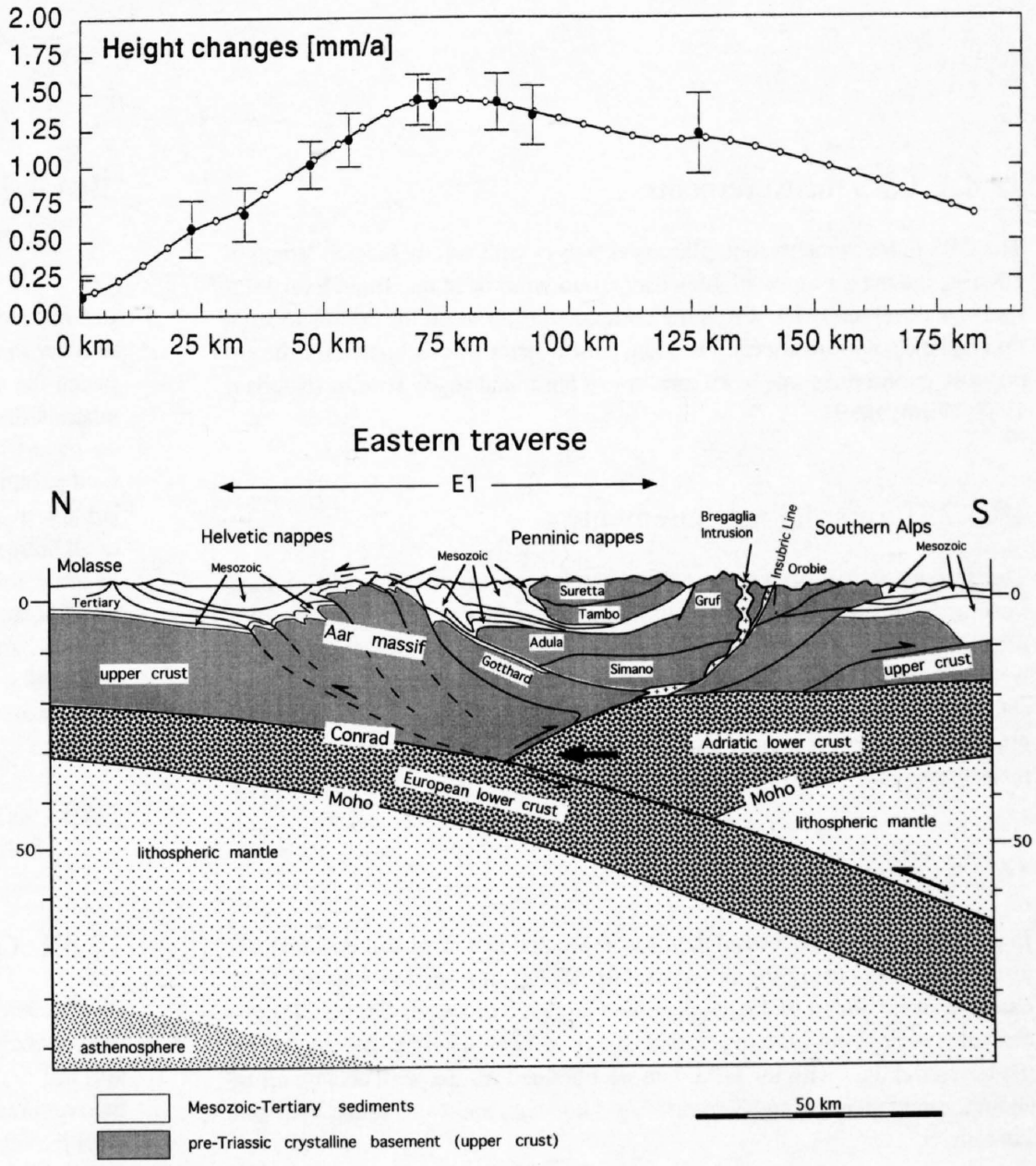

Figure 19-4 (continued)
Uplift and geologic profiles along various traverses of NRP 20.
c) Central traverse (seismic lines C1, C2 and C3).
d) Eastern traverse (seismic line E1, extended to the N and S).
See also Pfiffner & Hitz, Chapter 9.

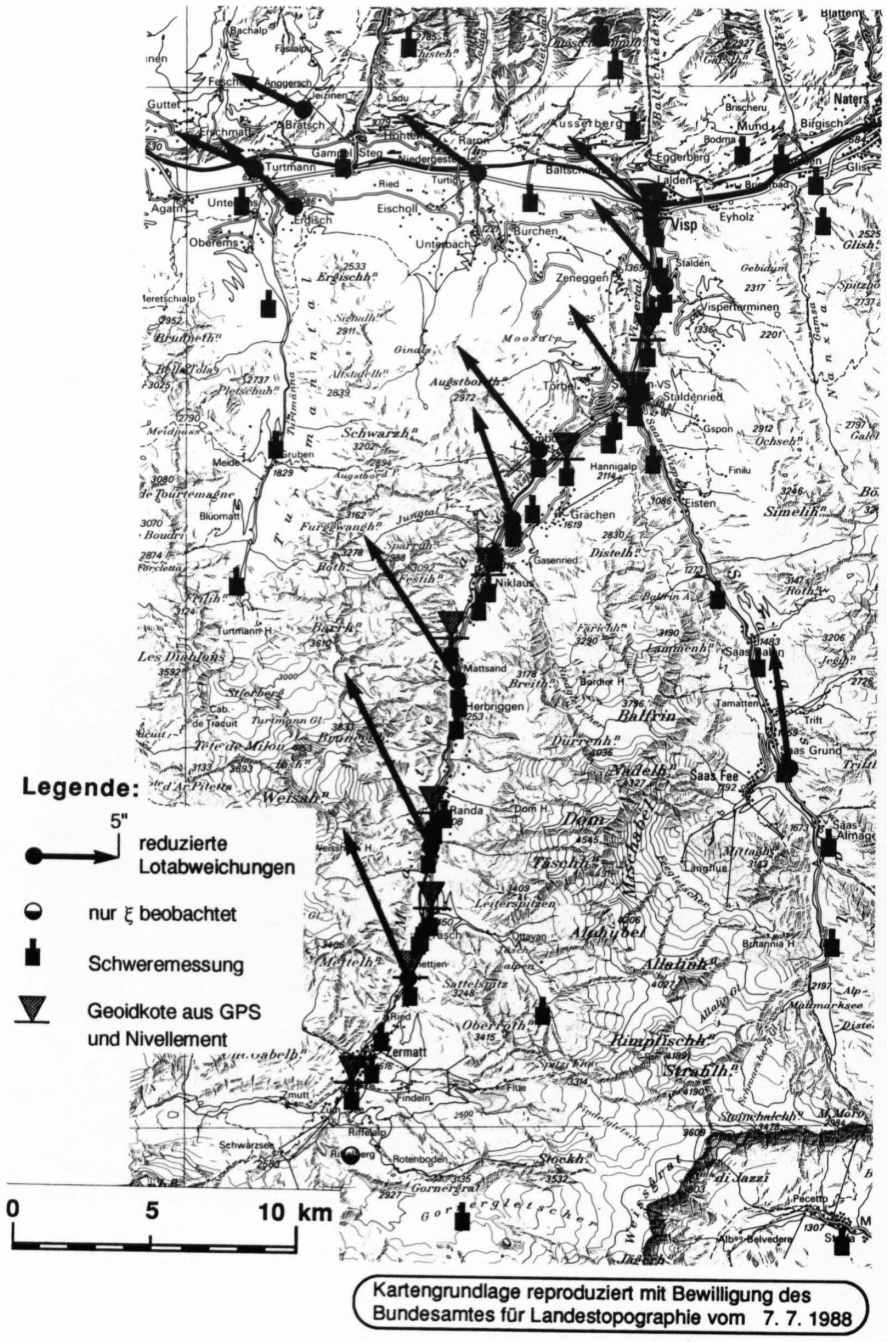

Figure 19-5
Stations of geodetic observations in the region of the leveling line Visp – Zermatt. Arrows: reduced deflections of the vertical (Wirth, 1990).

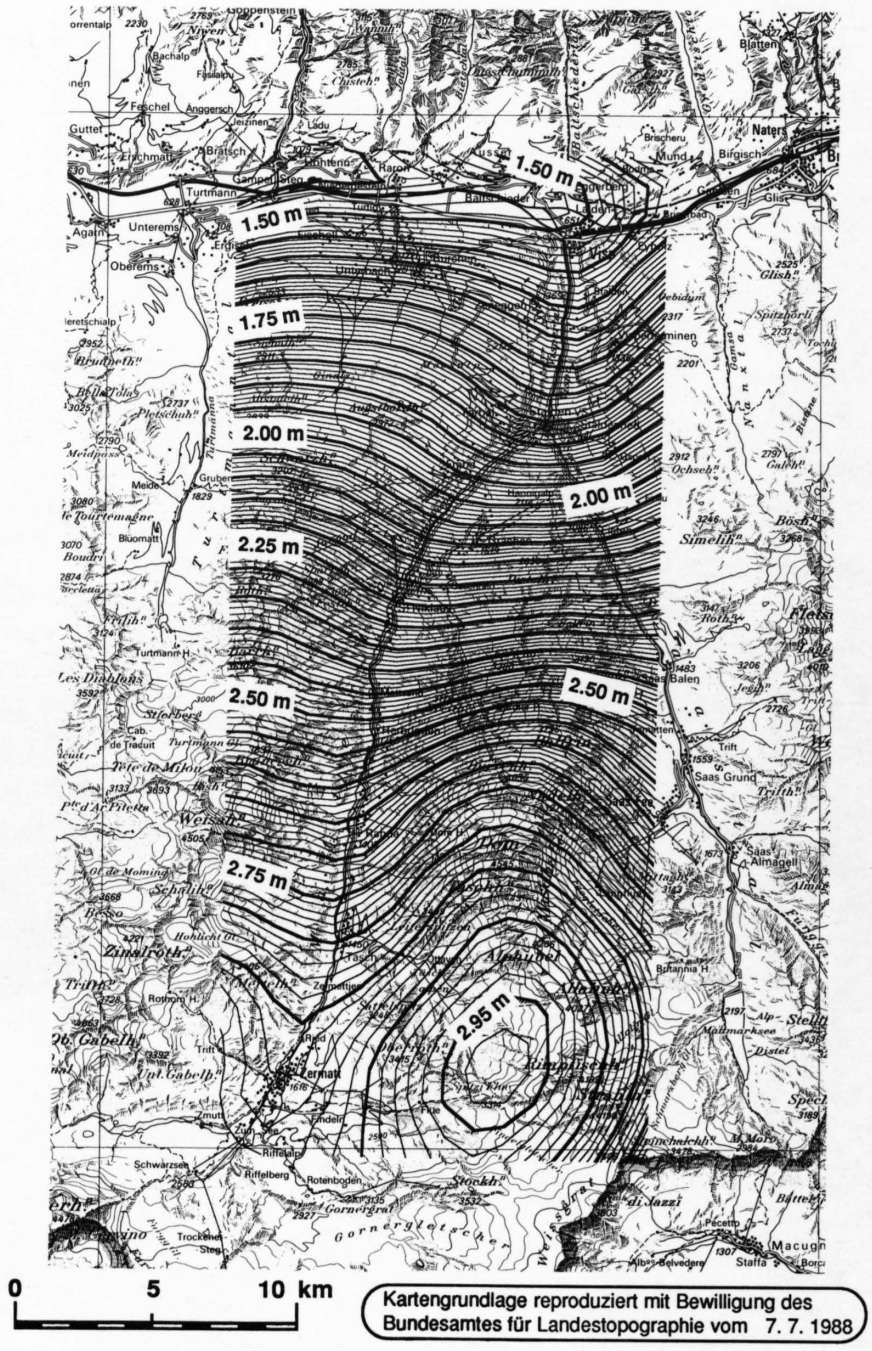

Figure 19-6
Local geoid in the region Visp – Zermatt (Wirth, 1990).

19.4.1 GPS measurements

The GPS measurements took place over 9 days with a daily session length of 3 hours, the maximum available observation window at that time. Every station was observed twice. From the comparisons between the complete solution and the solutions for each session, a mean error was estimated for the geocentric coordinates: m_X = 19 mm, m_Y = 6mm and m_Z = 10 mm (Nebiker, 1988; Wirth, 1989).

19.4.2 Terrestrial measurements

The terrestrial measurements consisted of observation of a 40 km long traverse from Visp to Zermatt using Mekometers (Kern) and precise theodolites. A total of 61 distances, 106 vertical angles and 61 horizontal angles were observed. In addition astronomical observations were performed at 8 stations and gravimetric measurements were carried out at 34 stations. The gravimetric data was mainly used for reduction calculations of the leveling measurements.

19.4.3 Evaluation

In a first step all the terrestrial data was evaluated in a three-dimensional adjustment process using the program RAUMTRI. In a second step the GPS baselines were added to the data set. The largest corrections on the GPS coordinates were about 2 cm in position and up to 5 cm in height. By combining the terrestrial data with the GPS data we obtained results with accuracies of about 2 cm in position and 3 cm in height between the two stations Visp and Zermatt.

19.4.4 Determination of orthometric heights and the local geoid

In a first step the raw leveling data was reduced together with the gravity data in order to obtain orthometric heights. The orthometric corrections differ between the stations Visp and Zermatt by more than 14 cm. This large value emphasizes the necessity of reducing leveling data in mountainous regions by means of gravity data. This is suitable for calculating the local gravity field parameters. For the investigations not only the NRP 20 measurements, but also available older data sets of the region were used. After the reduction of all known mass models, the residuals were interpolated by means of a multivariate collocation method using a 1/r covariance function. The calculated geoid is shown in Figure 19-6 (Wirth, 1990). It is clearly seen that there are lateral changes in the geoidal heights from Visp to Zermatt reaching more than 1.40 m. The maximum error of the calculated geoid difference between Zermatt and Visp is below 2 cm.

19.5 Astrogeodetic measurements and density estimations

19.5.1 Overview

Besides astrogeodetic observations along the line Visp-Zermatt it was part of the project to measure astronomical stations along the NRP 20 traverses. The aim was to use these to estimate density parameters of the topography and of the crust-mantle boundary. In 1986, 54 astrogeodetic stations were observed with the zenith-camera along the Eastern Traverse. 15 sites were selected

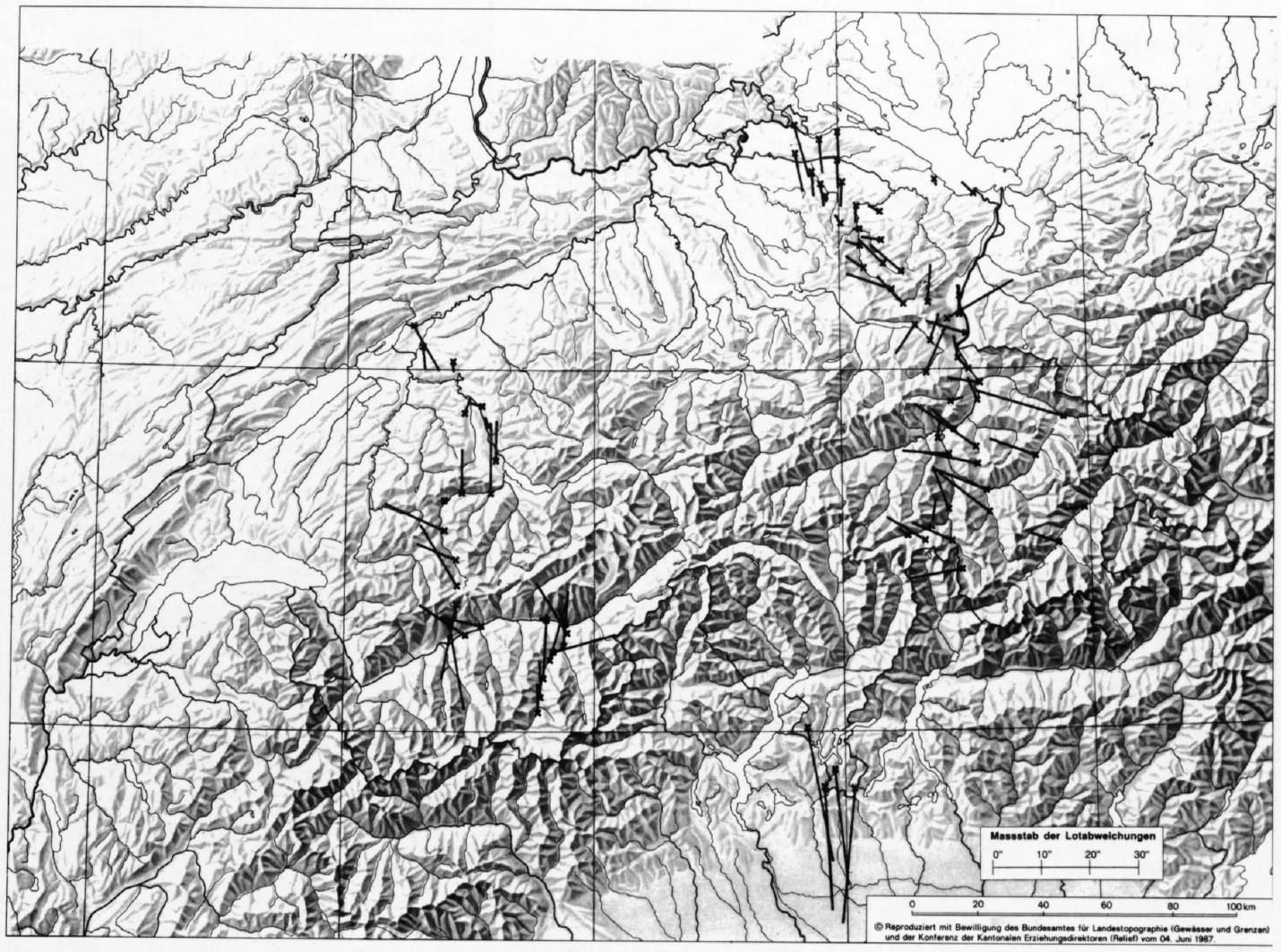

Figure 19-7
Astrogeodetic stations with observed deflections of the vertical (Wirth & Marti, 1988).

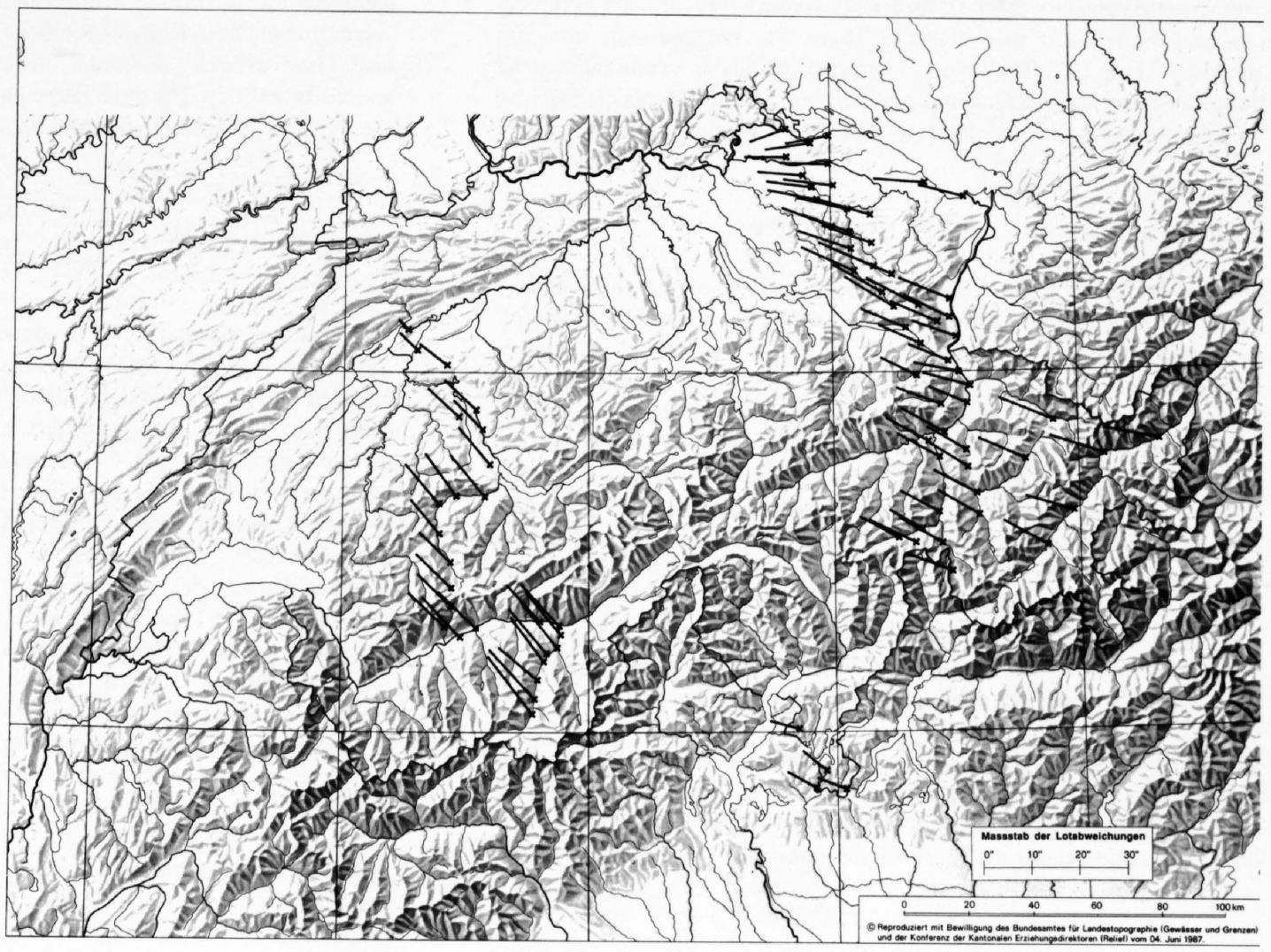

Figure 19-8
Deflections of the vertical, reduced by the effects of topography, Moho, Po plain and Ivrea body (Wirth & Marti, 1988).

near the border with Austria in order to connect the national astrogeodetic geoids of Austria and Switzerland.
25 stations were observed along the Western Traverse. The observations at the Eastern Traverse were completed in 1987 with an additional 4 stations in the Southern Traverse. This region is already well covered by astronomical stations. These were measured during the ETHZ Ivrea project between 1983 and 1986 (Bürki, 1989). In Figure 19-7 the stations are shown together with the observed deflections of the vertical. In general they have an accuracy of better than 0.5" (arc seconds). Because of the large influence of the Ivrea body the largest deflections are found in the southern part of canton Ticino (reaching almost 30").

19.5.2 Reduction of the observations

The observed deflections of the vertical (Figure 19-7) are masked by topographic effects (Wirth & Marti, 1988). In order to separate the signals from the effects of known mass inhomogeneities proper reductions have to be applied to the observations. The most significant effects are caused by the topography (see also Geiger et al., 1991; Marti & Kahle, 1995). In general we used a 500 meter digital terrain model (DTM) for its reduction. However, in order to increase accuracy a 50 meter DTM was applied in an area of 4 km^2 around each station. A common density of 2.65 g/cm^3 was used. As further

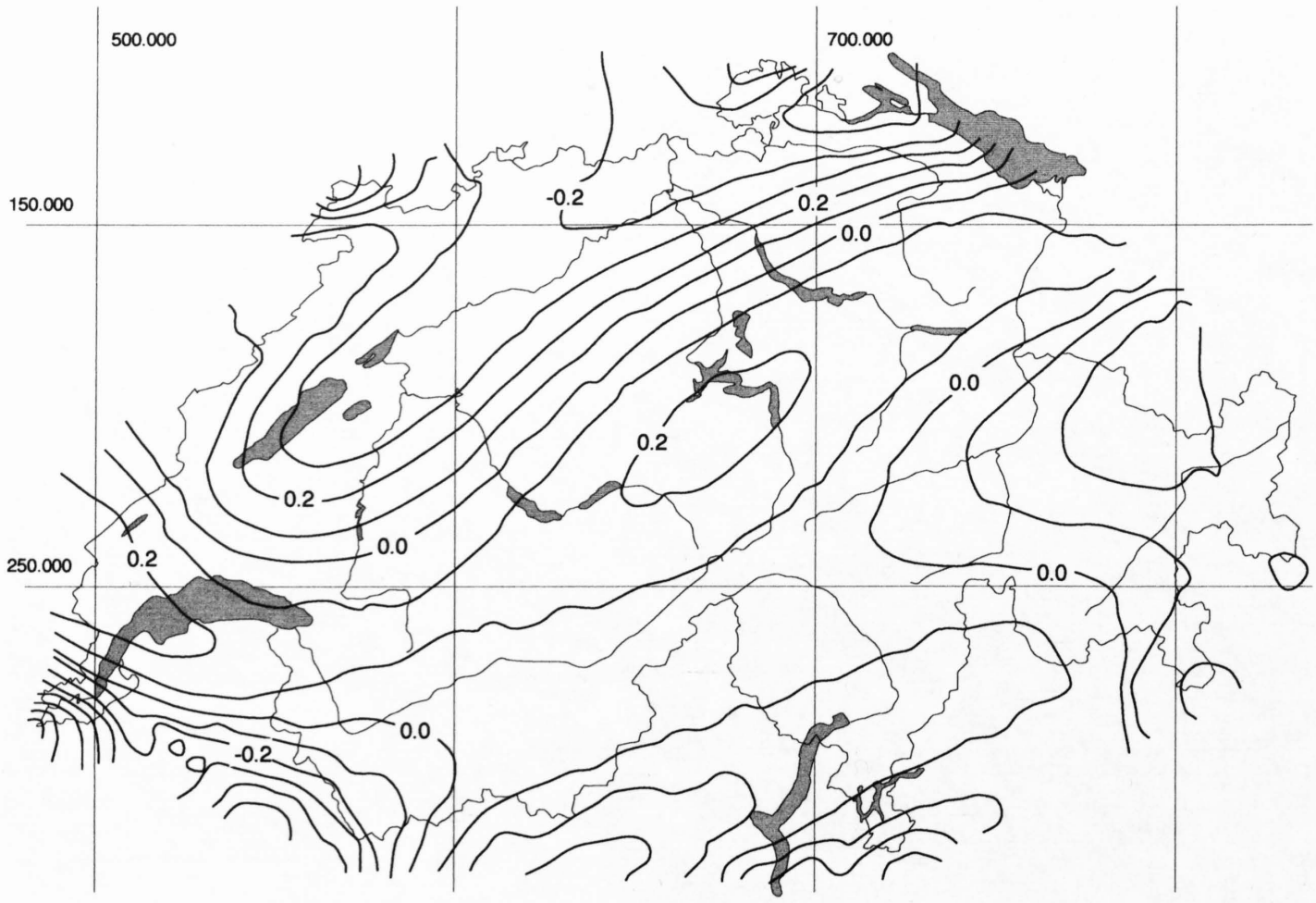

Figure 19-9
Estimated difference of density distribution [gcm^{-3}] of topography with a polynomial of degree 7 (after Geiger, 1990). Reference value: 2.67 gcm^{-3}.

models we considered the Ivrea body, the sediments of the Po plain and the crust-mantle boundary (Moho). Its density contrast was assumed as 0.43 g/cm^3 and the compensation depth as 34 km. The reduced deflections are shown in Figure 19-8. They can be interpreted mainly as a constant regional trend caused by the insufficient geographical extent of our models and also by the local Swiss geodetic datum to which the deflections are referred.

19.5.3 Interpretation of Astrogeodesy

One aim of the astrogeodetic measurements was to contribute to the density modeling of geological structures in Switzerland. We decided to set the following parameters:

a) The models of the Ivrea body (Bürki, 1989) and of the Po plain (Schwendener, 1984) had already been investigated in other projects. Their accuracy cannot be improved by the measurements of NRP 20.
b) The geometry of the topographic model remained unchanged but it was subdivided into two groups: One group with stations located in the Molasse Basin and one group with stations in the Alpine region. For both groups a best-fitting density value for the topographic effect was determined (Geiger et al., 1993).
c) The geometry of the Moho model remained unchanged. We used the model compiled from data of Mueller et. al. (1980). At the time of our analysis this model was considered to be the most reliable.

The density contrast at the Moho as well as density values for the topography were calculated in one computation. Similar to gravimetric Nettleton profiles, the horizontal components of the gravity vector can also be used to determine densities. Using the observation equation

$$\varepsilon_{meas} + v = \frac{\varepsilon^0_{moho}}{0.43} \cdot \sigma_{moho} + \frac{\varepsilon^0_{topo}}{2.65} \cdot \rho_{topo} + \Delta\varepsilon + \varepsilon_{Ivrea+Po}$$

for the deflections of the vertical ε, a density contrast σ_{moho} at the Moho of 0.40 ± 0.02 g/cm^3 was calculated. This value is 0.05 g/cm^3 higher than the one which was obtained by Kissling (1982) from regional Bouguer anomalies. The explanation for this difference will be examined further in this report. It is evident that a better result can be obtained by combining the two data sets of deflections of the vertical and gravity anomalies.
We also attempted to estimate a density contrast at the lithosphere – asthenosphere boundary from astrogeodetic and gravimetric data. The results, however, showed that the density contrasts at the Moho and at the lithosphere-asthenosphere boundary are highly correlated and cannot be estimated by the method described.

In a final step the density contrast at the Moho was calculated together with parameters for the density distribution of the topography using 2416 gravity values (mainly from Klingelé & Olivier 1980) over the entire area of Switzerland. These were also reduced by the influences of topography, of the Moho and the Ivrea body. The observation equations for gravity anomalies Δg_{meas}, used in the least squares adjustment system, are:

$$\Delta g_{meas} + v = \frac{g^0_{moho}}{0.43} \cdot \sigma_{moho} + \frac{g^0_{topo}}{2.65} \cdot \sum_{n=0}^{N} \sum_{i+j=n} c_{ij} x^i y^j + g_{Ivrea+Po}$$

The following parameters were introduced: Density contrast σ_{moho} at the Moho, and parameters for the density distribution of the topography (coefficients of a polynomial of degree 0 to 7).
Independent of the other parameters, a value of 0.34 g/cm^3 was obtained for the density contrast at the Moho in each calculation. This is 0.06 g/cm^3 lower than determined from the deflections of the vertical alone but it is in better agreement with the values Holliger & Kissling (1992) have inferred from their most recent gravity modeling.
In a next step a model for the Molasse basin (assuming an initial density contrast of -0.2 g/cm^3) was introduced. It was provided for us by the Institute of Geophysics at the ETHZ. The calculation combining gravity anomalies and reduced deflections of the vertical yielded a density contrast of 0.370 g/cm^3 at the Moho. Using the gravity values alone we calculateded 0.368 g/cm^3 and from the deflections we obtained 0.371 g/cm^3. Apparently the introduction of the Molasse model completely eliminated the differences between the two data sets. The statistical formal error for the estimated parameters resulted in very accurate values which may be too optimistic because the data in the adjustment system is considered to be uncorrelated.
An attempt was made to estimate a lateral density variation by means of a polynomial (see formula above) which also included the Molasse density contrast as an additional parameter. In our models the topography corresponds to masses between the Earth's surface and sea level. The results for the density distribution of the topography are shown in Figure 19-9 (Geiger, 1990). The negative density contrasts in northern Switzerland are clearly seen. This is an indication that most parts of the gravity anomalies in the region of the Molasse Basin are absorbed by density variations in the uppermost layers. The lower part of the Molasse Basin has much smaller effects. This result supports the assumption of increasing compaction of the Molasse near the Alpine front and with increasing depth. The other regions with negative density contrasts are located in the eastern parts of the Grisons and in the southwestern parts of the Valais. They cannot be explained by Molasse effects. These anomalies are not dealt with within NRP 20 but should be investigated in further projects. As a further result we note that the region of Switzerland is rather small for the calculation of a reliable density contrast at

the Moho. Because of the high correlation between the densities of deeper structures (lithosphere-asthenosphere boundary) estimates of these density contrasts failed in our calculations.

In a final calculation all the gravity stations, all deflections of the vertical and in addition 'observed' geoid undulations were used in the adjustment. Besides offset and trend parameters we introduced density values for the topography, the density contrast at the Moho and the density contrast of the Molasse as unknowns. The results obtained for the density of the topography (2.69 g/cm^3) and the density contrast at the Moho (0.37 g/cm^3) were in the expected range. The density contrast for the Molasse Basin, however, was smaller compared to the a priori assumption of –0.2 g/m^3. A value of –0.02 g/m^3 was obtained. Even if the Bouguer anomalies were reduced by a regional linear trend, anomalies in the order of 30 mgal are not identified as would be expected had they been caused by the Molasse Basin with a density anomaly of –0.2 g/m^3. Obviously it is difficult to interpret this effect solely from gravity anomalies and deflections of the vertical. The density contrast of –0.2 g/m^3 might only be valid at the surface and progressively diminishes with increasing depth. This conclusion is partly proven by well loggings in several regions of the Molasse Basin (pers. communication C. Schindler, ETH Zürich).

19.6 Summary

In NRP 20 it was demonstrated that geodetic measuring techniques are well suited for investigations to detect recent crustal movements. Leveling, triangulation and especially GPS are most useful tools and form the basis for interpretation and modeling work for geologists and geophysicists. Two leveling lines in the Cantons of Ticino and Valais were re-measured with high precision leveling instruments and annual calculated uplift rates reach values up to 1.5 mm/year with respect to a reference station near Aarburg in northern Switzerland. The second GPS campaign was performed along the leveling line from Visp to Zermatt, where geoidal undulations were calculated with an accuracy of better than two cm by combining GPS data, leveling data, astrogeodetic observations and gravity anomalies.
In the field of density determination we recognized that besides gravity measurements, deflections of the vertical and the combination of GPS measurements and leveling data are also suitable and can be used in constructing models for the density distribution of the Earth's crust.
A density contrast of 0.34 gcm^{-3} was determined at the Moho by means of least squares adjustments. A density model for the topography and Molasse Basin was generated using the same method. It was concluded that only the uppermost part of the Molasse shows a significant density anomaly of up to –0.3 gcm^{-3} with respect to the basement. The deeper layers of the Molasse Basin have a much smaller density contrast, most likely due to increasing compaction with greater depth.

Acknowledgement

We would like to thank all the numerous participating operators in the field and offices. In particular we thank the following institutes which supported us with their instruments: Alfred Wegener Institut, Bremerhaven (AWI), Geodätisches Institut, Hannover (GIH), Hochschule der Bundeswehr, Neubiberg (HSBW); Institut für Erdmessung, Hannover (IEMH), Observatorium Lustbüel, Graz (OLU), Technische Universität München (TUM), Leica AG Heerbrugg, Leica AG, Glattbrugg. Special thanks go to Dr. P. Heitzmann for the geological evaluation of the leveling benchmarks and to Prof. Dr. Steck for providing geological sections.

20 Alpine cooling and uplift

J.-C. Hunziker, A.J. Hurford & L. Calmbach

Contents

20.1 Introduction

One of the main goals of the NRP 20, was to study the deep structure and genesis of the Alpine edifice by means of seismic discontinuities, in order to establish mechanisms and models for the Alpine orogenesis. For this purpose a compilation of the available geochronological information should contribute the time axis. With the geochronological study today's measured uplift rates should be linked to paleo-uplift rates, established by cooling ages of different geochronometers, thus yielding a time integrated dynamic picture.
By means of Rb-Sr, K-Ar, as well as fission track zircon and apatite ages, time-temperature points are obtained, allowing the construction of time integrated cooling curves over the range of 500°C to ambient temperatures.
The establishment of critical blocking temperatures of radiogenic isotopes has always been a matter of debate. Nevertheless all determinations of temperature in geology have their uncertainties and problems in common, be it stable isotope thermometry, thermometry based on the distribution of elements between coexisting phases, or laboratory synthesis with a critical mineral paragenesis. Exceptions are common to all methods as is the extrapolation of results from experiments of short duration to geological times. A strong point in favour of the cooling and blocking temperature concept in geochronology is the relatively homogeneous distribution of the age data in the Alps grouped in age fields hundreds of square kilometers wide, and the commonly observed succession of mineral cooling ages. These facts make it possible to compare different rocks of a region, to establish cooling curves for this region and to compare these curves with those of other regions, by agreeing on certain temperature points, even if the absolute temperature scale remains open to discussion.
The preferred blocking temperature values are given in Hunziker et al., 1992 as well as a discussion of their relevance. The figure given there is reproduced in the present paper (Figure 20-1).
Over 350 new radiometric ages were measured in this project, thus enlarging the available database of the Central Alps to over 1000 age determinations. The analytical data were published separately: Cosca 1991, Cosca et al. 1991, 1992, Hunziker 1988, Hunziker et al., 1986, 1987, 1992, Huon et al., 1989, Hurford 1986, 1990, 1991, Hurford et al. 1989, 1991, Hurford & Hunziker, 1989, Michalsky & Soom 1990, Soom 1990, Zingg & Hunziker 1990. All ages are calculated using the IUGS recommended constants.

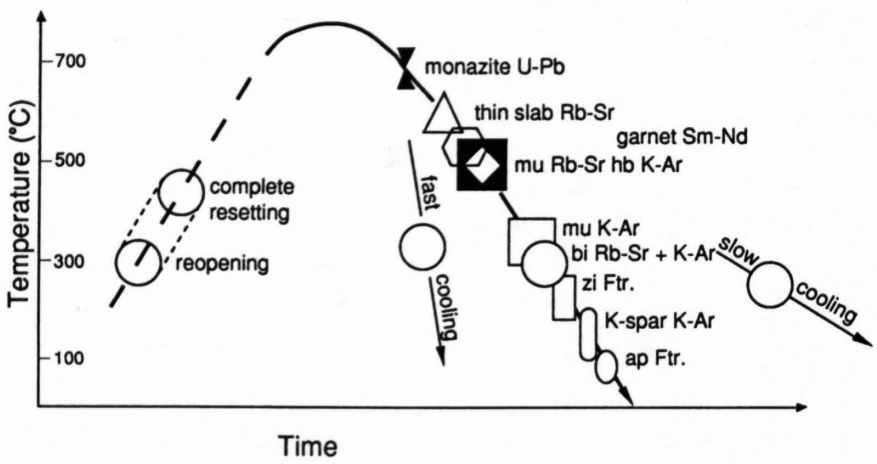

Figure 20-1
"Best estimates" of closure temperatures from regions cooling at a speed of around 30°C/Ma, for different systems as used in this paper in degrees centrigrade.

All the available Rb-Sr, K-Ar, and fission track age data on minerals of the Central Alps were compiled on 4 maps at a scale of 1:635 000 (maps IV,V,VI, and VII from Hunziker et al 1992).
The symbols on the map represent a mineral and the colour of the symbol stands for an age range (see legends on the maps). The radiometric ages were classified in age groups.
First the pre-Alpine ages were subdivided into Variscan = 380–280 Ma, and late Variscan = 280–240 Ma. No mica ages older than Variscan were measured in the Central Alps. After the Variscan orogeny, precursory Alpine events have been put into a single age group from 240–140 Ma. These Triassic-Jurassic periods are currently regarded as times of high heat flow and hydrothermal activity related to early rifting, as well as subduction and magmatic phases. Some, but only few, of these Triassic-Jurassic ages, however, may also be simply interpreted as mixed ages between pre-Alpine and Alpine.
We have chosen to subdivide the Alpine orogenies into Eoalpine = 140–60 Ma, Mesoalpine = 45–30 Ma, and Neoalpine = 30–0 Ma as discussed by Hunziker et al. 1989.
The Eoalpine orogeny has been subdivided into an early, eclogitic phase between 140 and 85 Ma, and a late, blueshist phase between 85 and 60 Ma, including cooling ages of the early Eoalpine event. The age group between 60 and 45 Ma characterizes a relatively quiescent period (the restoration phase of Trümpy 1961).
Most ages falling into this interval can be interpreted as mixed pre-Alpine/ Alpine or Eoalpine/Tertiary ages.
Alternative interpretations found in the literature are that the Eoalpine phase lasted longer in certain places, or that high P and T conditions of metamorphism do not show any pronounced break between the Eoalpine and the Mesoalpine; or else to a cooling of the eclogitic slab by underthrusting of a cool oceanic lithosphere suppressing the real recovery during uplift.
The ± 30 Ma calc-alkaline and alkaline magmatism represents a marked break in orogenic conditions, allowing for the ascent of partly mantle derived magmas, and subdivides the Cenozoic era into Meso-Alpine (45–30 Ma) and Neoalpine (30–0 Ma). A 15 Ma boundary between an early and late Neoalpine period has been chosen because of the relative quiescence around 15 Ma appearing in the data set.
Although the original title of the project was: Neogene to recent uplift and cooling history of the rocks along the geotraverses of NRP 20, it soon became evident, that the Neogene history cannot fully be understood without the beginning of Alpine orogeny in the Cretaceous. The heating of a stacked nappe pile, according to England 1978, England et al. 1977, 1984, requires a critical minimum time of 30 Ma. Thus a first stacking of cold Alpine nappes in the

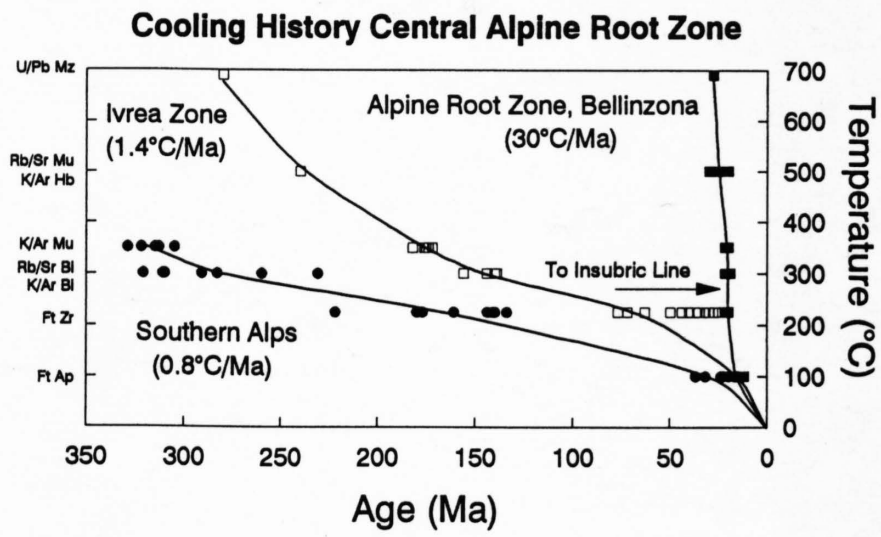

Figure 20-2
Cooling history of the Central Alpine root zone. The Alpine block underwent a rapid cooling, starting at the Meso-Neoalpine boundary, whereas slower cooling occurred in the southern block, already starting in Variscan times. In the Ivrea Zone, the closer we approach the Insubric line from the south, the more zircon fission tracks converge to values recorded north of the line in the Alpine metamorphic block. This observation can be interpreted as a consequence of the northern block, uplifting rather fast during Neoalpine time, and reheating the already cooled southern block.

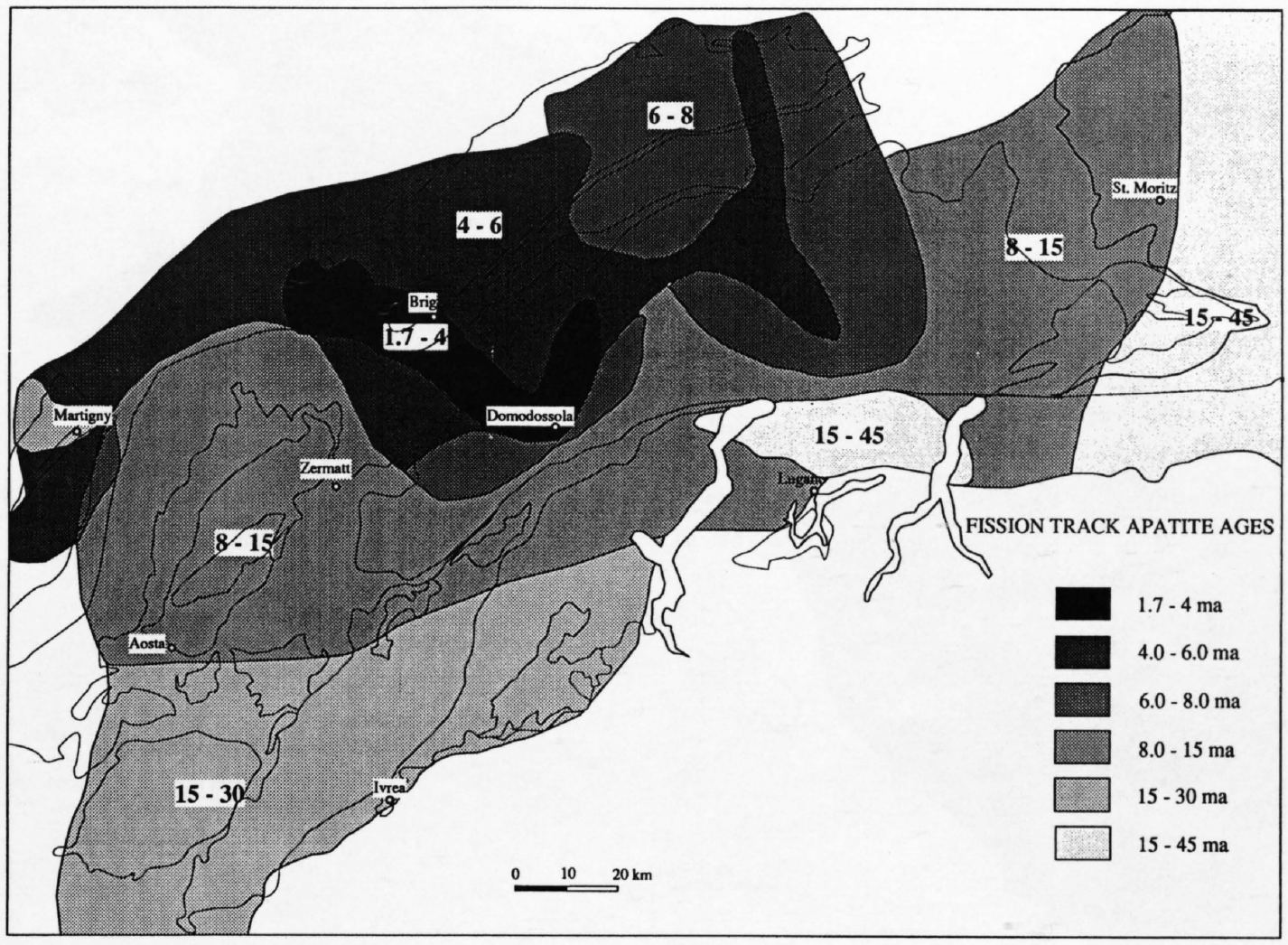

Figure 20-3
Fission track Apatite age distribution in the Central Alps based on map IV. For explanation see text

20.2 Discussion of the age data

20.2.1 Map IV Fission track apatite ages

Besides the new data measured in this project, map IV contains the compiled fission track apatite data from the literature (Wagner et al.1977 and Schaer et al.1975). The measured ages range between 42 and 1.7 Ma. The age data have been subdivided into Mesoalpine ages 45–30 Ma and Neoalpine ages 30–0 Ma. The latter have been further subdivided into groups 30–15, 15–8, and 8–0 Ma.

The most striking fact is, that the Insubric line does not show clearly on the fission track apatite map, in other words, that this main Alpine tectonic feature seems to be inactive for at least the time span since the cooling below 100°C, or expressed differently, that both northern and southern block form one block since their cooling below fission track apatite annealing.

The Austroalpine as well as the Southalpine domain cooled down below around 100°C already in the late Eocene – early Oligocene, while the Sesia-Zone and the Gran Paradiso area passed the 100°C isograd at the Oligocene/Miocene boundary and the Central Alps did not cool below this temperature before 15 Ma, certain regions of the Valais and Ticino not before 8 Ma bp. This zone of fission track apatite ages below 8 Ma coincides with a zone of present day hydrothermal activity as expressed by widespread thermal springs, a region running from the Mont-Blanc massif in the southwest along the Rhone valley over the Simplon, up the Toce and southeastwards down the Leventina to Biasca. The coincidence of young fission track apatite ages (i. e. of rocks cooled down below around 100°C only recently), with geothermal sources can be explained by rocks uplifted faster than their thermal relaxation speed of 0.5 mm/a (and therefore being still hot) thus heating up the percolating waters. In an attempt to delimit further hydrothermally active zones on Figure 20-3. fields of apatite fission track ages of 6-4 and 4-1.7 Ma are drawn, showing hot spots in the external massifs Aiguilles Rouges, Arpilles and SW end of the Aar massif, as well as the basal zone of the Simplon line, following the Antigorio valley. As already pointed out by Pfeifer et al., 1992, the Grimsel region with fission track apatite ages between 4 and 5 Ma shows a hydrothermal potential. Furthermore Figure 20-3 shows that along a narrow band from the Northern Aar massif down to Biasca a similarly warm zone is to be expected. Based also on these predictions our Italian colleague G. Martinotti drilled a 200 m well in the Verampio window actually producing 43°C water; further exploration wells South of the Simplon are under consideration.

20.2.2 Map V Fission track zircon ages

Zircon fission track ages range between 240 and 8 Ma, (see map V and Figure 20-4) the pre-Alpine ages being restricted to the Austroalpine/South-Alpine domain.

In the Central Alps a Mesoalpine zone of ages between 40 and 30 Ma can be seen, ranging from the central Sesia-Lanzo zone and the Gran Paradiso to the North as far as the region of Zermatt. Most of the remaining area of the Central Alps is characterized by 30–15 Ma Neoalpine ages with the exception of the analogous zone, already seen on the apatite map, ranging from the Mont-Blanc in the S–W, along the Rhone valley and over the Simplon, into the Ticino, with ages younger than 15 Ma. Here the western Aar massif, the Simplon and Ticino region again form an area of youngest zircon fission track ages of 12–8 Ma. Along the northern border of the Aar massif a field of Eoalpine zircon fission track ages was first interpreted as mixed ages, geologically meaningless (Soom 1990). In view of the zircon fission track annealing temperature of 225 ± 25°C and the kaolinite + quartz = pyrophyllite + H2O "isograd" (Frey, 1987) passing several kilometers north of the age points (i. e. at lower temperatures), these ages must be considered as geologically meaningful. Similarly south of the Insubric line an age field of Meso- and Eoalpine fission track zircons was tentatively drawn, showing that during the Alpine uplift the hot northern block reheated the already cooled southern block over a considerable distance (see Figure 20-2), thus resetting the fission track zircon ages of the southern block.

20.2.3 Map VI K-Ar and Ar-Ar mica ages

K-Ar and Ar-Ar mica ages are shown on map VI and Figure 20-5. Originally, in pre-Alpine times, all the pre-Alpine basement contained Variscan micas. Locally in the Penninic basement this can still be recognized by means of relict Variscan micas surviving Alpine deformation and metamorphism. In the Central Penninic, within the staurolite isograd, no such pre-Alpine micas are found.

The South-Alpine (+ Ivrea) /Austroalpine structural domain is characterized by widespread Variscan mica ages, ranging from Variscan to late Variscan ages in the Austroalpine nappes of the Western Alps and the South-Alpine domain, and Mesozoic ages in the Ivrea-zone and the Valpelline nappe of the

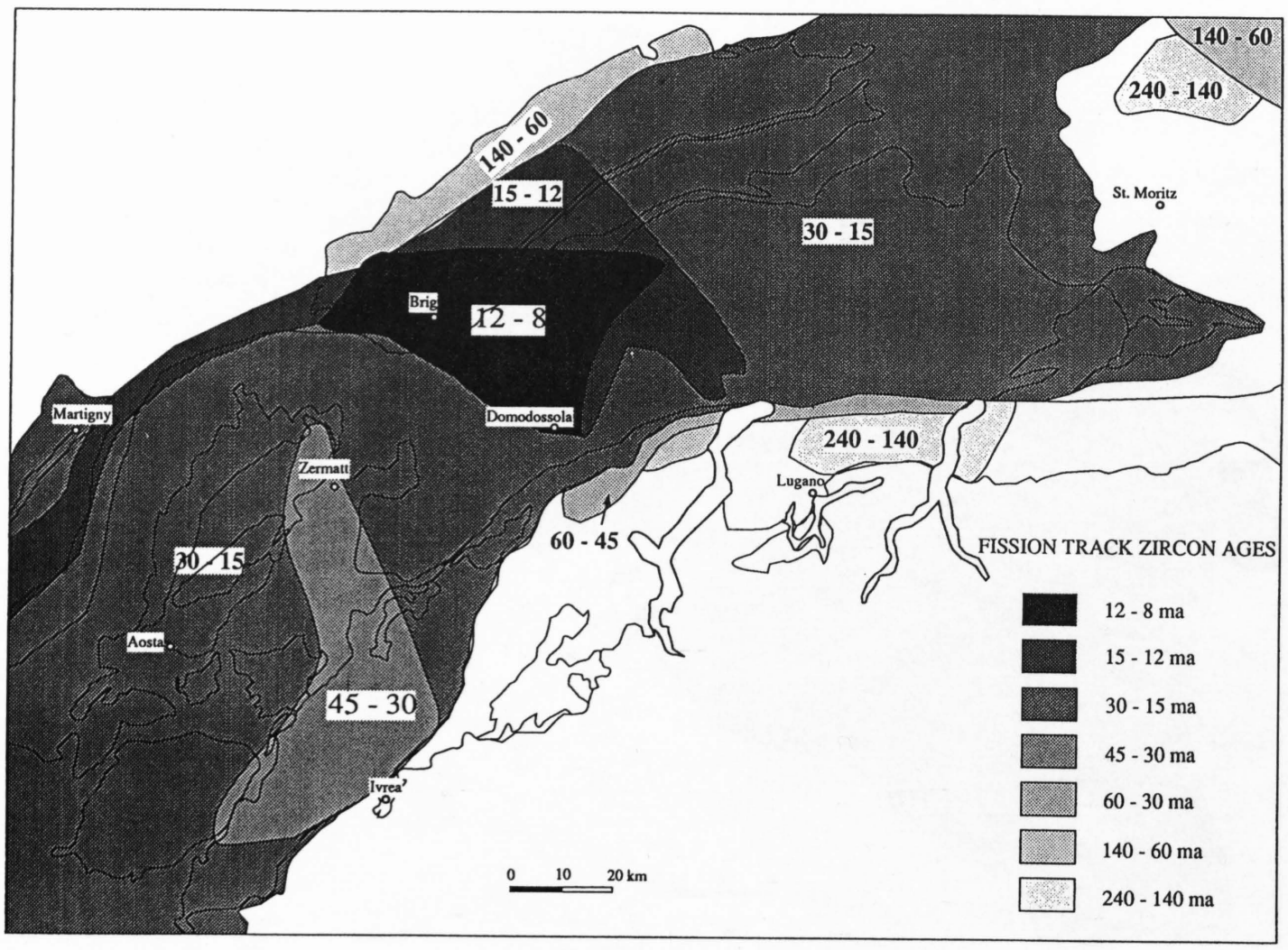

Figure 20-4
Fission track Zircon age distribution in the Central Alps based on map V. For explanation see text.

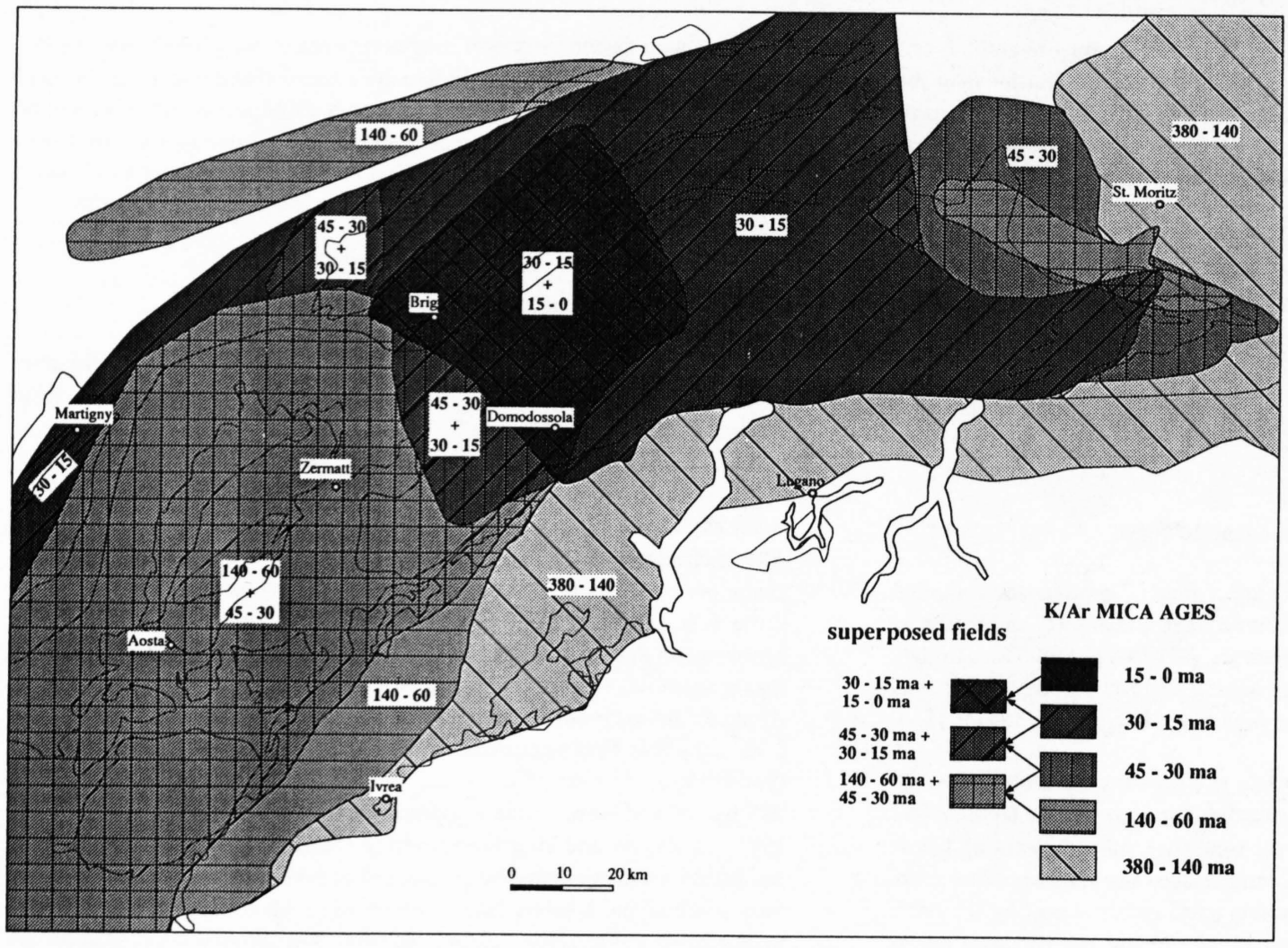

Figure 20-5
K-Ar age distribution in the Central Alps based on map VI. For explanation see text.

Western Alps. In these regions the Alpine overprint was of too low temperature to affect the old mica ages with the exception of local phenomena along Alpine thrust planes.

The Insubric line (see map VI and Figure 20-2) marks a pronounced boundary between pre-Alpine and Alpine mica ages, in that pre-Alpine ages can be found in low grade overprinted Alpine rocks north of the line, but that Alpine ages are extremely rare south of the Insubric lineament.

North of the Insubric line, the central Penninic nappes show a large field of Neoalpine ages between the Suretta nappe in the east and the Monte Rosa in the west, with a late Neoalpine overprint east of the Simplon line. This late Neoalpine field extends from the Simplon line to the Maggia valley and reaches north up to the central Aar massif.

East and West of this Neoalpine field of mica ages, Mesoalpine micas are found, partially overprinting a former blueschist to eclogite facies paragenesis of Eoalpine age.

Finally, in the internal Sesia zone a field of fresh, Eoalpine high-pressure paragenesis rocks are found, which later were only overprinted under brittle conditions, and locally more along also ductily deformed thrust planes.

As already discussed, the northern part of the Aar massif as well as the Prealps show locally a further low grade Eoalpine overprint.

20.2.4 Map VII Rb-Sr mica ages

On map VII the Rb-Sr mica ages of the Central Alps are compiled. As the distribution pattern of K-Ar and Rb-Sr mica ages is very similar, no additional figure for the Rb-Sr ages has been drawn. What has been said already for the K-Ar age also holds for Rb-Sr ages, and specific problems will be discussed in sections 20.3 and 20.4.

20.3 Dating movements

Due to the relatively low blocking temperature of the geochronometers used in the present paper, these systems are ideal for dating movements, both under ductile as well as brittle conditions. The combined fission track and mica dating approach evidenced multiphase deformation along the Insubric line. Zingg & Hunziker 1990 showed that in the region of Ivrea a ductile phase of deformation of the Insubric line was already active in Eoalpine times and that in this region the ductile/brittle transition was already crossed before Mesoalpine times. Conversely in the region of Locarno the ductile deformation outlasted the early Neoalpine with vertical uplift displacements of at least 10 km (see Figure 20-2).

In a similar study using geochronological data, Soom 1990, Hunziker et al., 1992 and Steck & Hunziker 1993 have shown a polyphase Neoalpine deformation along the Simplon line. On map IV and Figure 20-3 a further example of brittle vertical movements or at least vertical movement components can be seen along the Aosta-Ranzola fault, where fission track apatite ages change from over 20 Ma in the south to ages below 15 Ma in the northern block (Hunziker et al. 1992). Recent movements evidenced by horizontal striae on glacial deposits show that the general direction of movement has changed (Carraro et al. 1994).

Another possibility to date tectonic movements along ductile thrust planes by K-Ar and Ar-Ar dating of dynamically recrystallized potassic white micas was used by Hunziker et al., 1986 to date the Neoalpine movements along the Glarus thrust in the Helvetic nappes and by Crespo-Blanc et al., 1995 to date Miocene movements along the basal thrust of the Morcles nappe. A discussion of the uplift and deformation history concerning the external basement massifs (in particular the Aar massif) is given by Pfiffner et al. (Chapter 13.1).

20.4 Problems in dating Alpine metamorphism

The problems of dating high-grade Alpine metamorphic phases are considerable and complex. First of all most geochronometers have blocking temperatures lower than Alpine peak metamorphic temperatures; in addition we have to take into consideration that multiple deformation phases tend to enhance the possibilities of recrystallisation, as well as the access of fluids to the rock, both tending to rejuvenate radiogenic systems.

A good example for this behaviour is shown by the systematics of the U-Pb system of monazites in the Central Lepontine region, where Steck & Hunziker 1994 have shown, that monazite with a normally higher blocking temperature than muscovite Rb-Sr, always show younger U-Pb ages than the Rb-Sr muscovite system. This can be explained easily by pervasive fluid percolation during Neoalpine deformation of these rocks, selectively opening the U-Pb system of monazites.

As a general rule it can be stated that a precise age determination of a metamorphic phase requires a multimethod approach rather than the ultraprecise determination of one mineral with one method. Several geochronological methods applied hand in hand with a sound geological backup, will lead to a trustworthy model. Here still much interdisciplinary work remains to be done.

Nevertheless by means of such multimethod approaches we tentatively start to see in the Central Alps that we have to distinguish an Eoalpine metamorphic phase between 140 and 60 Ma, with first a subduction derived deformation phase, followed by a high to ultrahigh pressure eclogite facies phase, and ended by decompression and cooling, partly under blueshist conditions, starting around 90–80 Ma and ending 60 Ma B. P. The Eoalpine metamorphism goes together with several deformation phases and represents an independent orogeny, at least in the internal parts of the Sesia-Lanzo zone.

This Eoalpine orogeny, or at least parts of it, was presumably active throughout the Central and Western Alps, where it, was later overprinted partly to completely by the Mesoalpine metamorphism, which in turn was for a long time considered as "the Alpine metamorphism and deformation". As already stated in the introduction, due to the low heat conductivity of rocks, a first stacking of the Alpine nappe pile in Eocene times is incompatible with the heating to amphibolite grade as seen in the Central Alps with subsequent cooling in time, already cooling in the lower Oligocene. The nappe stack has to be, at least in part, older to allow for cooling before 30 Ma. In other words parts of the pre-Mesozoic basement of the Central Alps already started in Eocene times at an intermediate crustal depth, at elevated temperatures, possibly acquired during the Eoalpine orogeny. Along predetermined thrustplanes this embryonic nappe pile was further deformed, this time under shallower conditions of a compressional mountain chain in Mesoalpine times. This regime lasted until 30 Ma B.P., when a change of the tectonic factors led to a widespread calcalkaline magmatic activity along the Alpine "root zone", followed by an accentuated Neoalpine folding phase coupled with strong uplift, which continues to the present day (see Kahle et al., Chapter 19).

20.5 Summary

350 new Rb-Sr, K-Ar and fission track analyses performed during this project enlarged the available geochronologic dataset of the Central Alps to over 1000 age determinations. These data are compiled and presented on 4 geological sketch maps of the Central Alps, at a scale of 1:635 000 and allow the construction of time integrated cooling curves for the whole area of the NRP 20. On these maps the symbol form represents the analyzed mineral and a colour code stands for an age range.

On 3 figures, fission track apatite and zircon as well as K-Ar mica ages are summarized and tentatively represented as age fields.

This database leads to the proposal of three main Alpine events: Eoalpine, Mesoalpine and Neoalpine. The high degree of interlinking of these three events is shown, and the fact that presently we are still experiencing the cooling and uplift phase of the Neoalpine event becomes evident. This latter fact opens perspectives for the exploration of geothermal energy but also demands special attention for large scale construction projects.

Plates 20-1 to 20-4

Alpine Cooling and Uplift

J.C. Hunziker, A.J. Hurford and L. Calmbach

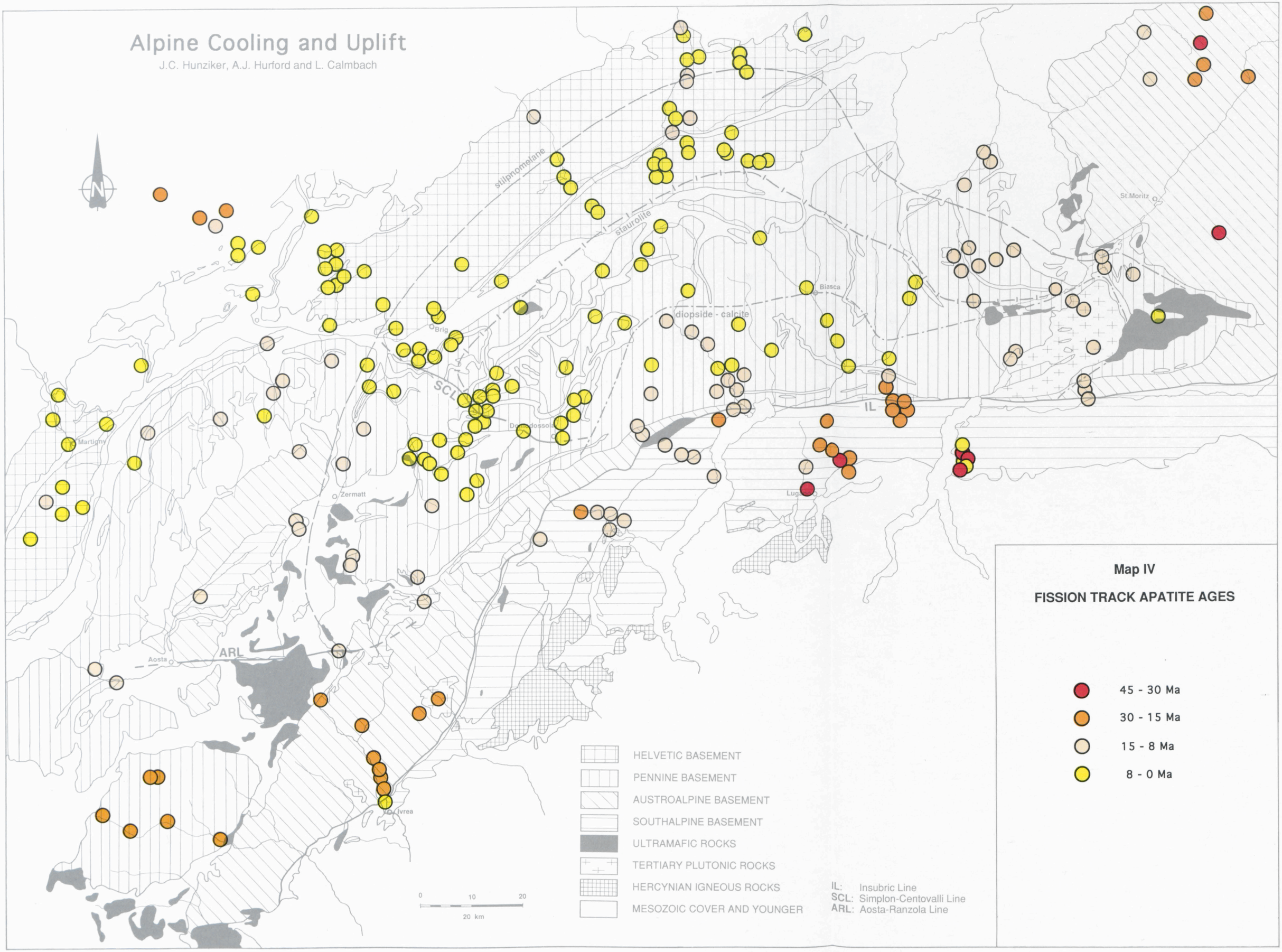

Map IV

FISSION TRACK APATITE AGES

- 45 - 30 Ma
- 30 - 15 Ma
- 15 - 8 Ma
- 8 - 0 Ma

Alpine Cooling and Uplift

J.C. Hunziker, A.J. Hurford and L. Calmbach

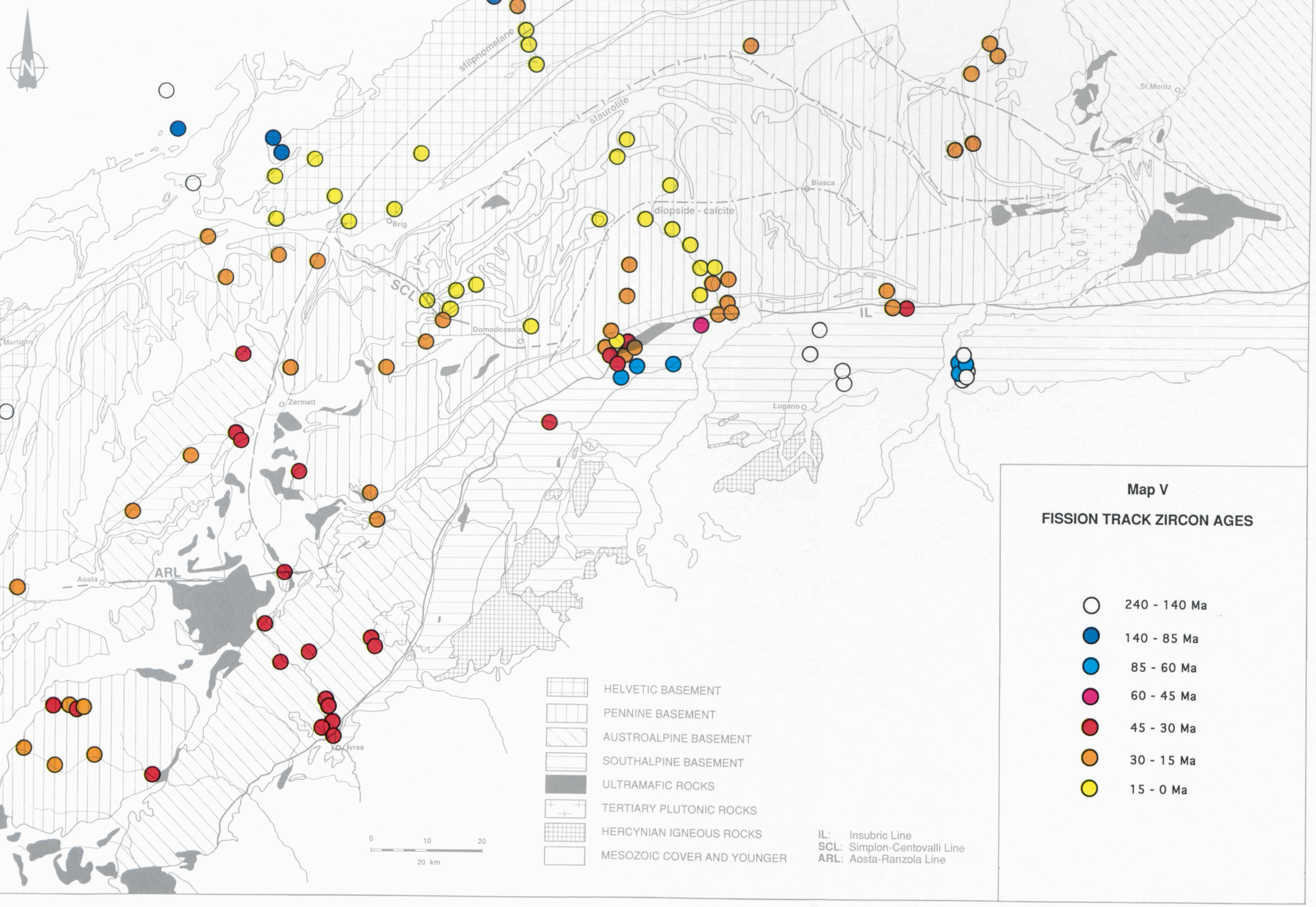

Map V

FISSION TRACK ZIRCON AGES

- 240 - 140 Ma
- 140 - 85 Ma
- 85 - 60 Ma
- 60 - 45 Ma
- 45 - 30 Ma
- 30 - 15 Ma
- 15 - 0 Ma

Alpine Cooling and Uplift

J.C. Hunziker, A.J. Hurford and L. Calmbach

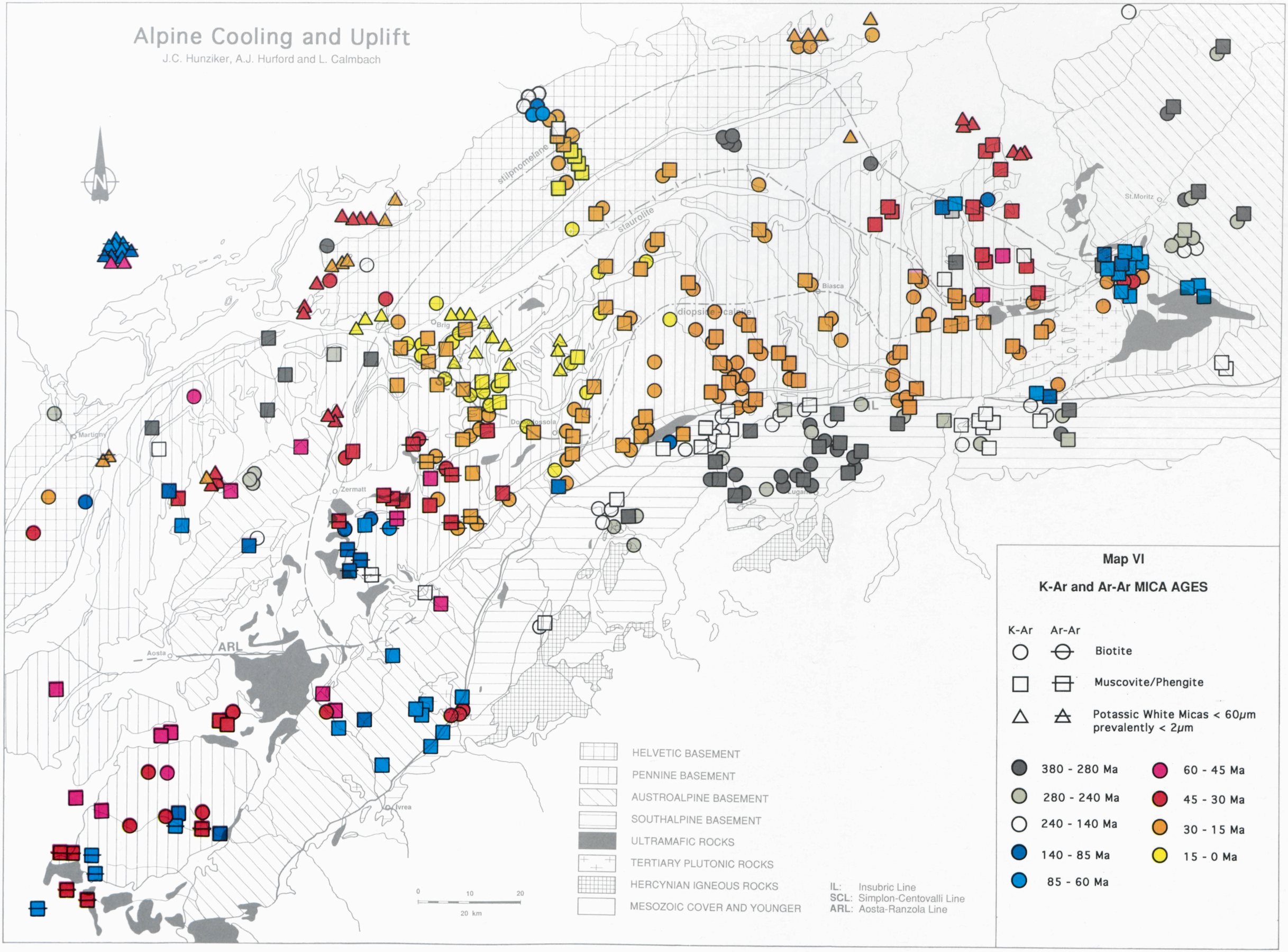

Map VI

K-Ar and Ar-Ar MICA AGES

K-Ar	Ar-Ar	
○	⊖	Biotite
□	⊟	Muscovite/Phengite
△	⧋	Potassic White Micas < 60μm prevalently < 2μm

380 - 280 Ma	60 - 45 Ma
280 - 240 Ma	45 - 30 Ma
240 - 140 Ma	30 - 15 Ma
140 - 85 Ma	15 - 0 Ma
85 - 60 Ma	

Alpine Cooling and Uplift

J.C. Hunziker, A.J. Hurford and L. Calmbach

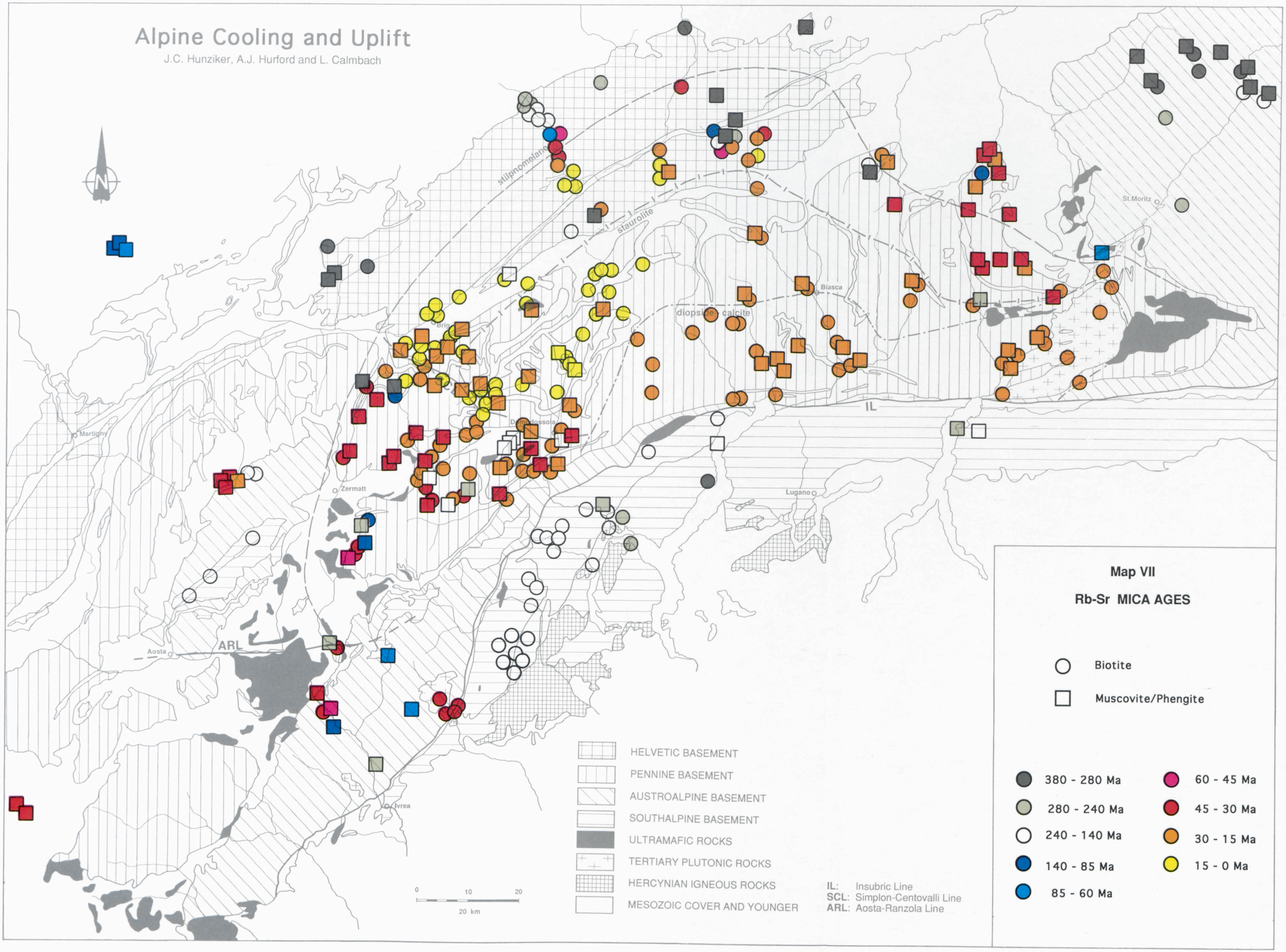

HELVETIC BASEMENT
PENNINE BASEMENT
AUSTROALPINE BASEMENT
SOUTHALPINE BASEMENT
ULTRAMAFIC ROCKS
TERTIARY PLUTONIC ROCKS
HERCYNIAN IGNEOUS ROCKS
MESOZOIC COVER AND YOUNGER

IL: Insubric Line
SCL: Simplon-Centovalli Line
ARL: Aosta-Ranzola Line

Map VII

Rb-Sr MICA AGES

Biotite
Muscovite/Phengite

380 - 280 Ma
280 - 240 Ma
240 - 140 Ma
140 - 85 Ma
85 - 60 Ma
60 - 45 Ma
45 - 30 Ma
30 - 15 Ma
15 - 0 Ma

21 Incision and backfilling of Alpine valleys: Pliocene, Pleistocene and Holocene processes

O.A. Pfiffner, P. Heitzmann, P. Lehner, W. Frei, A. Pugin & M. Felber

Contents

21.1 Introduction

O.A. Pfiffner, P. Lehner & A. Kühni

Valleys are an expression of the morphogenic evolution of the orogen in which they occur. They are the result of erosion due to crustal uplift, which in turn is directly linked to the deep structure of the orogen. Crustal uplift may be provoked by isostatic response to an overthickenned crust, or it may be due to ongoing crustal shortening. Valley incision may on its turn be responsible for additional isostatic uplift.

In the case of the Alps, the shape of the valleys has been deeply influenced by the action of the Quaternary glaciers, which overdeepened most of the valleys originally incised by rivers. Figure 21.1-1, derived from a digital elevation map, shows the present day relief of the Swiss Alps and the extension of the Quaternary glaciers into the northern and southern foreland of the Alps. One recognizes readily the dramatic overprint of the foreland's morphology brought about by the glaciers. Also visible in Figure 21.1-1 are the deeply incised valleys within the Alps. These valleys were incised by the combined action of ice and water flowing at the base of the glaciers and are known to be overdeepend in many places (see Wildi 1984 and Pugin 1988). In the case of

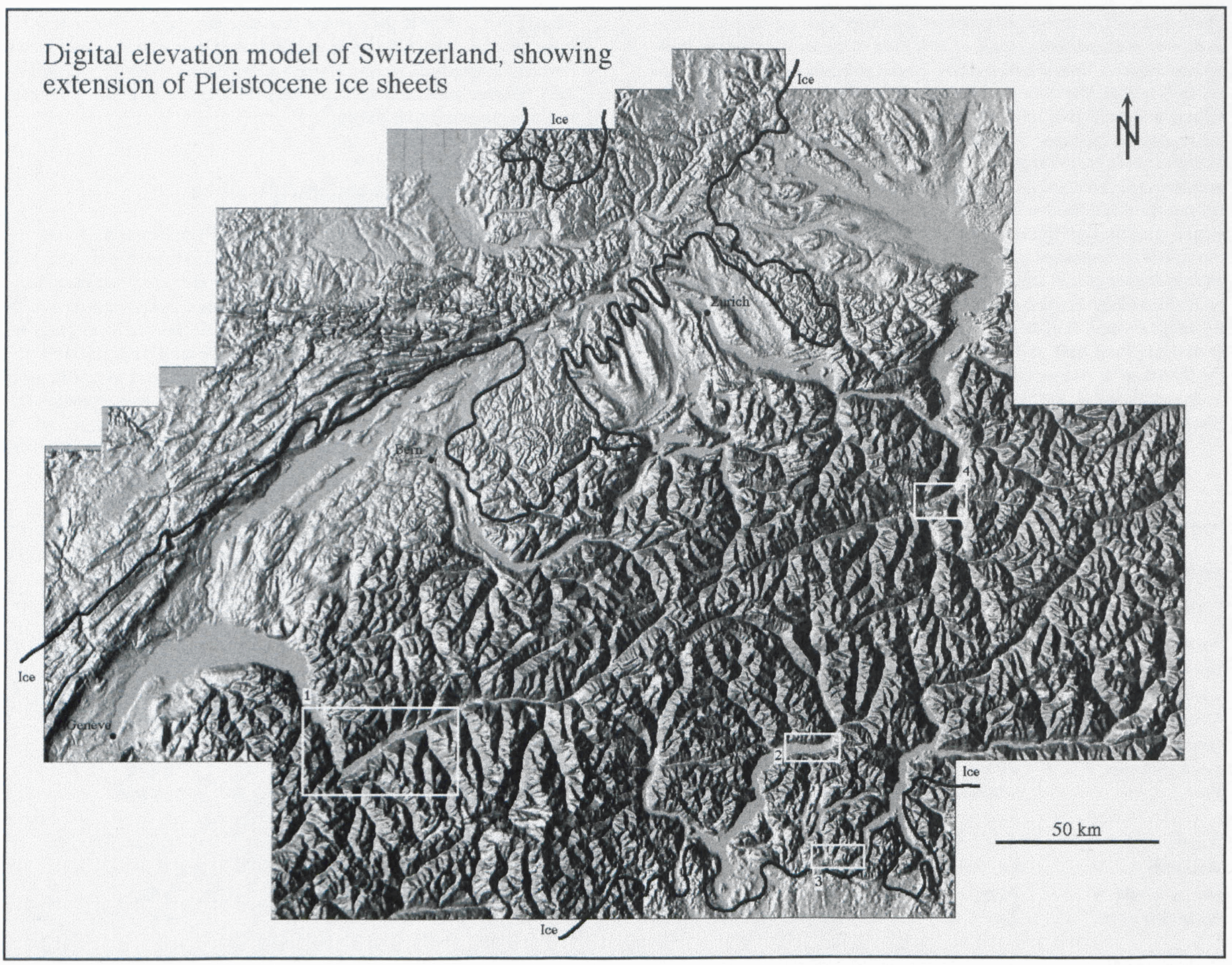

Figure 21.1-1
The Alpine relief imaged by a digital elevation map of Switzerland. The study areas are shown as rectangles: 1 = Rhone Valley, 2 = Piano di Magadino/Ticino, 3 = Sottoceneri, 4 = Rhine Valley. The morphology of the areas in the northern Alpine foreland not covered by the Pleistocene glaciers display a dendritic drainage pattern, which is typically missing in the areas formerly covered by ice.

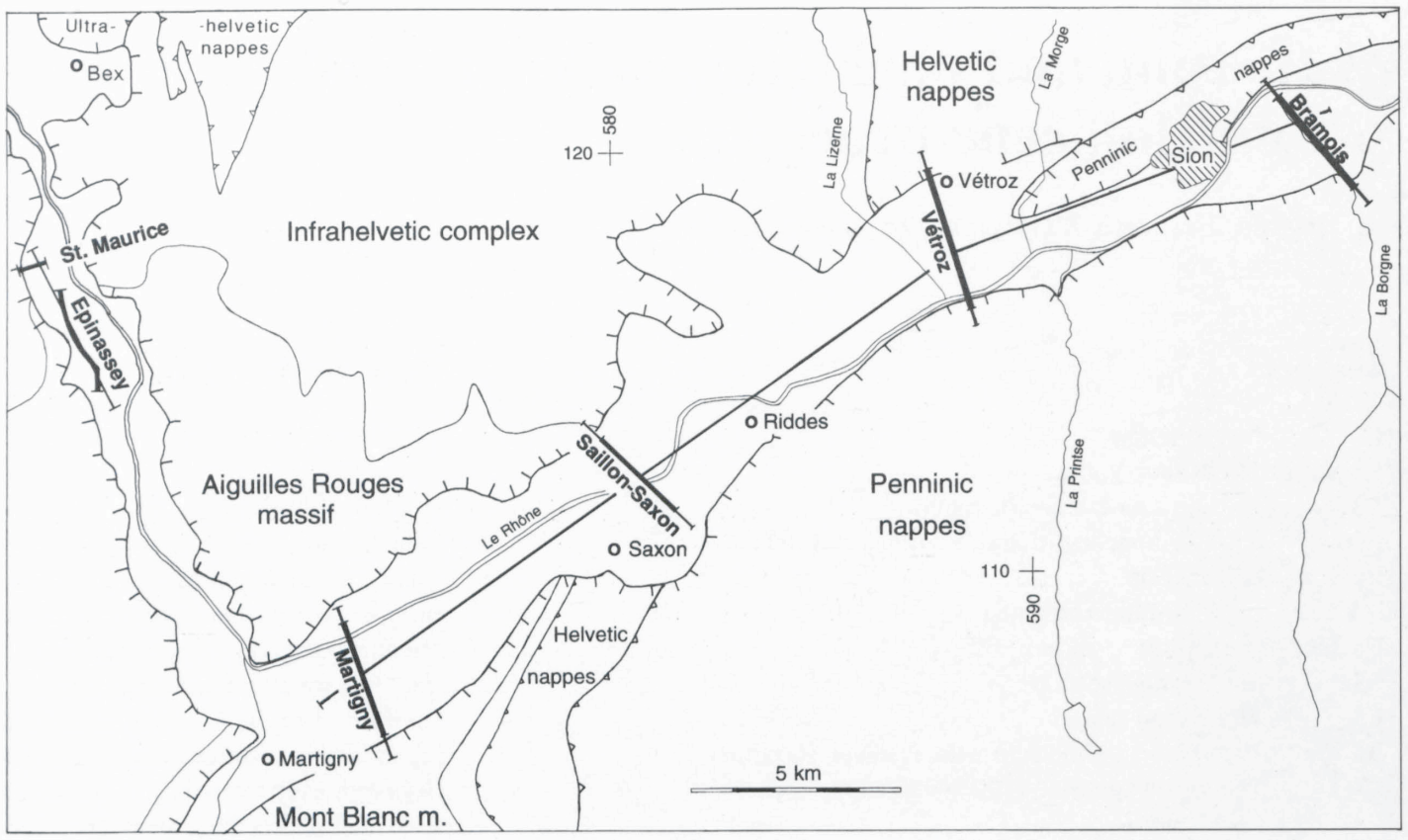

Figure 21.2-1
Map of the Rhone Valley between Martigny and Sion with location of the seismic lines (thick lines) and traces of cross sections (thin lines).

the Southern Alps, incision seems also related to fluviatile erosion during the Messinian, when the Mediterranean dried out at several occasions, thereby lowering the base level of rivers draining southward. All of the overdeepened troughs were subsequently backfilled with glacial and post-glacial sediments.

The concern for environmental problems involving water management is one of the important problems of our society. Most of the used aquifers in Switzerland originate from glacial and post-glacial sediments. One of the available tools to study the architecture of such sedimentary bodies is the seismic reflection method. Since the 70s, high-resolution seismic surveys revealed the structure of lacustrine and glacio-lacustrine sediments. Investigations by Matter et al (1971, 1973) and Finckh et al. (1984) analyzed seismofacies in overdeepened perialpine lakes; velocity calibrations were possible by simultaneous seismic refraction surveys. Sedimentological data became available from a scientific well in Lake Zürich (Hsü & Kelts 1984). Lister (1984) has shown that the sedimentary fill of such overdeepened troughs are in part glacigenic. Similar glacial sequences have also been reported from the Gruyère basin (Pugin1989) or the Canadian Rockies (Eyles et al.1990).

It is in the framework of these considerations that NRP 20 made some efforts at shedding some light on the understanding of the shape and fill, as well as the formation of Alpine valleys. Research was concentrated on two major valleys draining to the northern and northwestern foreland (Rhine and Rhone), and on two valleys draining to the south (Ticino and Mendrisiotto). The locations of these study areas are indicated in Figure 21.1-1.

21.2 The Rhone Valley

O.A. Pfiffner, W. Frei, P. Lehner & A. Pugin

The Rhone river takes its source within the Alps and flows into a deep valley running first parallel to the regional structures but making a 90° turn to become an axial valley before draining into lake Geneva (see Figure 21.2-1). Previous geophysical surveys (Finger & Weidmann 1988, Finckh & Frei 1991, Wagner 1984) document the very thick Quaternary valley fill, estimated in places to reach 900 m.

21.2.1 Seismic data and interpretation

Six high-resolution seismic lines, each about 3 km long and crossing the Rhone valley, were recorded between 1989 and 1991 (see Figure 21.2-1) in cooperation with the "Centre de Recherches Scientifiques Fondamentales et Appliquées de Sion" (CSRFA). The data acquisition and processing was the responsibility of the Institute of Geophysics ETH-Zürich. The spacings between the source and geophone group stations, the most important recording parameters, were set to 10 m. The seismic sources used were weight droppers and explosives with charges of 100–300 g buried in 2 m deep boreholes. Details about the acquisition parameters for the individual lines can be found in Table 21.2-1. Processing of the first acquired seismic lines was carried out by

Line	Bramois	Vétroz	Saillon-Saxon	Martigny	Epinnassey	St.-Maurice
Recording instrument	DFS-V	BISON 9048 & DFS-V	DFS-V	DFS-V	Sercel 368	BISON9024 & DFS-V
Number of channels	48	96	48	48	144	72
Spread details	symmetrical	symmetrical split	symmetrical split	symmetrical split	symmetrical	symmetrical split
Geophone group spacing	10 m	10 m	10 m	10 m	10 m	10 m
Geophones per group	6	6	6	6	12	6
Geophone type	4.5 Hz	20 / 4.5 Hz	4.5 Hz	4.5 Hz	10 Hz	4.5 Hz
Filter	LC 4 Hz/HC 125 Hz	LC 4 Hz / HC 125 Hz	LC 4 Hz / HC 125 Hz	LC 8 Hz	LC 8 Hz	LC 8 Hz
Source type	Dynamite + Thumper	Dynamite	Dynamite	Dynamite	Vibroseis	Dynamite
Coverage	24	48	24	24	72	1
Sampling rate	2 ms	2 ms	2 ms	2 ms	2 ms	2 ms
Recording length	2 s	2 s	2 s	2 s	2 s	1 s
Date recorded	Sept. 1989	Feb. 1991	Sept. 1989	Dec. 1989	Oct. 1990	Dec. 1989

Table 21.2-1
Field parameters of the Rhone Valley seismic lines.

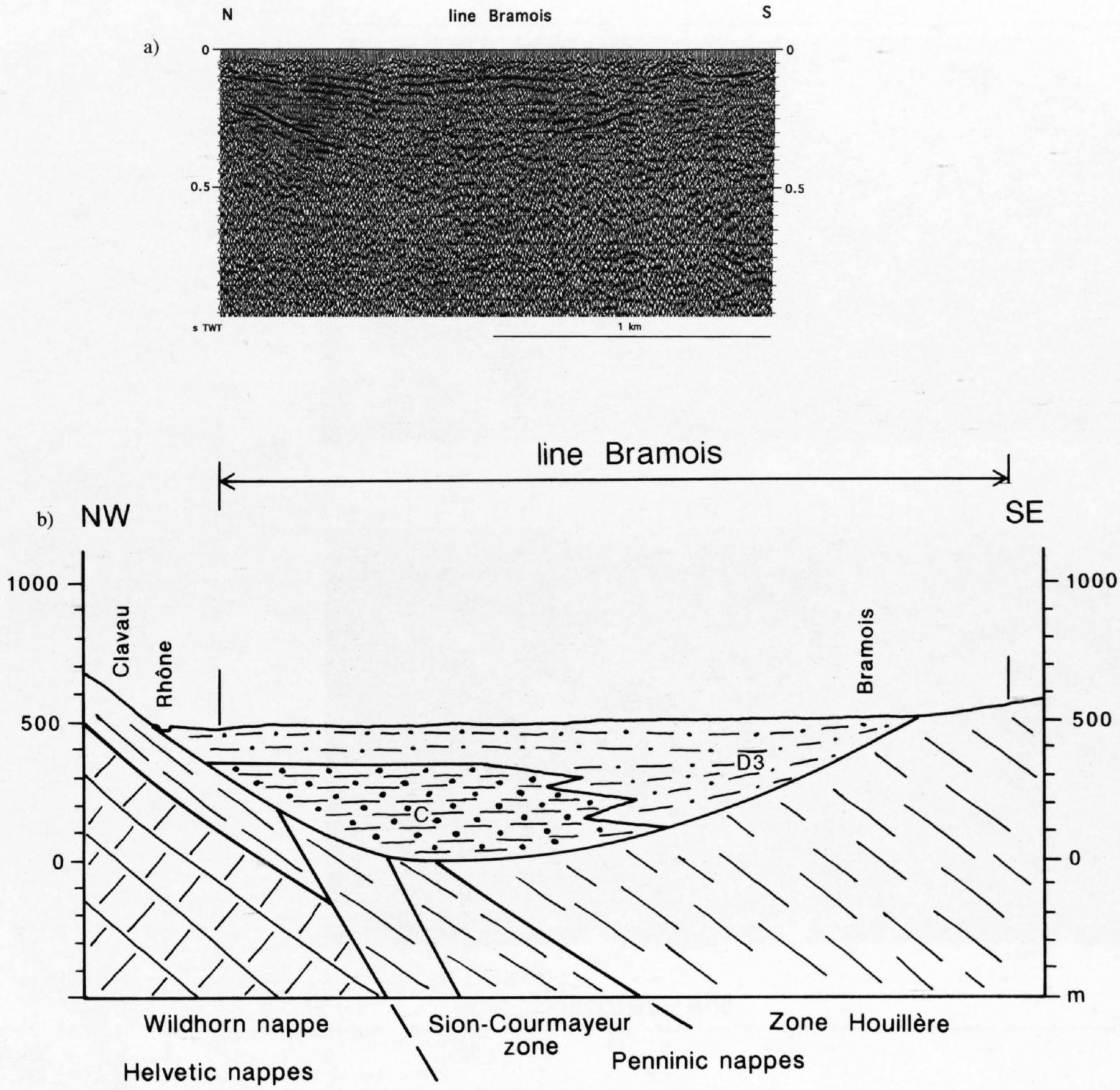

Figure 21.2-2
Line Bramois (northern part).
a: Final stack,
b: geologic interpretation.
C: Glacio-lacustrine deposits,
D2: Deltaic sediments

R. Lehner (1990) and W. Frei. A first geological interpretation of some of the seismic lines has been published by Besson et al. (1991). Two of those profiles (Vétroz and Martigny), which are of particular high quality, were analyzed in more detail by seismic modeling and are discussed in Section 21.2.2. Since there is no deep well control down to the bedrock in all these lines, the seismostratigraphic interpretation of the valley fill remains tentative.

Line Bramois (Sion-East)

This line is located 5 km east of Sion (Figure 21.2-1) and crosses the Rhone Valley on the fan of a tributary (La Borgne). The Rhone river itself is deviated to the NW side of the valley floor by the building of this fan. The seismic data show a moderately SE-dipping band of reflections at the NW end extending form 200 ms TWT down, and a shallow NW-dipping band of reflections in the center at around 300 ms TWT (see Figure 21.2-2a). Some subhorizontal, low-frequency reflections extend across the NW half of the section.

The two dipping reflections can be attributed to the bedrock surface (see also Besson et al.,1991). The top of this bedrock surface in the deepest portion of the trough is at least at 400 ms TWT or roughly at sea level. There is a slight indication of a deeper trough, with somewhat steeper flanks below the axial portion of the vallley down to 550 ms TWT or some 150 to 200 m below sea level. Such steeper, often canyon-like channels in the basal portion of the glacially overdeepened valleys may be attributed to fluvial erosion by sub-glacial rivers. The subhorizontal reflections from the valley fill were interpreted as a package of well bedded glacio-lacustrine sediments (siltstones) by Besson et al. (1991). Similar low-amplitude reflections are observed in the seismic lines in the Rhine Valley (see Section 21.4) where they are calibrated by wells and turn out to stem from fluviatile gravel deposits. Considering the location of line Bramois precisely on the fan of La Borgne, these low-amplitude reflections are also interpreted as stemming from fluviatile gravel fans making up the upper 200 m of the valley fill (see Figure 21.2-2b).

Line Vétroz (Sion-West)

Line Vétroz crosses the Rhone Valley downstream of the confluence of two tributaries (La Printse and La Morge), where the valley suddenly broadens (Figure 21.2-1). The seismic line (Figure 21.2-3a) shows two pronounced bands of reflections, one dipping south, the other dipping north, and curved reflections beneath their intersections. Subhorizontal, high-frequency reflections occupy the space above the two dipping reflection bands.

A first interpretation by Besson et al. (1991) is reproduced in Figure 21.2-3b. These authors assigned the two dipping reflection bands on either side of the profile to the bedrock surface. The deepest point of the valley trough must be sought at around 800 ms TWT, i.e. at around 400 m below sea level. Apart from a terrasse on the southern flank the valley is remarkably symmetric and V-shaped. A more detailed interpretation of this line is given in Section 21.2.2.

Line Saillon-Saxon

Line Saillon-Saxon traverses a segment of the Rhone Valley not affected by tributary rivers or glaciers (Figure 21.2-1). The seismic data show symmetrically dipping reflections, defining a conspicuous V-shaped bedrock surface (see Figure 21.2-4a). The symmetrically dipping reflections give way in the NNW to convexely curved reflections at around 200 ms TWT. Very regular, horizontal high-frequency reflections occupy the lower part of the space within the V-shape. These reflections grade into horizontal low-frequency reflections which dominate the uppermost 100 ms TWT.

As pointed out by Besson et al. (1991), the V-shaped bedrock surface is at the deepest point at about 400 m below sea level. The total thickness of the valley fill is thus around 750 m. The plateau in the NNW is a subsurface continuation of the elongate hill "Les Combes" passing to the NW of the village Saillon which consists of Liassic and Triassic sediments. The depression be-

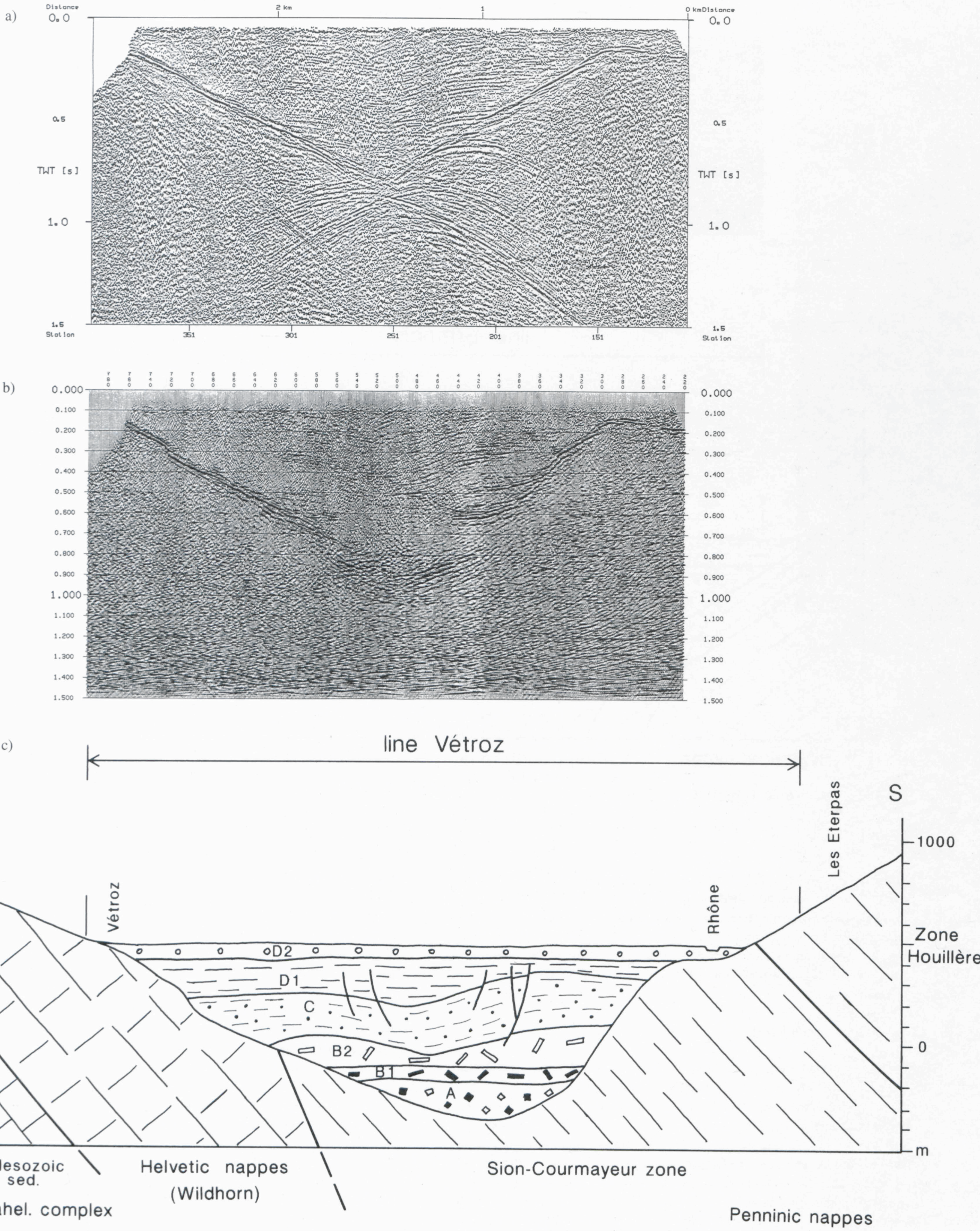

Figure 21.2-3
Line Vétroz (Sion-West). a: Final stack; b: migrated seismic section; c: geologic interpretation.
A: Subglacial deposits, B1: Lodgement till, B2: Meltout and reworked till, C: Glacio-lacustrine deposits, D1: Lacustrine deposits, D2: Fluviatile gravels.

tween this hill and the mountain flank to the NW follows Aalenian shales and can be interpreted as a classic longitudinal valley (or combe). The deepest point of the V-shaped bedrock in the main valley is likely to follow the Chamonix zone, which consists of Mesozoic sediments sandwiched between crystalline basement rocks of the Aiguilles Rouges and Mont Blanc massifs. Downstream to Martigny the Rhone Valley follows geologic contacts marked by easily erodable formations. These units dip to the SSE and if the Rhone Valley's incision was controlled by these units the thalweg – seen in cross section – migrated down and to the SSE in time. It thus may well be that the longitudinal valley of "Les Combes" represents the deepest point of an ancient Rhone Valley. Besson et al. (1991) evoke the possibility that the entire hill "Les Combes" represents a block which slid down the valley flank after melting of the big glaciers of the Last Ice Age; the longitudinal depression would then mark the limit between the stable flank and the moving block.

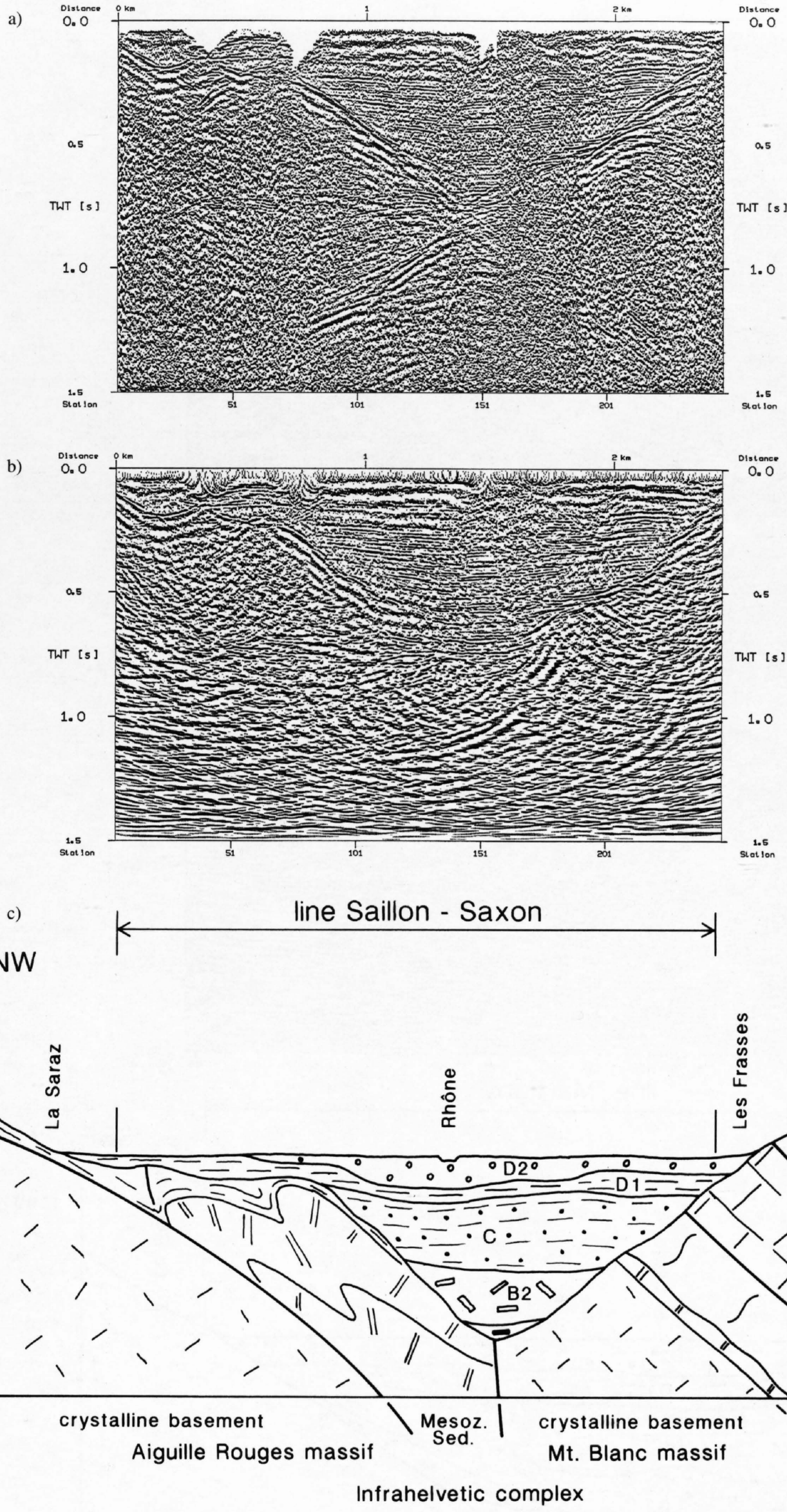

Figure 21.2-4
Line Saillon-Saxon. a: Final stack; b: migrated seismic section; c: geologic interpretation.
B1: Lodgement till, B2: Meltout and reworked till, C: Glacio-lacustrine deposits, D1: Lacustrine deposits, D2: Fluviatile gravels.

By comparison with lines Vétroz and Martigny (as discussed in Section 21.2.2 below), the horizontal reflections just overlying the intersection point of the dipping reflection associated with the bedrock surface, could be correlated to the lodgement tills. The overlying zone of poor reflectivity between 400 and 500 ms TWT resembles the meltout or till (unit B2 in Figure 21.2-4b). The subhorizontal narrowly spaced reflections between 200 and 400 ms TWT of the Valley fill resemble the glacio-lacustrine deposits recognized in lines Vétroz and Martigny (unit C in Figure 21.2-4b). The uppermost, low-frequency reflections, finally, resemble the seismic facies typical for fluviatile gravel deposits as discussed in line Bramois and the seismic lines in the Rhine Valley (Section 21.3).

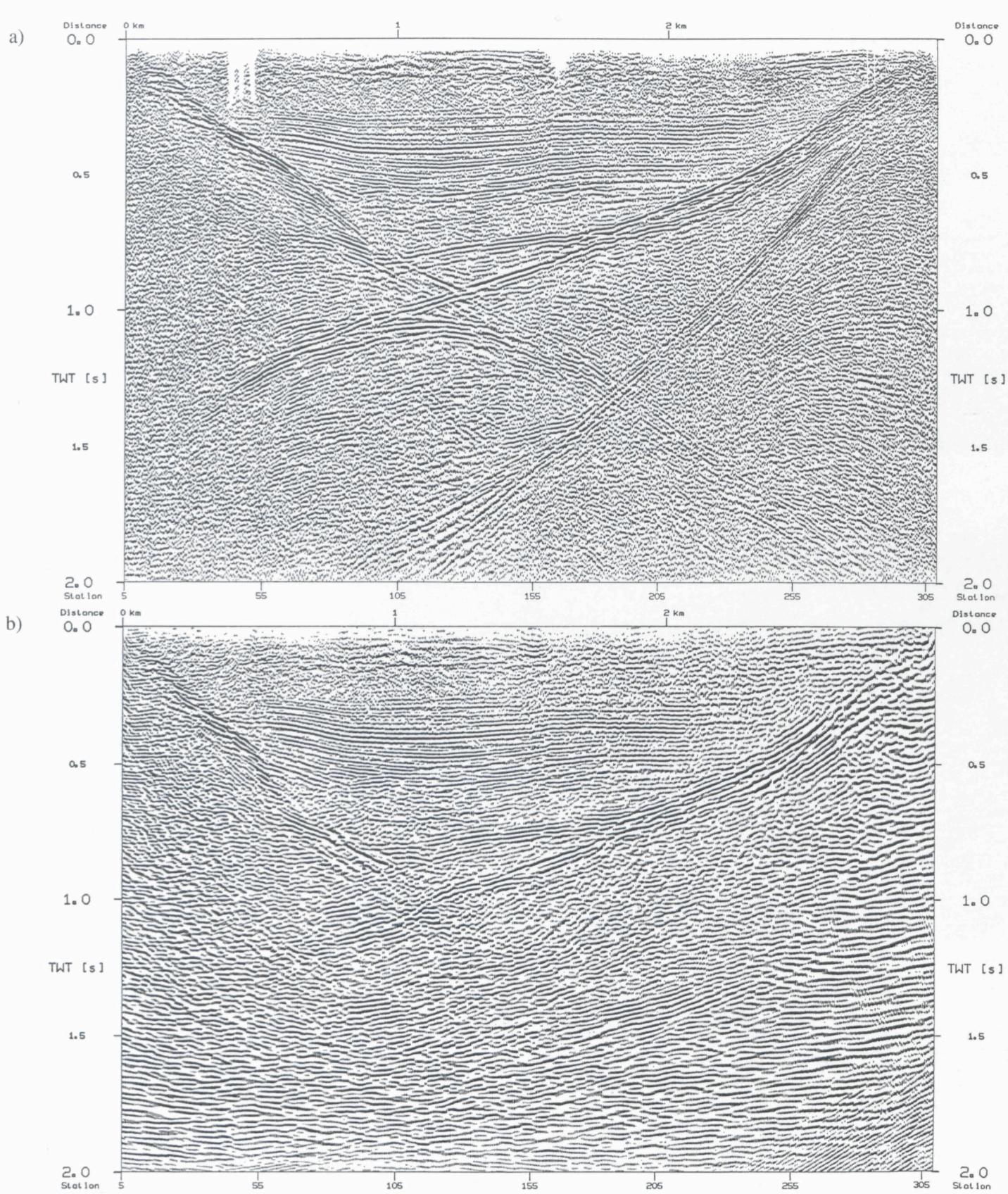

Figure 21.2-5
Line Martigny. a: Final stack; b: migrated seismic section; c: geologic interpretation. A: Subglacial deposits, B1: Lodgement till, B2: Meltout and reworked till, C: Glacio-lacustrine deposits, D1: Lacustrine deposits, D2: Fluviatile gravels, D3: Deltaic sediments.

a)

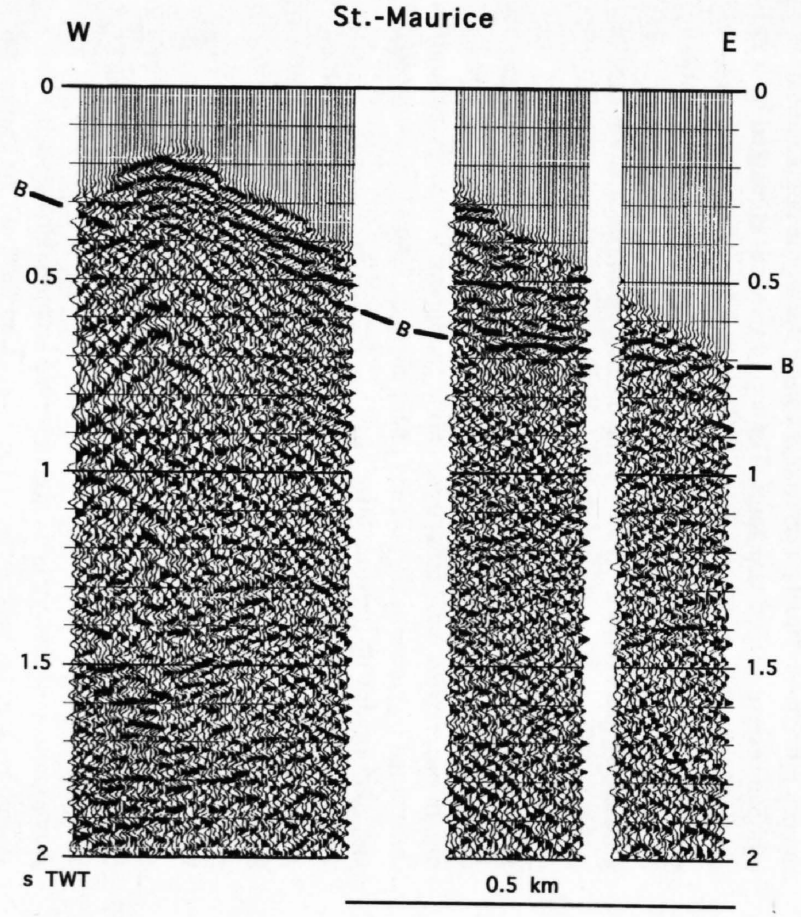

b)

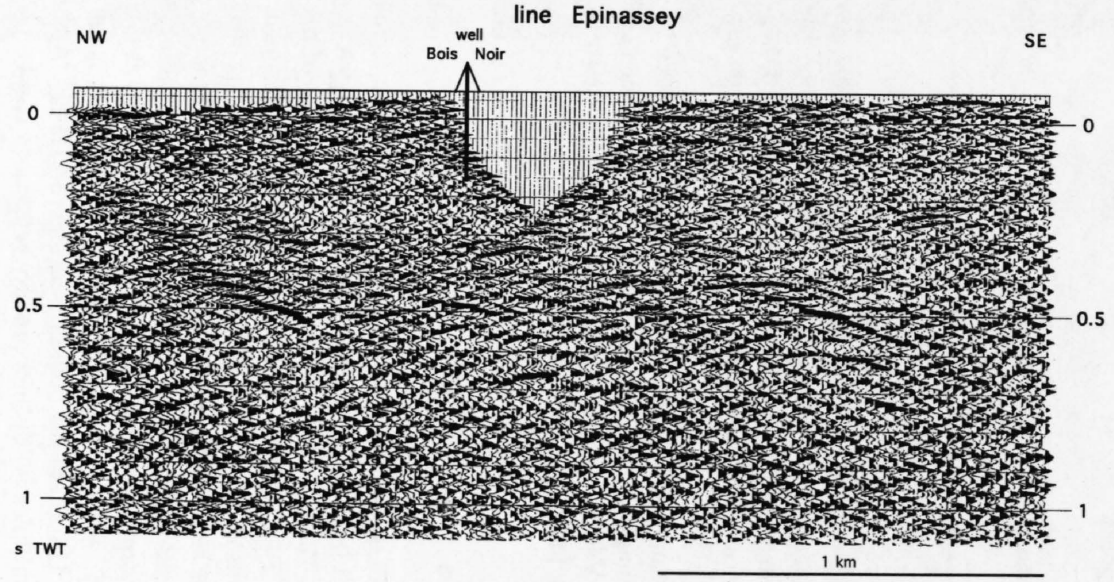

c)

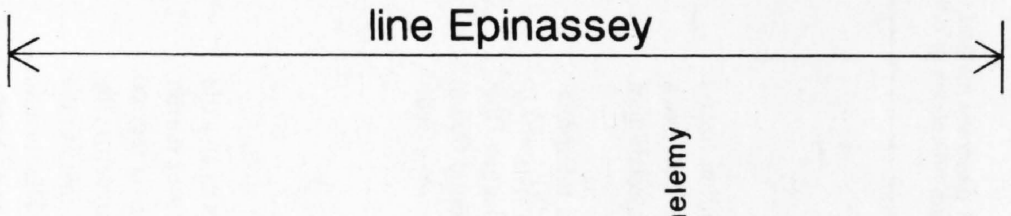

Figure 21.2-6 b

Lines Epinassey and St.-Maurice. Line Epinassey is a longitudinal line following the axes of the Rhone Valley, while line St.-Maurice was laid out across the valley.
a: Final stack of line St.-Maurice, b: Final stack of line Epinassey, c: geologic interpretation of line Epinassey.
B: top bedrock, B2: Meltout and reworked till, C: Glacio-lacustrine deposits, D2: Fluviatile gravels, D3: Deltaic sediments.

Units	Reflection character	Geological interpretation	P-Velocities
D2	discontinuous, undulating reflections	deltaic sediments	1650-1800 m/s
D1	poor reflectivity, some diffractions	lacustrine deposits	1800 m/s
C	strong, coherent, continuous reflections, where disturbed poor reflectivity	glaciolacustrine deposits	1900-2000 m/s
B2	discontinuous, undulating reflections, poor reflectivity	meltout and reworked till	1900-1950 m/s
B1	strong, continuous low-frequency reflections	lodgement till	2300-2400 m/s
A	almost transparent, few low-amplitude reflections	subglacial deposits	2050 m/s
bedrock	top bedrock generally marked by strong discontinuous reflections or diffractions	limestones, sandstones, shales, gneisses	5000 m/s

Table 21.2-2
Comparison between reflection character, geological interpretation and P-wave velocities of the seismostratigraphic units recognized in lines Martigny and Vétroz.

Line Martigny

This line crosses the same segment of the Rhone Valley as line Saillon-Saxon (Figure 21.2-1). The seismic data are shown in Figure 21.2-5a as final stack and in 21.2-5b as migrated stack. A detailed discussion and interpretation of this line is given in Section 21.2.2.
The geologic interpretation given in Figure 21.2-5c relies on the interpretation of the valley fill discussed in Section 21.2.2, but has been extended to include the geologic structure of the bedrock. Besson et al. (1991) argued that the deepest point of the Rhone Valley's bedrock surface is at around 600 m below sea level and that the thalweg possibly follows the Mesozoic sediments of the Chamonix zone.

Lines Epinassey and St.-Maurice

Line Epinassey follows the Rhone Valley where the Rhone flows as an axial river to the NNW, towards Lake Geneva (Figure 21.2-1). A major rock barrier crosses the valley just downstream of line Epinassey. The Rhone river incised a narrow gorge through this barrier. The line Epinassey was set out across the alluvial fan of the Torrent de St. Barthélemy. During growth of this fan the Rhone river was deviated to the eastern flank of the main valley. The seismic data shown in Figure 21.2-6a and b. Four seismostratigraphic units can be recognized. The topmost comprizes horizontal, low-frequency reflections, the middle unit is more or less transparent, a lower unit consists of an irregular bundle of laterally discontinuous reflections and is bound by some high amplitude reflections at its base.
These lowermost reflections are interpreted as the bedrock surface in Figure 21.2-6b, and – by analogy to the other seismic lines further upstream – the overlying discontinuous reflections as meltout or lodgement till. The transparent section are glacio-lacustrine deposits, which were drilled by the well Bois Noir near the center of the seismic line. The uppermost, low-frequency events are attributed to the alluvial fan of the Torrent de St. Barthélemy.
Two dynamite shots were used for line St.-Maurice, a short line across the Rhone Valley. The line is situated at the NW extension of line Epinassey and just upstream of the rock barrier of St.-Maurice (see Figure 21.2-1) and is shown in Figure 21.2-6a. A dipping event, marked B in Figure 21.2-6a, is recognized in the western half of the section and levels off at 0.7 s TWT to the east. This event is interpreted as originating from the bedrock surface which would suggest that the valley bottom is at around 200 m below sea level. By analogy to line Martigny, the high-amplitude horizontal reflections immediately above might be explained as stemming from well compacted lodgement tills and meltout tills.

21.2.2 Seismic modeling of lines Martigny and Vétroz

A. Pugin, R. Marchant, O. Besson & G.Stampfli

In the first stage, the processed, stacked and migrated seismic data were loaded on a CHARISMA (GECO^{TM}) workstation, an interactive seismic interpretation system. The resulting interpretation were then tested with a new modeling system developed by Pugin (in prep.) which simulates shot records of 48 or 96 channels which are reprocessed with a similar sequence used for the field data. Depths and velocities were changed iteratively until a satisfactory match between model and field processed data was obtained. The velocities used for modeling were based on those obtained from processing and velocities observed from previous seismic studies on glacial sediments. The velocities that turned out to fit the data best are listed in Table 21.2-2. Densities, absorption and spherical divergence factors have been admitted proportionally to the velocities.
Two seismic profiles were modeled. The first, line Martigny, was chosen because it shows the most complete seismic stratigraphy of the Pleistocene valley fill. The second, line Vétroz, was chosen because of the collapse structures contained within the Pleistocene valley fill.

21.2.2.1 Seismofacies

To characterize the infill of the glacial basin on the basis of geometry, signal continuity, amplitude and frequency, six main seismofacies have been defined (see Table 21.2.-2). These facies will be discussed on the basis of line Martigny (see Figure 21.2-8), which is the deepest and the most complete profile. The following units are distinguishable:
The **Bedrock-Pleistocene sediment** interface is likely to possess the largest acoustic impedance contrast in these formations, given the high velocities to be expected in the metamorphic bedrock. High-amplitude reflections clearly outline the ancient valley, which generally appears to be V-shaped, sometimes being truncated in U-form at the bottom (see Figure 21.2-8a). Apart from various types of multiples no distinct primary reflections can be observed beneath this reflector.
Unit A is almost transparent with only very few discontinuous and low-amplitude reflections. It is triangular shaped and lies at the bottom of the valley. The top of this unit has a relatively high reflectivity but is rather difficult to follow precisely because of interference with reflections from the valley wall.
Unit B1 is characterized by a series of very strong, continuous low-frequency reflections. Small phase changes along the profile might indicate normal and reverse faulted structures. The top of this unit is marked by a pronounced reflection. In line Martigny (Figure 21.2-8a) this unit is seen to follow the bedrock contact on the southern flank of the valley. The next units up, units C and D, are onlapping over it.
Unit B2 has poor reflectivity with some undulating and discontinuous reflections. As evident from Figure 21.2-8a this facies is onlapping over unit B1 and offlapping under unit C.
Unit C consists of a remarkable succession of coherent and continuous reflections. Some of the basal reflections are oblique with regard to the general dip. In line Vétroz, these reflections define continuous trough-shaped curves interrupted by subvertically aligned phase changes. Unit C passes gradually and conformably up into unit D1.
The seismofacies of **unit D1** is characterized by poor reflectivity. Diffracted arrivals in this part of the section may be generated by some local lateral inhomegeneities within unit D1. This seismofacies can be observed in line Martigny only.
Unit D2 is characterized by undulating and discontinuous reflections with medium-sized amplitude and a high-frequency content. Disconformities due to intraformational thickness changes as well as vertical faults appear to be affecting this uppermost unit.
A comparison of the synthetic and observed seismograms reveals a striking resemblence of the geometries of the bedrock surface and the various interfaces between the different Pleistocene sedimentary units. This gives some confidence in the ultimately chosen velocity functions, layer geometry and, hence, the depth conversion.

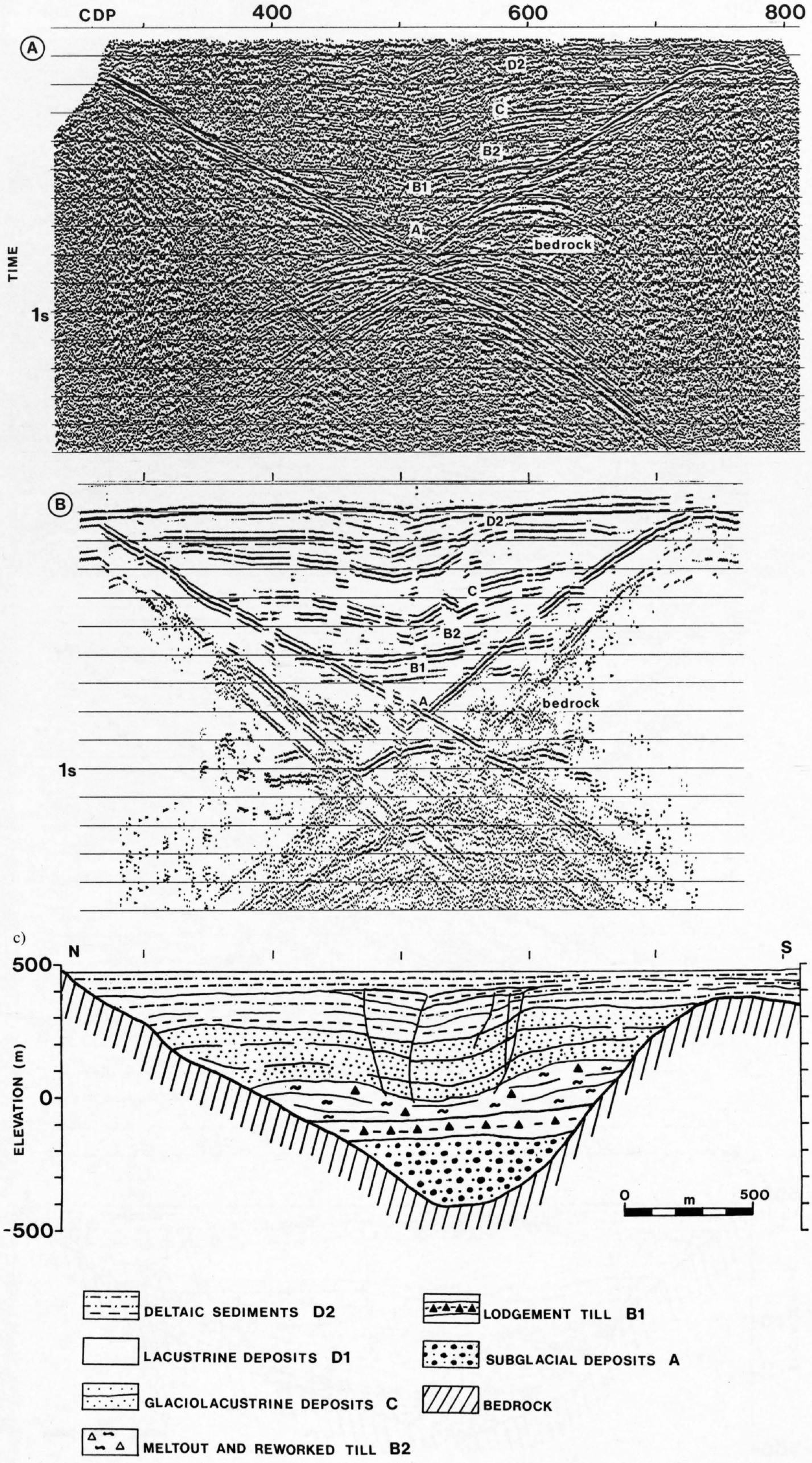

Figure 21.2-7
Seismic modeling and geologic interpretation of Line Vétroz.
a: unmigrated seismic data,
b: synthetic seismic data,
c: geologic interpretation.

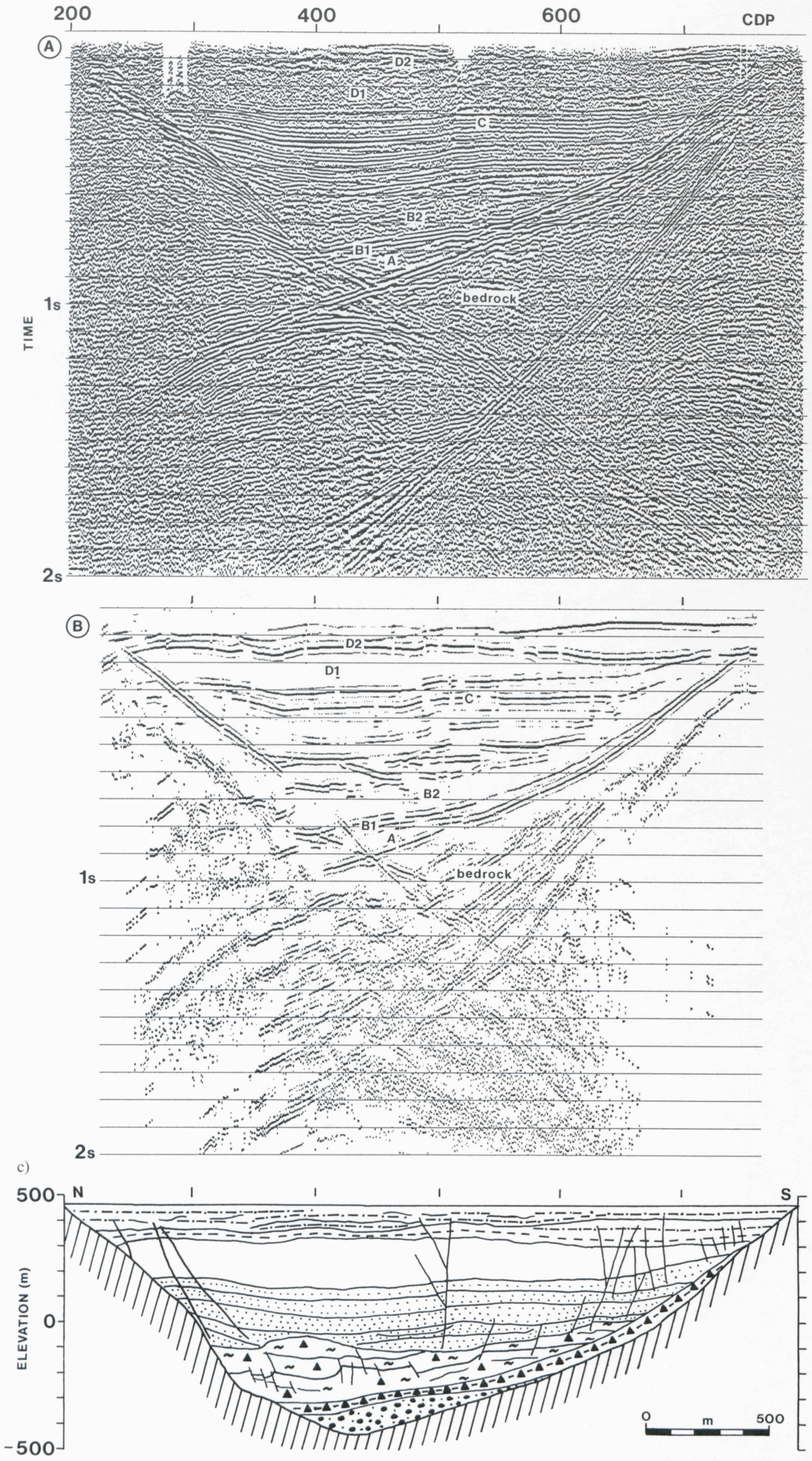

Figure 21.2-8
Seismic modeling and geologic interpretation of Line Martigny.
a: unmigrated seismic data,
b: synthetic seismic data,
c: geologic interpretation.

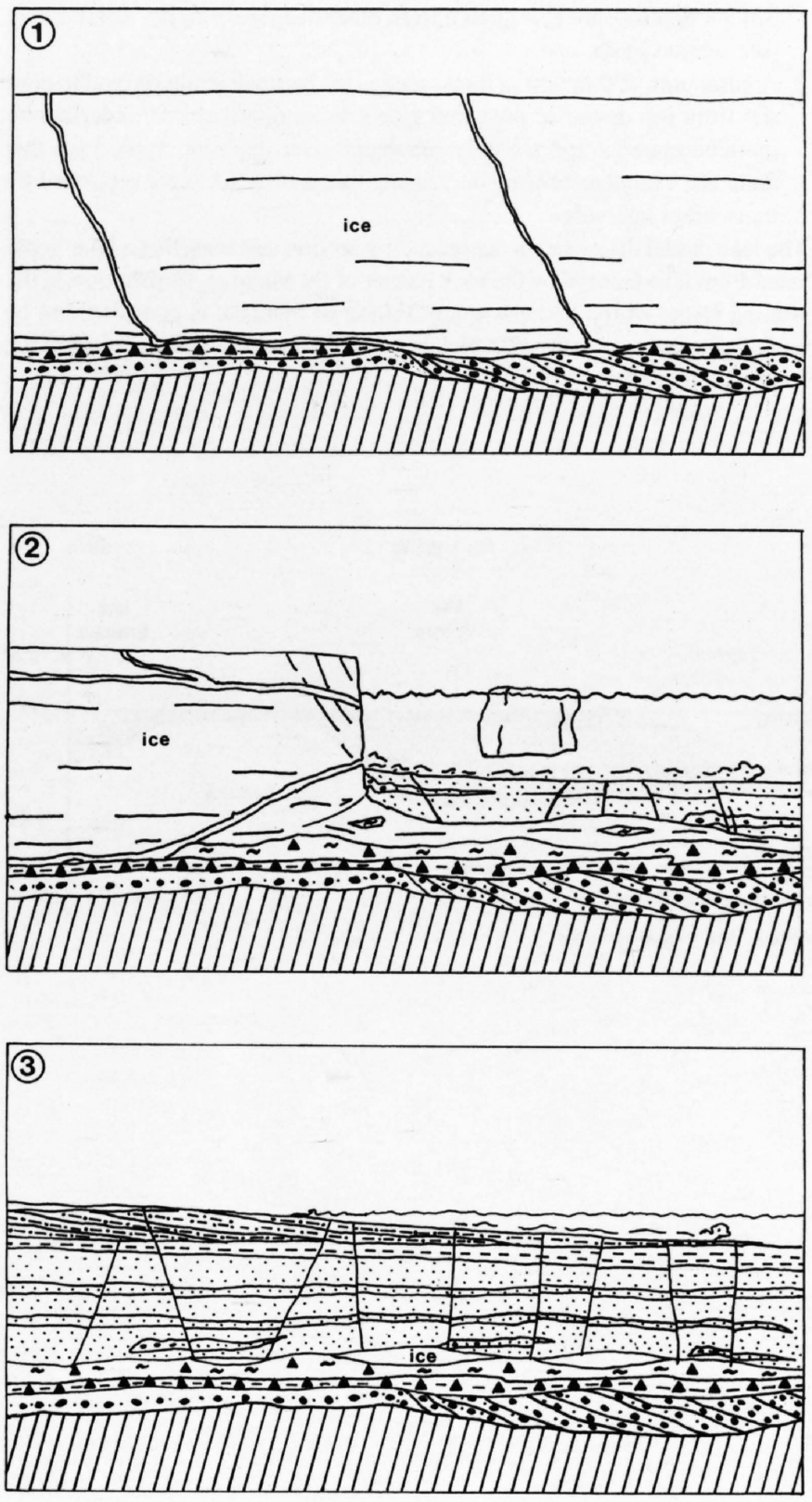

Figure 21.2-9
Model showing three stages of backfilling of the Rhone valley. Stage 1: Subglacial channel deposits, Stage 2: Glacio-lacustrine sedimentation in a supra- and proglacial lake, Stage 3: Deposition of a deltaic sequence.

21.2.2.2 Geological interpretation

The geological interpretation is shown in Figures 21.2-7c and 21.2-8c. The two lines will be discussed in parallel. As previously shown by Finckh et al.(1984), the **bedrock interface** suggests that glacial valleys like the Rhone Valley are strongly overdeepened. The deepest point of the bedrock surface is as deep as 550 m below see level in line Martigny. This means that a total of about 1000m of Pleistocene sediments were infilled into this glacial valley in the Martigny area. The valley itself is neither true V-shaped nor U-shaped. The asymmetrically dipping slopes grade into a U-shape at the bottom. This may result from a combined action of ice and water erosion processes as in glacial tunnel valleys (Boulton & Hindmarsh, 1987), or in overdeepened troughs (e.g. Mullins & Hinchey 1989, Eyles et al. 1990).
The transparent facies of **unit A** is analogous to the unit observed at the bottom of the glacial series of Lake Zürich, which has a P-wave velocity of 2500 m/s (Finckh et al. 1984). A borehole drilled into the bottom of lake Zürich has revealed that this unit is a well sorted gravel lying over the bedrock (Hsü & Kelts 1984). It has been interpreted as subglacial channel deposits (Lister 1984). Such features have also been reported from outcrops in the Gruyère basin (Pugin 1988). The transport and deposition must have occurred in a subglacial channel (Röthlisberger 1972). From Shreve (1972) it is known that water flows along the base of a glacier, giving rise to such subglacial channel deposits.
The strong acoustic contrast between **unit B1** and the layers above and below show that sediments of unit B1 must be significantly compacted. Only lodgement tills accumulating beneath a shearing glacier have this characteristic (Boulton 1978).
The chaotic aspect and the low reflectivity of **unit B2** could be correlated with a poorly sorted sediment (Eyles et al.1990). Such sedimentary structures result from residual sedimentation during the melting of the glacier and correspond to melt-out or reworked tills (Boulton 1978).
The continuous reflections of **unit C** are expressing a complex of well stratified turbiditic lacustrine sediments. The divergent dips at the base of this unit suggest collapsed strata or foresets in a proglacial sedimentation environment. Such turbiditic environments have already been described in outcrops in the Gruyère basin (Pugin 1989) or in the Canadian Rockies (Eyles & Clague 1987). Sedimentary collapses related to trapped ice have been discussed by McDonald & Shilts (1975) and Pugin (1989). They show characteristically syn-sedimentary deformation or faulting with extension towards the sides and compression in the center of the valley. Unit C is thus identified as glacio-lacustrine deposits.
The transparent seismic character of **unit D1** suggests that the sediments are either massive or very finely laminated, or else well stratified but slumped. Finely laminated sediments are typical for bottom-set beds of a delta. Unit D1 is tentatively considered as representing a lacustrine sequence.
The disconformities observed in the upper unit, **D2**, can be interpreted as a proximal deltaic system with imbricated lobes. Although the explanation as foresets of a delta seems plausible, a seismic line parallel to the valley would be more suitable for a further interpretation (Pugin & Rossetti 1992).

21.2.2.3 Discussion

The discussion of the filling of this valley by sediments is illustrated by a three phase model (see Figure 21.2-9). Similar to the situation in Lake Zürich (Lister 1984) and the Sarine basins (Pugin 1989) one single deglaciation event can satisfactorily explain such a sedimentary sequence.
The first stage, the deposition of the coarse sediments of unit A, is related to subglacial channels (Röthlisberger 1972) and is illustrated in the Figure 21.2-9a. Lodgement tills or deformation tills (unit B) may be deposited on top of such very permeable sediments (Boulton 1987). The presence of only one compacted till at the base of the sequence would suggest that these sediments are related to the Last Ice Age (the late "Würm" maximum).
The second phase shown in Figure 21.2-9b is characterized by supra and proglacial lakes. The ice is now melting rapidly at the water contact (deposition of the unit C). The deep trapped ice covered by sediments is melting at a lower rate. The presence of such dead ice is indicated by collapse structures in the center of the valley. Synsedimentary faults were active at that time. Some of the roll-over structures present on the sides of the valley are possibly due to differential compaction.
The last stage encompasses deposition of a deltaic sequence (unit D). The last trapped ice is now melting. The presence of fractures near the top of the sedimentary sequence suggests a very high deposition rate. This sedimentation occurred during the last deglaciation, i.e. within a maximum interval of 5000 years, between 18000 and 13000 years BP. Accumulation rates were thus of the order of 6 cm/a (300 m sediments within 5000 years). Similar rapid accumulation rates in equivalent sequences have been described in the Seez valley of eastern Switzerland by Müller (1994) and the Rocky Mountains by Eyles et al. (1990).
Several boreholes a few tens of meters deep have been drilled in the Rhone Valley close to lines Martigny and Vétroz (Finger & Weidmann 1988). They show different post-lacustrine deposits, which were dated by the C14 method. The ages range up to 10390 ±190 years BP.

21.2.3 Longitudinal section

A longitudinal profile linking the seismic lines discussed above is shown in Figure 21.2-10. Besson et al. (1991) have already drawn a similar profile including some seismic and well data. Figure 21.2-10 encompasses the segment of the Rhone Valley down to Martigny and includes the insight gained from seismic modeling (Section 21.2.2). Part of the segment from Martigny to St.-Maurice is shown in the context of the longitudinal line Epinassey (Figure 21.2-6).
The Rhone valley between St. Maurice and Brig represents an elongated, V-shaped sedimentary basin with a length of about 90 km and a width of 2–4 km, as measured on the level of the present-day valley floor. The thickness of the valley fill decreases from a maximum of about 1000 m near Martigny to around 500 m upstream, at Bramois near Sion. It decreases also in a downstream direction to about 600 m at Epinassey and ends at the rock barrier of St. Maurice.
Comparing the various seismic profiles shows that the sedimentary fill has some common features which can be traced across the entire basin. Remark-

able similarities emerge for lines Martigny, Saillon and Vétroz. The distinct reflection character and the continuity of the individual seimostratigraphic units made it possible to present a tentative interpretation of the lithofacies, in spite of the absence of well control between Martigny and Vétroz. Three major units can be distinguished:

1. An uppermost unit, some 200 to 300 m thick with chaotic reflectivity, consists of deltaic and fluvial gravels and sands, documented by numerous shallow wells.
2. A middle unit, 400 to 500 m thick with distinct, continuous, narrowly spaced reflections, is interpreted to consist of lacustrine and distal glacio-lacustrine beds. Several hundred meters of lacustrine beds were penetrated in the well Bois Noir near St.-Maurice (see line Epinassey, Figure 21.2-6). Similar deposits are also known from other deep wells in the Rhine valley (see section 21.4).
3. A basal unit, 400 to 500 m thick, resting on bedrock is interpreted to consist from top down, of proximal glacio-lacustrine deposits underlain by moraine material and possibly subglacial river deposits. Typical for this units are a number of irregular, strong bands of reflections, separated by transparent intervals.

The lake model discussed in the preceding section assumes, that a lake, separated from lake Geneva by the rock barrier of St. Maurice, formed during the waning stages of the last glaciation. Filling of this lake is considered to be essentially a one cycle event, which began after the retreat of the ice from the lower Rhone valley.

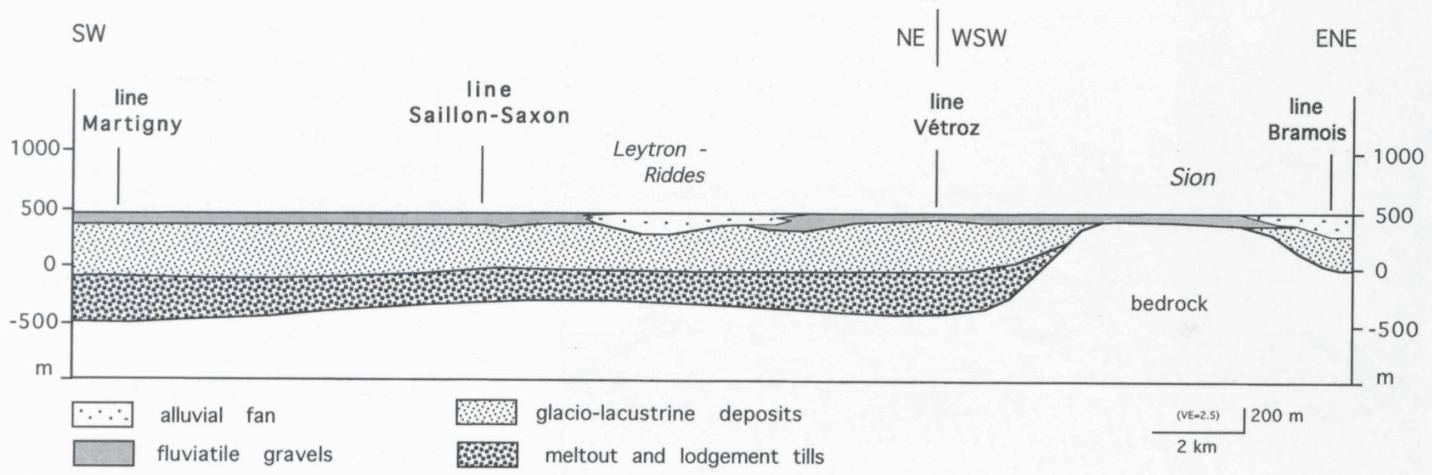

Figure 21.2-10
Longitudinal profile of the Rhone Valley. The shallow bedrock surface beneath Sion results from the profile trace being off the central axis of the valley.

21.3 The Ticino region

P. Heitzmann, M. Felber & W. Frei

Compared to the inneralpine valleys of the Rhone (see Section 21.2) and the Rhine (see Section 21.4), which both drain to the northern side of the Alps, the Ticino region on the southern slope of the Alpine chain has actually a different climatic, and therefore also hydrographic regime. In addition, this region underwent a completely different geologic evolution during latest Tertiary to Quaternary times (Bini et al. 1978, Cita et al. 1990, Felber 1993, Felber et al. 1995). With the goal to improve our understanding of the complex morphogenic evolution of the Southern Alps, high frequency reflection profiles were recorded, one across the Piano di Magadino and five short profiles across suspected sites of buried paleovalleys in the Mendrisiotto region (see Figure 21.1-1).

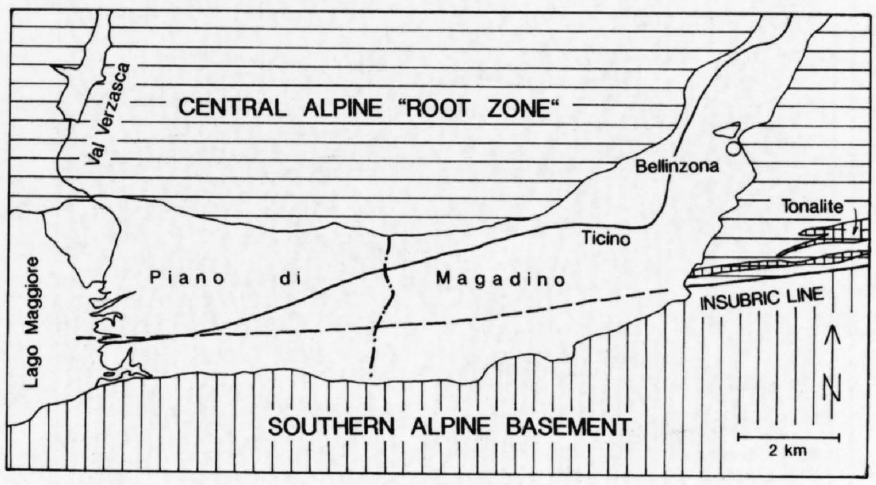

Figure 21.3-1
Geologic sketch map of the Piano di Magadino showing location of the seismic line.

21.3.1 The seismic profile across the Piano di Magadino

The experience acquired in the Rhone Valley during the previous years was applied in 1992 to investigate the depth of the bedrock below the Piano di Magadino (Figure 21.3-1). The Ticino river has its origin in the Gotthard region and crosses the tectonically lowermost units of the Central Alps. From Bellinzona to Lago Maggiore, the Ticino river follows the E-W running Insubric Line. This valley segment, the Piano di Magadino, therefore separates the subvertically foliated gneisses of the Central Alpine "root zone" from the gneisses of the Southern Alpine Strona-Ceneri Zone. Previous geophysical investigations gave evidence for a very deep incision along the trace of the Insubric Line (Bächlin et al. 1974, Spicher & Wenk 1981).
A 3 km long profile was recorded perpendicular to the valley axis about 8 km upriver of Lago Maggiore (Felber 1993, Felber et al. 1995). Data acquisition was carried out by GeoExpert AG, Schwerzenbach and data processing executed at the Institute of Geophysics ETH-Zürich. The field parameters are listed in Table 21.3-1. As seismic sources a weight dropper BISON EWG III and – in the central part of the line – explosives were used.
The data quality in this line is comparable to that obtained in the Rhone Valley lines (Section 21.2), making it possible to subdivide the valley fill into a sequence of seismostratigraphic units. The geometry of the bedrock surface is well outlined by high-amplitude reflection bundles dipping N and S.

Based on reflectivity, six seismostratigrphic units can be identified within the valley fill (Figure 21.3-2); from bottom to top they are:

1. A lowermost zone characterized by short irregular reflections indicative for a poorly layered sedimentary complex as for example fluvial deposits.
2. A thin zone with low reflectivity, interpreted as a body of coarse fluviatile sediments.
3. A reflective zone with long continuous reflections might stem from well stratified, fine grained lacustrine sediments.
4. The lower part of the valley fill terminates with a thin zone of low reflectivity similar to zone 2 which may also consist of coarser, poorly layered sediments.
5. The main part of the valley fill is characterized by a highly reflective zone with continuous reflections. This very thick formation (> 2.5 s, or about 250 m) may be composed of a complex succession of fine grained, well layered lacustrine sediments, deposited in the greater Lago Maggiore.
6. The uppermost zone with low reflectivity represents the most recent fluvial (deltaic) deposits.

The shape of the valley as it is outlined by the bedrock surface is strongly asymmetric (Figure 21.3-2). The southern flank with a continuous slope between 25 and 30 degrees contrasts with a well structured northern slope where a shoulder at about 0.4 s (or about 400 m) below the surface separates a very gentle upper part from a steeper lower part. The general valley section does not resemble the typical U-shape valley section thought to be typical for glacial erosion. Instead, the steep lower part may well be explained by fluvial erosion.
The reflectivity pattern of the valley fill and the shape of the bedrock surface in the profile across the Piano di Magadino are very similar to those of the Line Martigny in the Rhone valley (see Section 21.2). But it cannot be assumed that both valleys have the same incision and backfilling history. Whereas the Rhone valley forms a basin probably closed at St. Maurice, the Ticino valley with the Lago Maggiore is open towards the Po Plain, where a lower erosional base level during Messinian times must be taken into account (see following section 21.3.2).

Line	Magadino	Novazzano	Ronago-Seseglio	Pizzamiglio	Chiasso	Cantone-Vignoo
Recording instrument	BISON9048	DFS-V	BISON9048	BISON9048	BISON9048	BISON9048
Number of channels	48	48	48	48	48	48
Spread details	symmetrical split	symmetrical split	symmetrical split	symmetrical split	symmetrical split	symmetrical split
Geophone group spacing	5m	10 m	5 m	5 m	5 m	5 m
Geophones per group	6	6	6	6	6	6
Geophone type	20 Hz	4.5 Hz	20 Hz	20 Hz	20 Hz	20 Hz
Filter	16-250 Hz	8-125 Hz	16-250 Hz	16-250 Hz	16-250 Hz	16-250 Hz
Source type	EWGIII + dynamite	Vakimpak	Vakimpak	Vakimpak	EWGIII	EWGIII
Source spacing	5 m	10 m	5-7.5 m	5 m	5 m	5 m
No. of vertical stacks	6	4	6	4-6	6	4-8
Multipicity	24	24	24	24	24	24
Samling rate	1 ms	2 ms	1 ms	1 ms	1 ms	1 ms
Registration time	1 s	2 s	1 s	1 s	1 s	1 s
Date recorded	March 1992	Sept. 1988	Oct. 1991	May 1991	March 1992	July 1993

Table 21.3-1
Field parameters of the southern Ticino seismic lines.

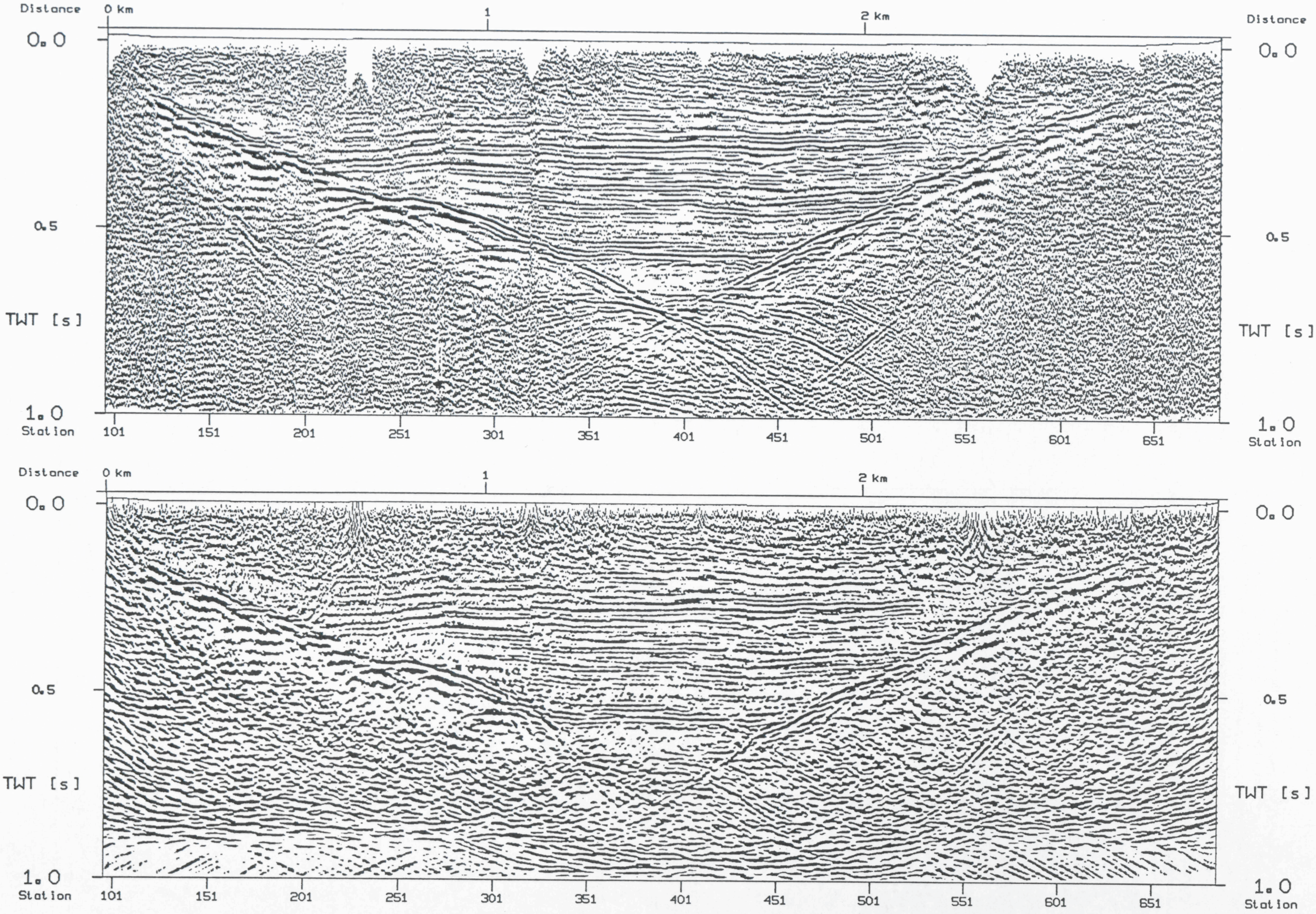
Distance
0 km
1
2 km
Distance
0.0
0.5
TWT [s]
1.0
Station
101
151
201
251
301
351
401
451
501
551
601
651

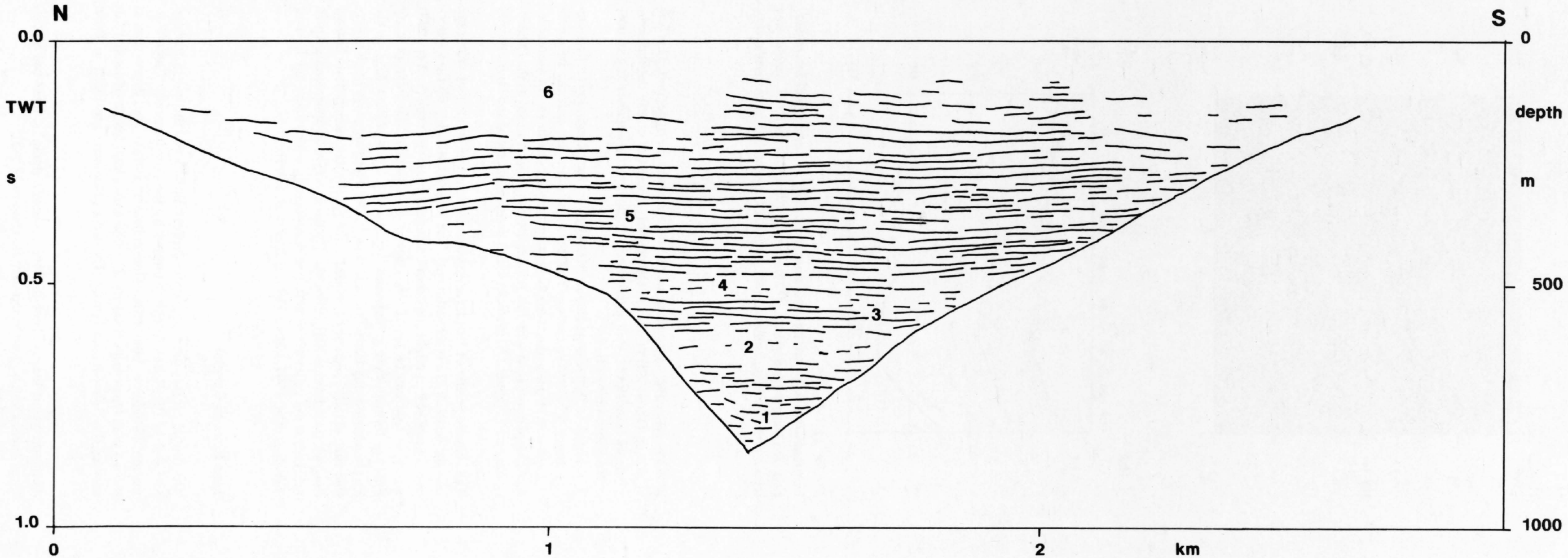

Figure 21.3-2
Seismic section of the Piano di Magadino line: (a) final stack, unmigrated; (b) migrated section; (c) geologic interpretation. 1: fluvial deposits, 2: coarse fluviatile sediments, 3: fine grained lacustrine deposits, 4: coarse fluviatile sediments, 5: lacustine sediments (Lago Maggiore), 6: recent alluvial deposits.

a)

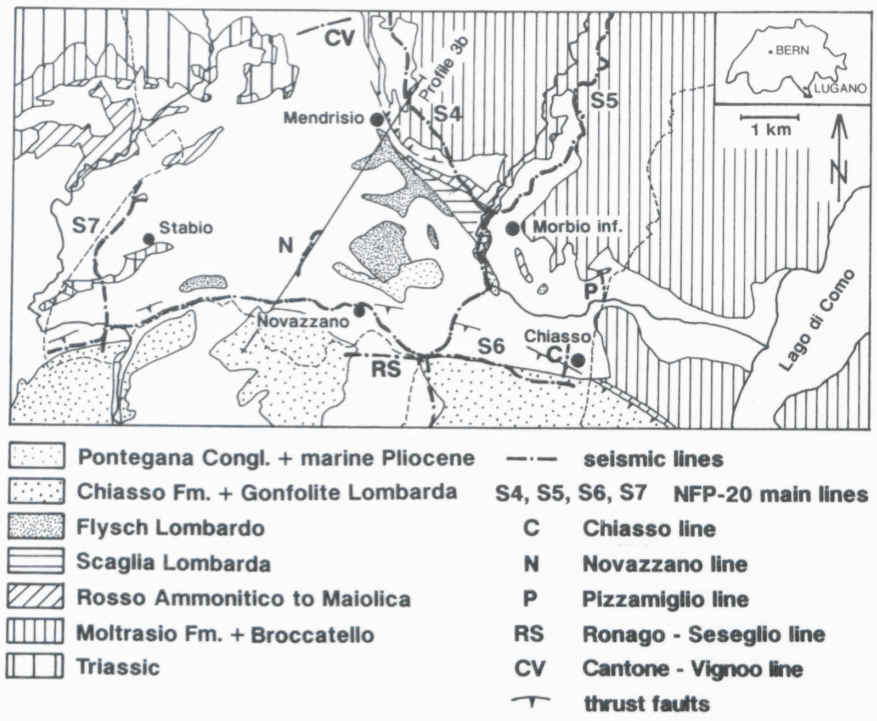

b)

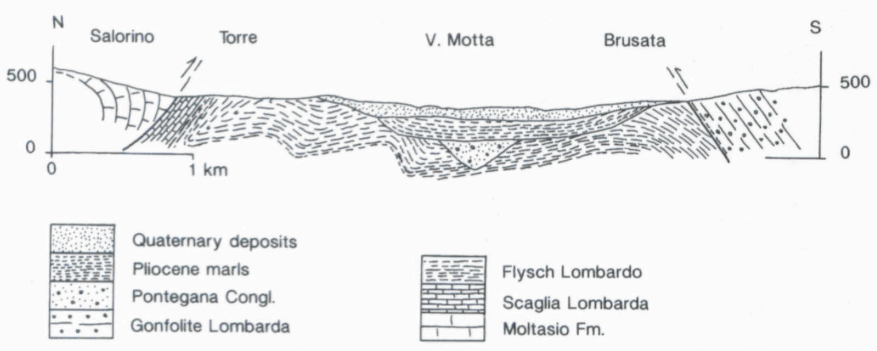

Figure 21.3-3
a) Simplified geological map of the Mendrisiotto region with location of the NRP-20 main seismic lines and the valley lines.
b) General geological profile through the Mendrisiotto region drawn along line Novazzano N in (a).

a)

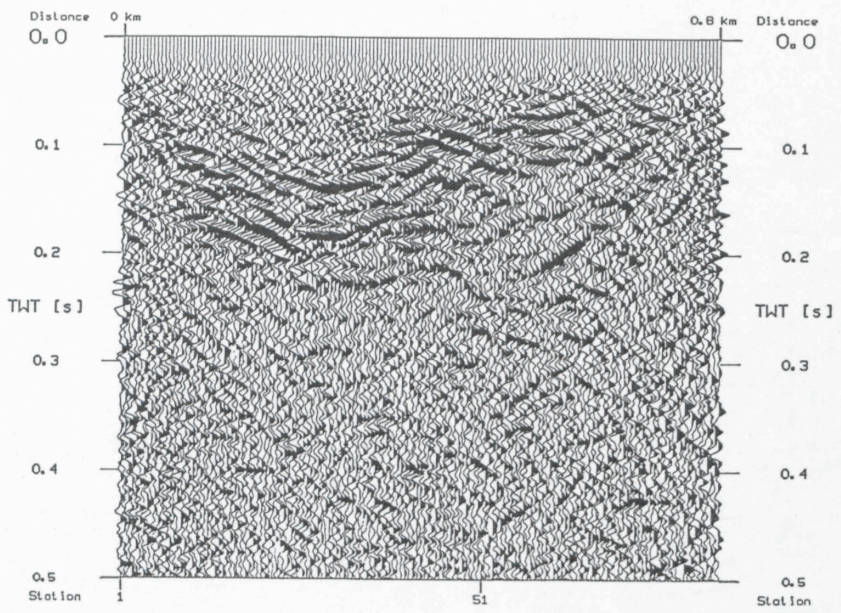

b)

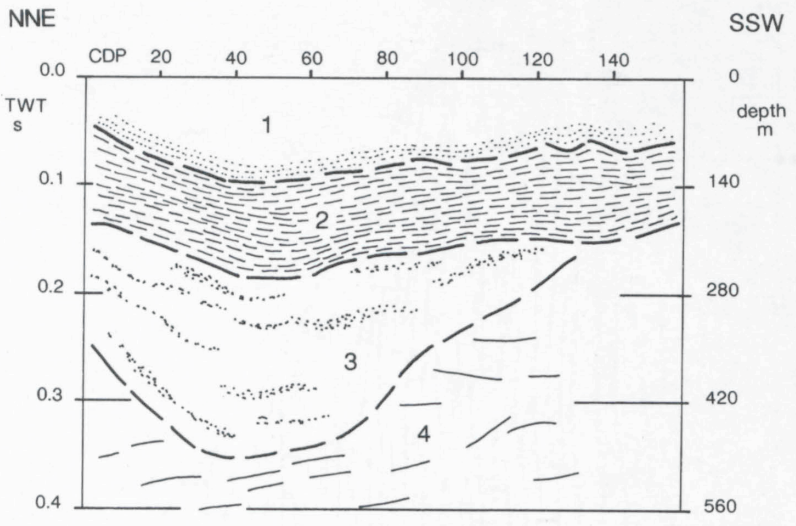

Figure 21.3-4
Novazzano line: (a) unmigrated seismic section; (b) geological interpretation. 1: Quaternary deposits, 2: Pliocene argillaceous marls, 3: sandstones with interbeded conglomerates (Messinian), 4: bedrock (Flysch Lombardo).

21.3.2 The seismic profiles in the Mendrisiotto region

A number of experimental, shallow seismic surveys were carried out in the Mendrisiotto region, the southernmost part of the Canton of Ticino. The lines are situated near Novazzano (Valle della Motta), between Ronago and Seseglio, at Pizzamiglio, in the town of Chiasso and near Mendrisio (see Figure 21.3-3). The main goal of these profiles was to study the paleohydrographic system. The possible presence of pre-Pliocene (Messinian) valleys in this area was suggested by Bini et al. 1978, Finckh 1978, Finckh et al. 1984, Cita et al. 1990, Felber et al. 1991, Felber 1993 and Felber et al. 1995.
The Mendrisiotto region forms the frontal part of the Mesozoic-Tertiary South-Alpine sedimentary cover nappes (see Chapters 10 and 15). In Late Tertiary time a last marine transgression reached this region (marine, Early Pliocene shales of the Argille di Castel di Sotto Formation; Premoli-Silva 1965, Longo 1968, Violanti 1991, Felber 1993), flooding also the Messinian valleys and their earliest sedimentary fill (Conglomerato di Pontegana Formation). The topographic depressions of the Mendrisiotto region were subsequently filled with late Pliocene-Pleistocene clastic sediments (Conglomerati di Mendrisio Unit) and Pleistocene-Holocene glacial, lacustrine and postglacial deposits (Felber 1993).

Line Novazzano

The line is situated in its total length on Quaternary sediments (glacial, fluviatile and deltaic deposits). the Cretaceous flysch crops out to the north, and in the south the basin is bounded by hills formed by the Teritary conglomeratic Gonfolite Lombarda formation. In the valley located further to the east, Pliocene marls and Pliocene-Pleistocene clastics are exposed. During the 1988 seismic survey of NRP 20 a 800 m long seismic profile was recorded. The field parameters are listed in Table 21.3-1.
The seismic section (Figure 21.3-4) displays four zones with different reflectivity patterns. From bottom to top one can distinguish:

1. A lowermost zone without significant traceable reflections. It represents the bedrock, probably Flysch sediments. The valley bottom appears to be at about 0.35 s , i.e. at around 140 m below sea level.
2. A low reflective zone with some rare reflections in the upper part. This formation (about 220 m thick) may possibly consist of coarse detrital sediments (sandstones with interbeded conglomerates) representing almost the entire valley fill.
3. A highly reflective zone characterized by very long continuous reflections forming a basin-like feature. This seismostratigraphic unit can be correlated with Pliocene marls cropping out in the valley to the east of the profile.
4. An uppermost zone with low reflectivity can be interpreted as the Quaternary cover (about 140 m thick) which consists of glacial and fluvio-glacial deposits.

The seismic profile of Novazzano shows evidence of an ancient valley cut into the bedrock of Flysch sediments. The lowermost valley fill (low reflective zone of unit 2) might consist of Pontegana conglomerates (Felber 1993) which in turn can be tentatively correlated to similar Messinian or early Pliocene formations (e.g. Sergnano Formation or Caviaga Formation) in the Po plain underlying Early Pliocene shales. The overlying clays (high reflective zone of unit 3) can be correlated to the Argille di Castel di Sotto Formation, which is dated as Early Pliocene. These clays give an upper stratigraphic bracket for the valley fill of unit 2, thus supporting a Messinian age for unit 3 (Felber et al. 1991, Felber 1993, Felber et al. 1995).

Line Ronago-Seseglio

The profile crosses the topographic depression between the hill of Ronago and that of the Penz (Seseglio) formed by the conglomeratic Como Formation (Gonfolite Lombarda; Gunzenhauser 1985). The depression is topped with Quaternary deposits. The line with a total length of about 1 km crosses the Swiss-Italian border. The field parameters are listed in Table 21.3-1.

In the profile of Ronago-Seseglio five seismostratigraphic units can be distinguished. From bottom to top they are (Figure 21.3-5):

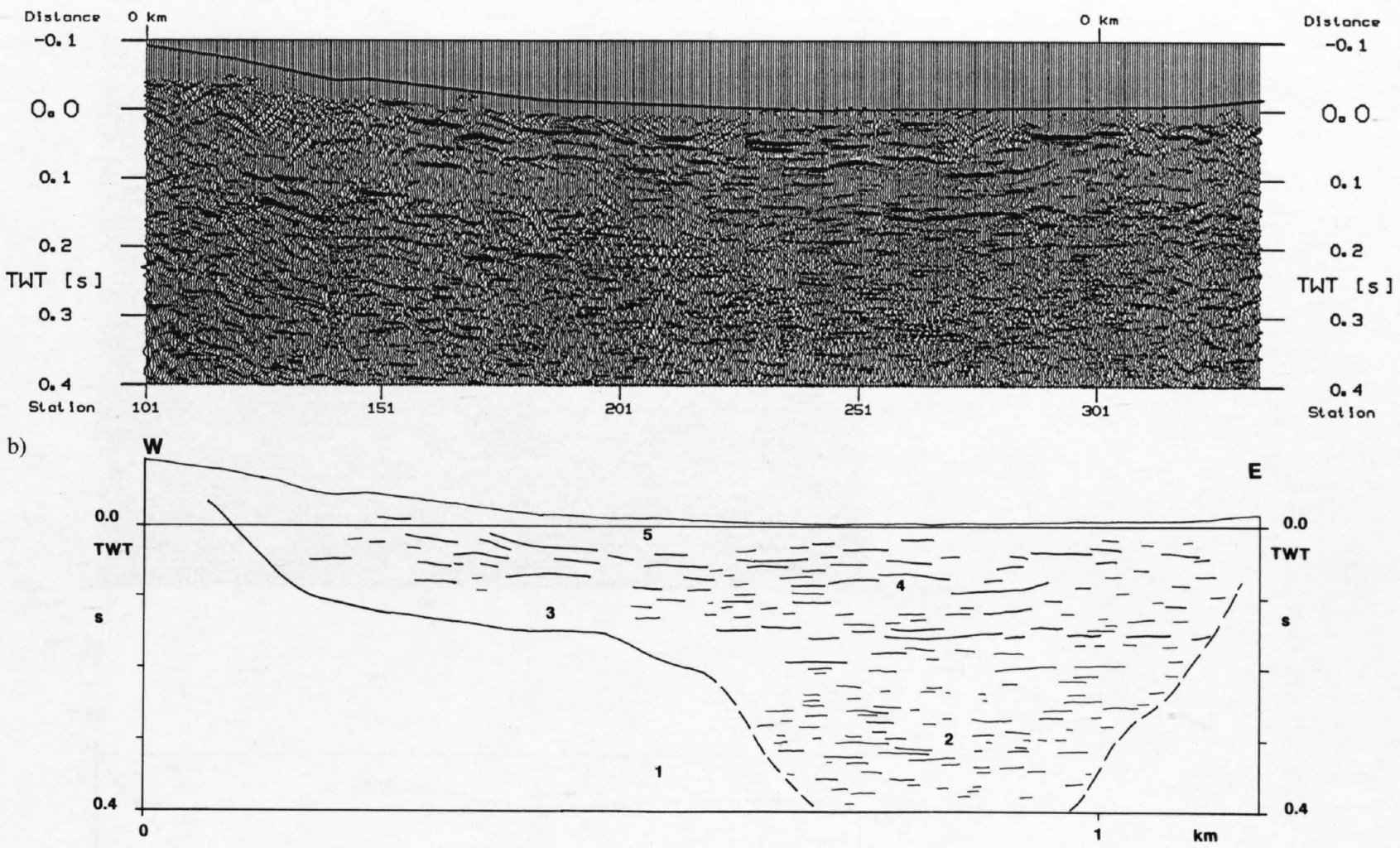

Figure 21.3-5
Ronago-Seseglio line: (a) unmigrated seismic section; (b) geological interpretation. 1: bedrock (Gonfolite lombarda), 2, 3: sandstones (2) with interbeded conglomerates (3) (Messinian), 4: argillaceous marls (Pliocene?), 5: alluvial deposits.

1. A lower part with few, questionable sporadic reflections stemming from the bedrock, i.e. conglomerates of the Gonfolite Lombarda which crops out in the hills on both side of the profile. The limit between this bedrock and the overlying fill is not clear (an irregular trough-shaped morphology could be suspected).
2. In the central and eastern part, between CDP 420 and 580, at a depth between 0.2 s and 0.3 s, a complex with short, high-frequency reflections can be identified. It may be correlated with sandy bodies in analogy to the Novazzano line.
3. In the western part, above the bedrock (about 1.5 s), a zone with very low reflectivity could be interpreted as a coarse grained (conglomeratic) formation.
4. Overlying the formations 2 and 3 and onlapping on bedrock at the western and the eastern end of the profile, a highly reflective zone characterized by long reflections can be interpreted as the Pliocene shale formation, in analogy with the Novazzano profile.
5. The uppermost zone in the central part of the profile corresponds to the Quaternary cover, cropping out in the depression between the two hills.

In the Ronago-Seseglio profile, the ancient valley cut into the Oligo-Miocene Gonfolite Lombarda Formation is filled with coarse grained clastic deposits, which in turn are overlain by the Pliocene Castel di Sotto Formation. The results of the Ronago-Seseglio recording complement the data obtained from the Novazzano line and suggest a possible course of a Messinian paleovalley.

Line Pizzamiglio

The line crossing the Breggia river straits of Pizzamiglio to the north of Chiasso was recorded in order to obtain information about the bedrock depth and the valley fill between the basins of Chiasso and Lago di Como (Lario). The actual valley is cut into the bedrock formed of Liassic limestones of the Calcare di Moltrasio Formation (Figure 21.3-3). The seismic recording was executed in a highly populated area under difficult logistic problems, specially the intense traffic crossing the Swiss-Italian border. Field parameters are listed in Table 21.3-1.

The seismic profile (Figure 21.3-6) displays three seismostratigraphic units:
1. A lowermost, dipping zone between 0.2 and 0.3 s, observable only between CDP points 235 and 345.
2. A zone with slightly south dipping continuous reflections between 0.1 and 0.2 s. The zone begins in the central part and dips towards the southern end of the section.
3. An uppermost zone with irregular strong reflections (uppermost 0.5 s).

The geological interpretation of this profile (Figure 21.3-6) shows a deeply eroded valley (depth about 450 m, with the valley bottom at about 200 m be-

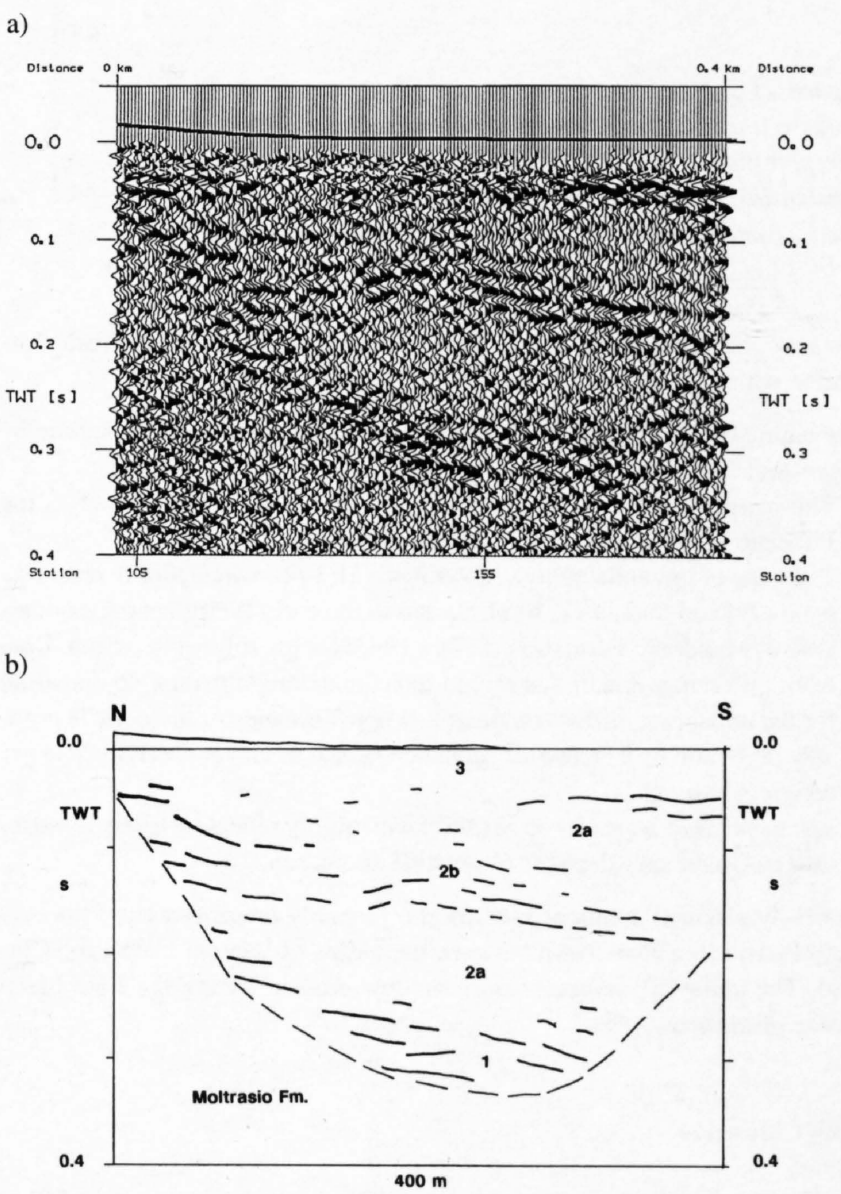

Figure 21.3-6
Pizzamiglio line: (a) unmigrated seismic section; (b) geological interpretation. 1: argillaceous marls (Pliocene?), 2: glacial deposits with morainic material (2a) and interbeded lacustrine deposits (2b), 3: alluvial deposits.

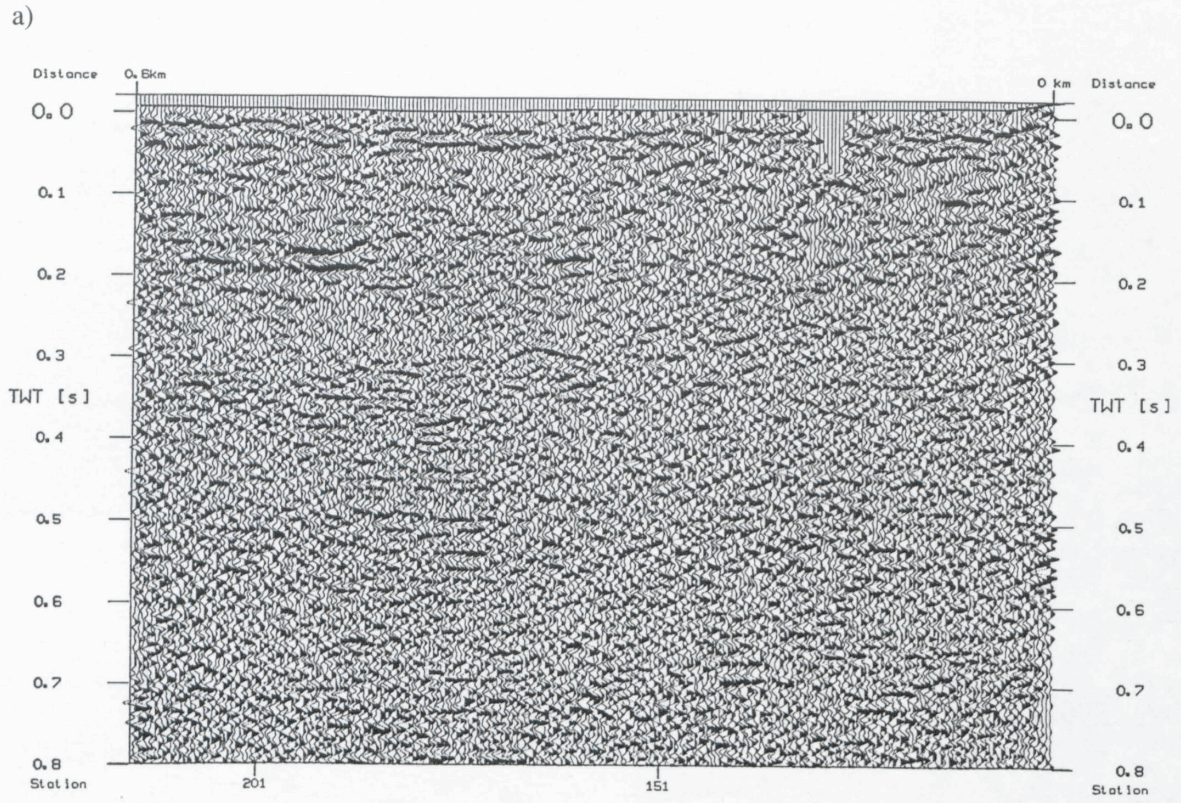

Figure 21.3-7
Chiasso line: (a) unmigrated seismic section; (b) geological interpretation. 1: bedrock (Moltrasio Formation and Gonfolite Lombarda), 2: shales (Pliocene?), 3: lodgement till, 4: fluvial and lacustrine deposits, 5: lacustrine deposits (Chiasso lake).

low sea level), cut into the Liassic limestones of the Calcare di Moltrasio Formation which is outcropping on both side of the valley.

The nature of the fill is difficult to define; three tentative correlations can be suggested:

1. The lower southward dipping reflective zone may be compared to the Pliocene shales in the Novazzano and Ronago-Seseglio lines.
2. The zone of low reflectivity (2a in Figure 21.3-6b) with a highly reflective band (2b) can tentatively be attributed to the early Pleistocene Conglomerati di Mendrisio Formation (Felber 1993) for the following reason. Data from different wells in this region indicate a conglomeratic composition for the upper part of this complex; this upper conglomeratic body is probably underlain by a lacustrine sequence, which in turn is overlying a lower conglomeratic body.
3. The uppermost zone (60-70 m thick) with highly reflective layers is attributed to Quaternary deposits observable at outcrop.

The E–W oriented straits of Pizzamiglio probably presents a late Pliocene/early Pleistocene connection between the basins of Lago di Como and Chiasso. The valley fill indicates only shallow erosion during the Late Pleistocene glaciations.

Line Chiasso

To get information about the sedimentary fill of the Chiasso basin, a 560 m long seismic profile was recorded within the town of Chiasso. In the south, the line begins at the hill of Penz, composed of the Oligocene/Miocene Gonfolite Lombarda Formation (Bernoulli et al. 1989). Further north the line was laid out on the Quaternary deposits of the Chiasso basin. Well data reveal that the uppermost part is characterized by Holocene lacustrine sediments (Chiasso lake) underlain by medium to coarse grained glacial and fluvial deposits. The field parameters are listed in Table 21.3-1.

For this particular line recording meant overcoming major logistic problems:

- the international railway station of Chiasso had to be closed for some hours;
- the interurban and regional traffic had to be diverted through the old town of Chiasso;
- special care had to be given to water and gas pipelines;
- to maximize the signal/noise ratio, recording across the town took place during night time.

The seismic section (Figure 21.3-7) is hardly interpretable. The following seismostratigraphic units are tentatively distinguished:

- An uppermost interval down to 0.05 s characterized by some low-frequency reflections;
- An interval (0.1-0.2 s) with a few curved, high-amplitude reflections;
- A transparent interval (0.2-0.3 s) in the northern part;
- A reflective interval (0.3-0.4 s) with short, high-frequency reflections in the northern part of the profile.

The following geological interpretation can be proposed tentatively (Figure 21.3-7b):

1. The bedrock of the Chiasso basin is composed of the Mesozoic-Tertiary sedimentary succession (Moltrasio Formation in the northern part, conglomeratic Gonfolite Lombarda, Como Formation, in the south). The valley bottom has to be sought at a depth of about 0.45 s (i.e. at about 350 m below sea level).

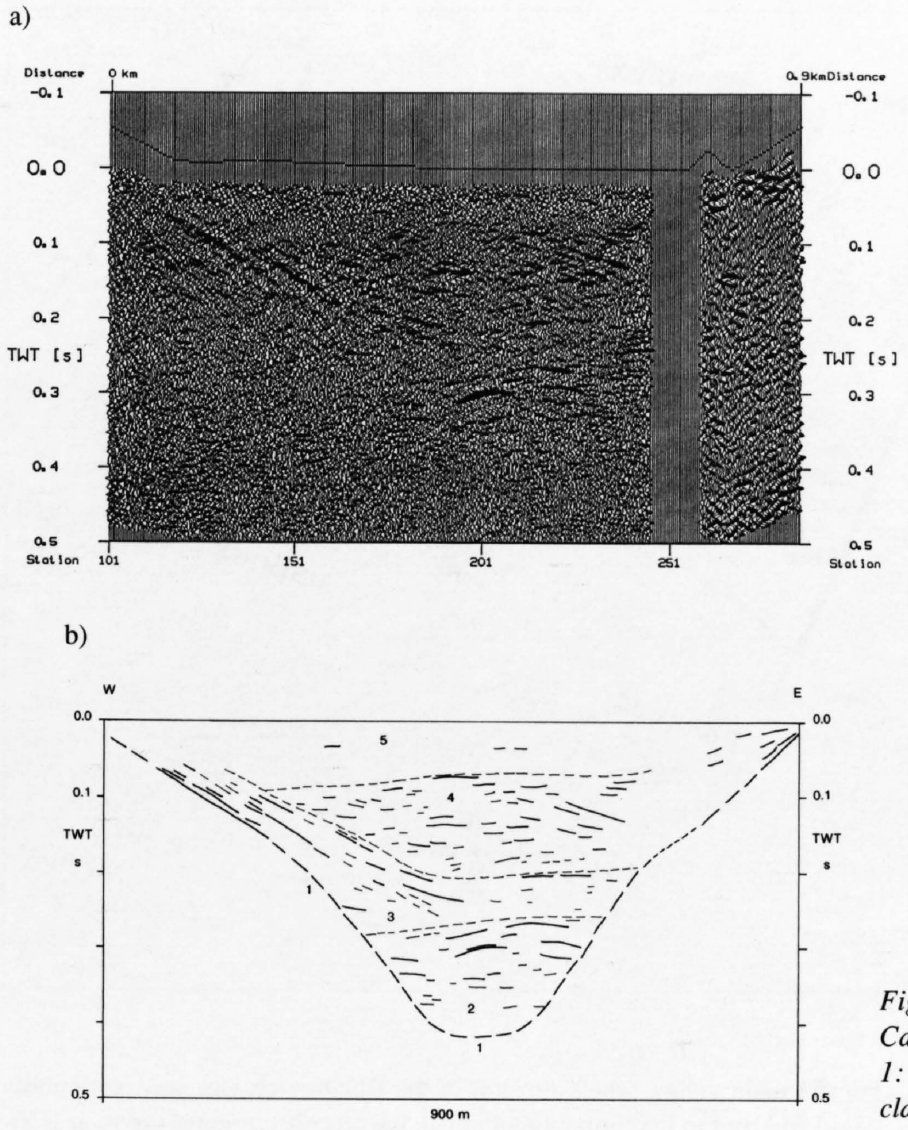

Figure 21.3-8
Cantone–Vignoo line: (a) unmigrated seismic section; (b) geological interpretation. 1: bedrock, 2: sand and gravel, 3: coarse grained slope deposits, 4: coarse grained clastics, 5: fluvioglacial clastics.

2. The lowermost formation of the valley fill might consist of a sequence of fine grained well stratified sediments, similar to the Pliocene shales.
3. The non reflective interval may represent a lodgement till.
4. The overlying formation is characterized by a mixed sedimentation; fluvio-lacustrine fine grained well stratified sediments are interbedded with fluvial coarse grained flood deposits.
5. The uppermost zone represents the lacustrine deposits in the postglacial Chiasso lake.

Line Cantone – Vignoo

The 890 m long profile between Cantone (Rancate) and Vignoo (Mendrisio) was recorded in order to check an eventual buried connection between the basins of Lago di Lugano (Ceresio) and the Mendrisiotto. The valley is cut into Mesozoic sediments, Triassic on the western side, Liassic (Moltrasio Formation) on the eastern one. The extension of the Lugano fault (Bernoulli 1964, Bertotti 1991) follows this valley. The field parameters are listed in Table 21.3-1.

Based on reflection character, shape and sequence (see Figure 21.3-8), the following seismostratigraphic unites can be tentatively distinguished:
5. An uppermost zone of poor reflectivity;
4. Below it a zone with irregular strong reflections;
3. On the western side of the profile a number of E-dipping high-amplitude, low-frequency reflections, which flatten out at depth;
2. At the bottom of the valley fill several conspicuous curved reflections;
1. Bedrock without reflectivity.

The following tentative geological interpretation is proposed (Figure 21.3-8b):
1. The enveloppe of the detrital valley fill suggests a narrow valley with the lowest point at 100-150 m below sea level.
2. The lowermost unit of the valley fill consists possibly of sand and gravel of Late Pliocene/Early Pleistocene age, comparable to the Mendrisio or Pontegana conglomerates.
3. Above it a fan of coarse grained clastics, which can be traced into a sequence of calcite-cemented slope deposits outcropping near the western end of the profile.
4. Above it a coarse grained valley fill.
5. Fluvioglacial clastics with some lacustrine layers, as encountered in nearby shallow wells. This unit cuts deeply into unit 4.

21.3.3 Conclusions

The seismic recording in the Ticino region reveals a series of very deeply eroded valleys with a bedrock surface reaching far below the present-day sea level:

Line	Total thickness of valley fill	Altitude of valley bottom below sea level
Magadino	800 m	-600 m
Novazzano	490 m	-140 m
Ronago-Seseglio	550 m	-300 m
Pizzamiglio	430 m	-200 m
Chiasso	500 m	-350 m
Cantone-Vignoo	420 m	-100 to -150 m

The results of these experimental lines confirm the postulated presence of a complex system of fossil valleys of Early Pliocene, possibly even Late Miocene age, buried underneath the Quaternary deposits. The origin of these valleys may be explained partly by the lowering of the base level during the Messinian eustatic sea-level low. In this period the Mediterranean dried up several times and, as a consequence the streams cut themselves deep into the bedrock. With the reflooding of the Mediterranean basin, these valleys were drowned and filled by clastic deposits (conglomerates of the Messinian Pontegana Formation) and marine shales (Early Pliocene Argille di Castel di Sotto Formation). The duration of the dessication period of only 500'000 years (Gauthier et al. 1994) is too short to explain the formation of such a complex hydrographic system, and a pre-Messinian configuration of this valley system must thus be assumed. It appears probable that the valley system originated in the context of the Miocene (Tortonian) folding and thrusting of the Southern Alps (see Bernoulli et al. 1989, Gelati et al. 1988, Cita et al. 1990, Schumacher et al., Chapter 16 and Schmid et al., Chapter 22). A subsequent rejuvenation in the course of the intensive erosion during the Messinian period is possible. An overdeepening of these Late Tertiary valleys in the Mendrisiotto region by the action of the Pleistocene glaciers, on the other hand, can be ruled out on the basis of the stratigraphic evidence. The morphologic similarity between the profile across the Piano di Magadino and the Rhone valley lines (discussed in section 21.2) may be accidental.

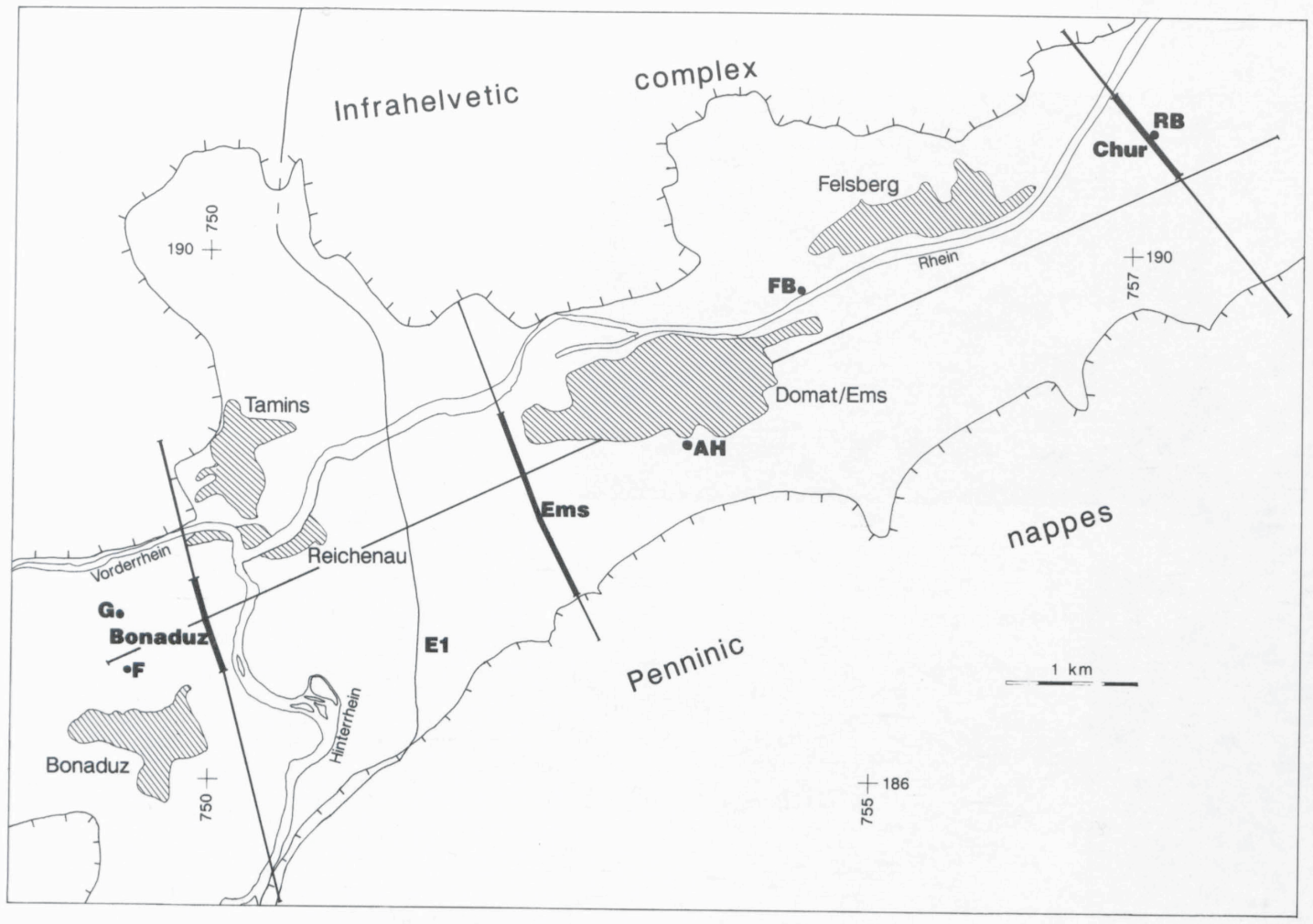

Figure 21.4-1
Map of the Rhine Valley between Reichenau and Chur with location of the seismic lines (thick lines) and traces of cross sections (thin lines). Wells: RB = Rossboden, FB = Felsberg, AH = Altersheim, G = Gurgs, F = Foppa. E1: trace of seismic line of Eastern Traverse (discussed in Chapter 9).

21.4 The Rhine Valley

O. A. Pfiffner & W. Frei

21.4.1 Geologic framework

A shallow seismic reconnaissance survey was carried out in the upper Rhine Valley between Reichenau and Chur with the aim to image the bedrock surface and the valley fill (see Figure 21.4-1). The bedrock surface has been drilled 25 km north of the study area in Balzers (Liechtenstein) at 32 m above sea level. A compilation of the bedrock surface (Wildi 1984) suggests that this surface could be expected at around or slightly above sea level in the area investigated. The Quaternary sedimentary valley fill consists of lacustrine siltstones which directly overly bedrock in the Balzers well. These beds have also been drilled in the Chur-Rossboden well (SGD/AGS document 18078; see Figure 21.4-1). The lake sediments are overlain by coarse clastic fluviatile gravel sediments. The limit between lake sediments and fluviatile clastics is located at a rather constant datum of 400–450 m above sea level. The fluviatile gravel sediments interfinger towards the valley slopes with coarse clastic sediments which are derived from the various tributary creeks. The latter built up some spectacular deltas on the south and east side of the main valley, where erosion in the Bündnerschiefer was particularly easy and lead to the formation of small, but steeply cut gorges (e.g. near Zizers-Sais). In the area of Reichenau several landslides have been mapped, the largest of which, the Flims landslide moved a total mass of about 10 km^3. Several smaller landslides produced the characteristic hills in the area of Domat/Ems (the so-called tumas). The base of the landslide mass is known to be quite shallow (20 m beneath the valley floor as evident from well "Altersheim"). More information on the geology and geomorphology of the area can be found in Nabholz (1975), Abele (1970), Remenyik (1959), Scheller (1970), Pavoni (1968).

21.4.2 Seismic data and interpretation

Three experimental lines were shot across parts of the upper Rhine valley (see Figure 21.4-1). Data acquisition was carried out by GeoExpert AG Schwerzenbach. For the first line shot, Ems, a weight dropper was used and only poor results were obtained (see below). It was thus concluded to continue using dynamite as source, which ultimaltely turned out to be the correct decision. Details about the acquisition parameters of the three lines are given in Table 21.4-1. Processing of the data was carried out at the Institute of Geophysics ETH-Zurich by A Roose (1993) and W. Frei.

Line	Chur	Ems	Bonaduz
Recording instrument	BISON 9048	BISON 9048	BISON 9048
Number of channels	48	48	48
Spread details	symmetrical split	symmetrical split	symmetrical split
Geophone group spacing	5 m	5 m	5 m
Geophones per group	6	6	6
Geophone type	20 Hz	20 Hz	20 Hz
Filter	LC 25 Hz / HC 250 Hz	LC 25 Hz / HC 250 Hz	LC 25 Hz / HC 250 Hz
Source type	Dynamite	Dynamite	Dynamite
Coverage	24	24	24
Sampling rate	2 ms	2 ms	2 ms
Recording length	1 s	1 s	1 s
Date recorded	Nov. 1992	Nov. 1992	Nov. 1992

Table 21.4-1
Field parameters of the Rhine Valley seismic lines.

a)

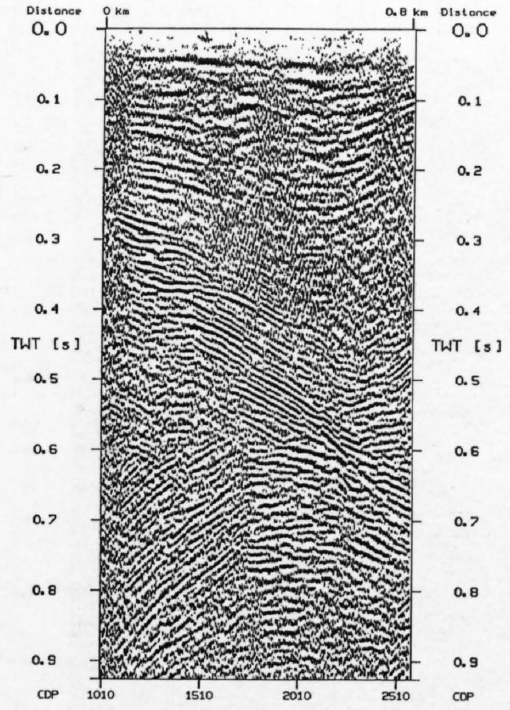

b)

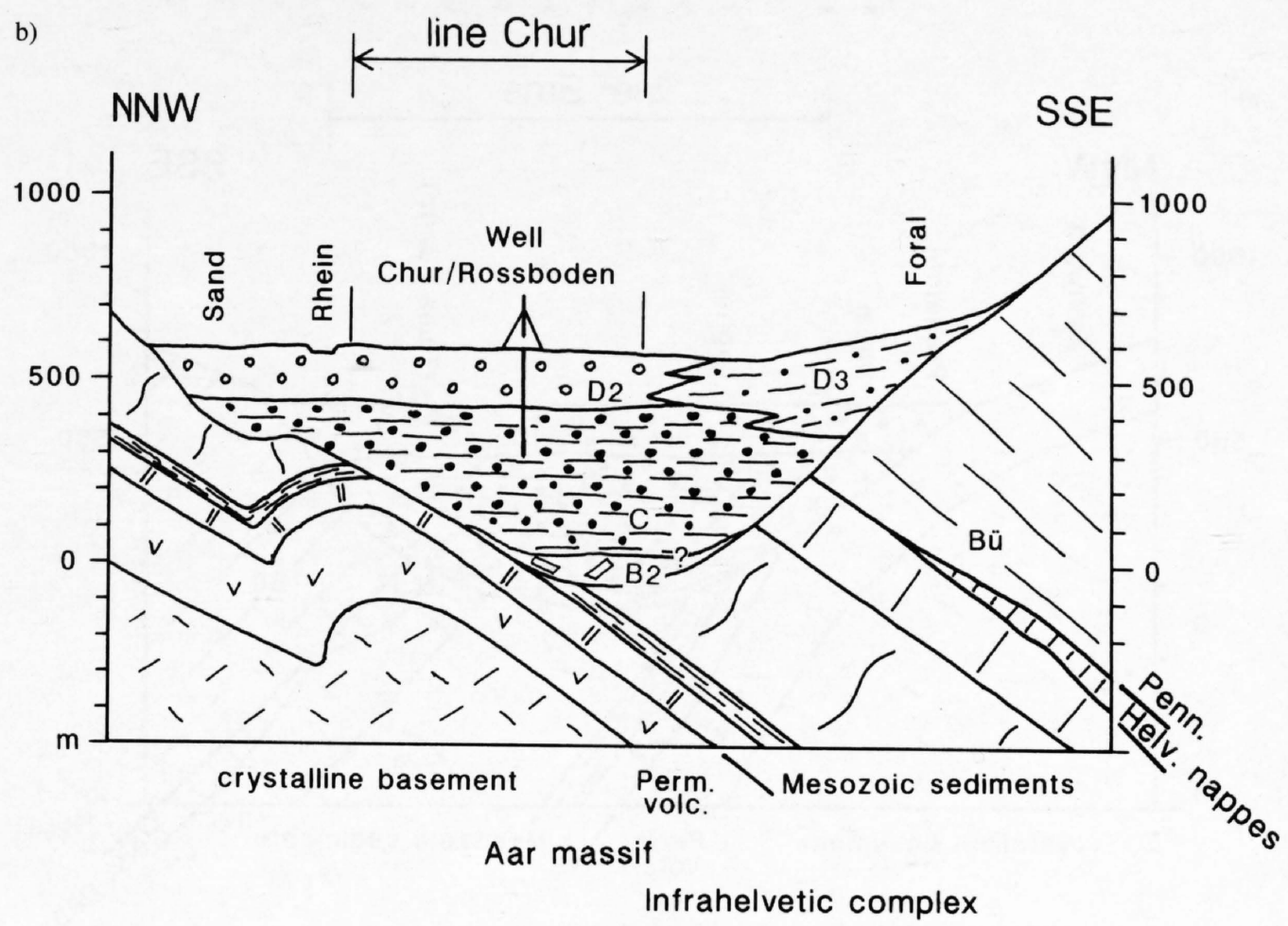

Figure 21.4-2
Line Chur.
a: Unmigrated, final stack,
b: geologic interpretation
(horizontal equals vertical scale).
B2: Meltout and reworked till,
C: Glacio-lacustrine deposits,
D2: Fluviatile gravels,
D3: Deltaic sediments.
Bü: Penninic Bündnerschiefer
(Tomül nappe).

Line Chur

Line Chur crosses the Rhine Valley in the bend, where the valley changes from a longitudinal to an axial valley. The line is slightly upstream from the confluence of the Plessur, which built up a fan pushing the Rhine river to the NW side of the valley floor. The line is also slightly upstream of the confluence of the Pleistocene Rhine glacier and the Julia glacier (which transfluenced across the wind gap of Lenzerheide).
Line Chur traverses only one third of the width of the entire valley. The seismic data are displayed in Figure 21.4-2a and show low frequency reflections in the uppermost 100 msec TWT. Beneath that continuous reflections occupy much of the section between 100 and 250 msec TWT. A SE-dipping band of high amplitude reflections extend from 300 msec TWT downward and southeastward and intersects a NW-dipping band at the SE end of the section. A concave upward band of reflections, finally, can be recognized in the lower part of the section and might represent a buried-focus effect.
The seismic data of line Chur can be correlated with the Chur-Rossboden well (SGD/AGS document 18078), which is located exactly on the seismic line. This well encountered 150 m of fluviatile gravels, followed by fine grained, glacio-lacustrine clastics. Thus the low-frequency reflections correspond precisely to the layer of fluviatile gravels. The underlying continous reflections correlate with the fine-grained glacio-lacustrine sediments, the interface between the two being located at around 120 msec TWT (equivalent to 410 m above sea level in the Chur-Rossboden well). The high-amplitude SE-dipping band most likely stems from the bedrock surface on the valley side. The topography of the area to the NW of line Chur suggests that the seismic line is located above the junction of a tributary valley merging with the main Rhine valley. The bedrock surface is therefore expected to be rather complex, with reflections likely to be sampled from several places of this bumpy surface. The bottom of the main valley can be correlated with the reflection groups at 720 msec TWT, which corresponds to a position of about 100 or 200 m below sea level. The meltout tills shown in the tentative interpretation of Figure 21.4-2b are not based on seismic data.

Line Ems

Line Ems crosses the Rhine Valley downstream of the confluence of Vorderrhein and Hinterrhein and traverses about half of the entire valley floor. The line is located within the area occupied by tumas (hills) consisting of rockslide deposits.
Line Ems is more or less impossible to interpret due to the poor data qualtity (Figure 22.4-3a). Low frequency reflections above 100 msec TWT might stem from fluviatile gravels and their discontinuous nature may be due to the occurrence of large limestone rockslide blocks. A number of such blocks can be observed in the immediate vicinity of the seismic line. Moreover, several

a)

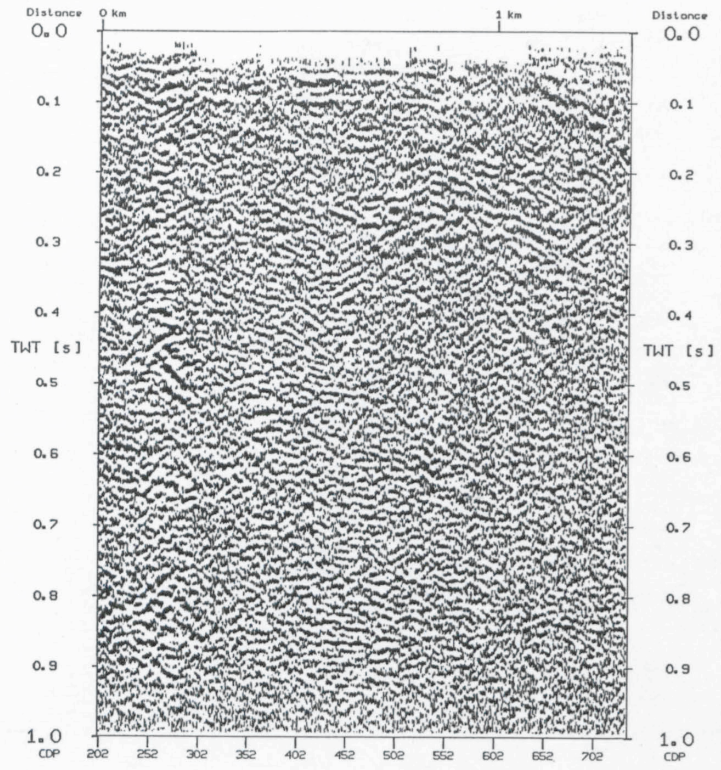

b)

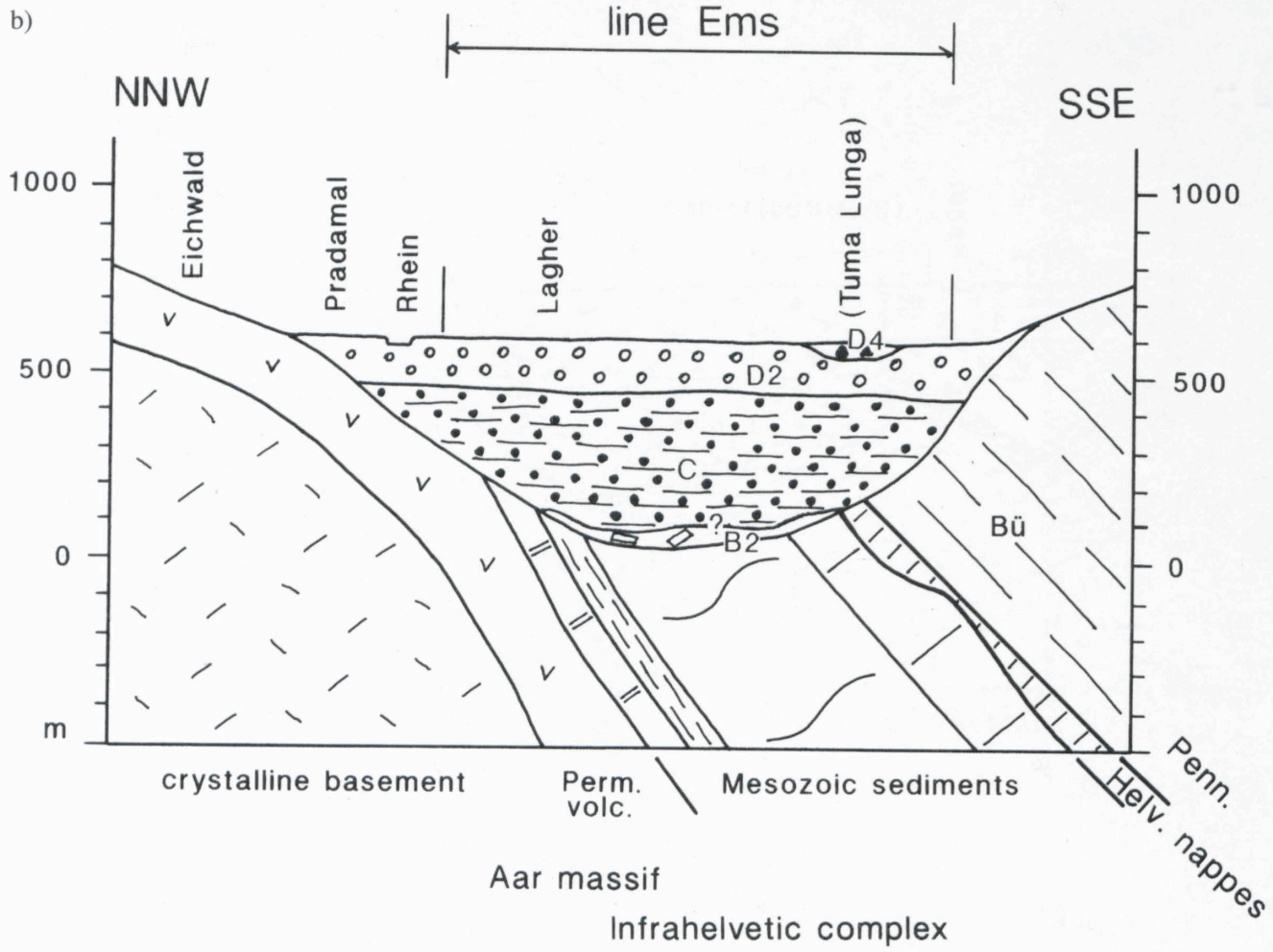

Figure 21.4-3
Line Ems.
a: Unmigrated, final stack,
b: geologic interpretation (horizontal equals vertical scale).
B2: Meltout and reworked till,
C: Glacio-lacustrine deposits,
D2: Fluviatile gravels,
D4: Rockslide deposits.
Bü: Penninic Bündnerschiefer (Tomül nappe).

hills, rising 10 to 100 m above the flat valley floor are spread across the valley and consist mainly of rockslide material. From well data it is known that this rockslide material, which consists essentially of Quinten limestone (Upper Jurassic of the Helvetic zone), is a superficial deposit that extends only about 20 m beneath the surface (SGD/AGS documents 17007 and 18078). The irregular nature of this material (compact limestone blocks of all sizes next to finely crushed material and gravels) may in part be responsible for the poor quality of this line.

Reflections from the bottom of the valley cannot be distinguished clearly (the S-dipping reflections at 500 msec TWT in the north, the horizontal reflections at 550 msec beneath CDP 360 and in the S-dipping events extending from 300 msec at the S end to 500 msec near the the center of the line are not really interpretable). In the geological cross section of Figure 21.4-3b the valley bottom is tentatively placed at around 200 m above sea level, assuming more overdeepening at the convergence of the valley glaciers in the vicinity of lines Chur and Bonaduz. In addition a thin veneer of meltout till is shown in the geological profile of Figure 21.4-3b as a speculative possibility.

Line Bonaduz

Line Bonaduz crosses the area of confluence of the Vorderrhein and Hinterrhein rivers and the confluence of two large Pleistocene glaciers. One thus might expect the Rhine Valley to be particularly overdeepened at this locality. Two wells, Gurgs and Foppa (see SGD/AGS document 17009) are located 2 km to the west of line Bonaduz. They encountered 100 m of Bonaduz gravels, 30 to 100 m of till, 200 m of fluviatile gravels and finally stopped in finer grained clastics (till or glacio-lacustrine deposits?). The so-called Bonaduz gravels lack internal stratification and have been interpreted as representing the deposit of a catastrophic event (violent outflow of the Pleistocene Lake Ilanz after burst of the natural dam).

Line Bonaduz, shown in Figure 21.4-4a, was shot at a low elevation of 600 m above sea level, i.e. beneath these Bonaduz gravels. Again an uppermost band of low-frequeny reflections extending to 130 msec TWT can be recognized. Beneath, a continuous band of reflections extends all the way across the line and down to 200 msec TWT. Still deeper down, two branches dipping to the N and the S, respectively, overly a concave upward reflection, suggesting a buried-focus effect.

The uppermost low-frequency reflections are likely to stem from fluviatile gravels. Their lower limit at 130 msec TWT corresponds to an elevation of about 430 m above sea level. The continuous reflections beneath 130 msec

a)

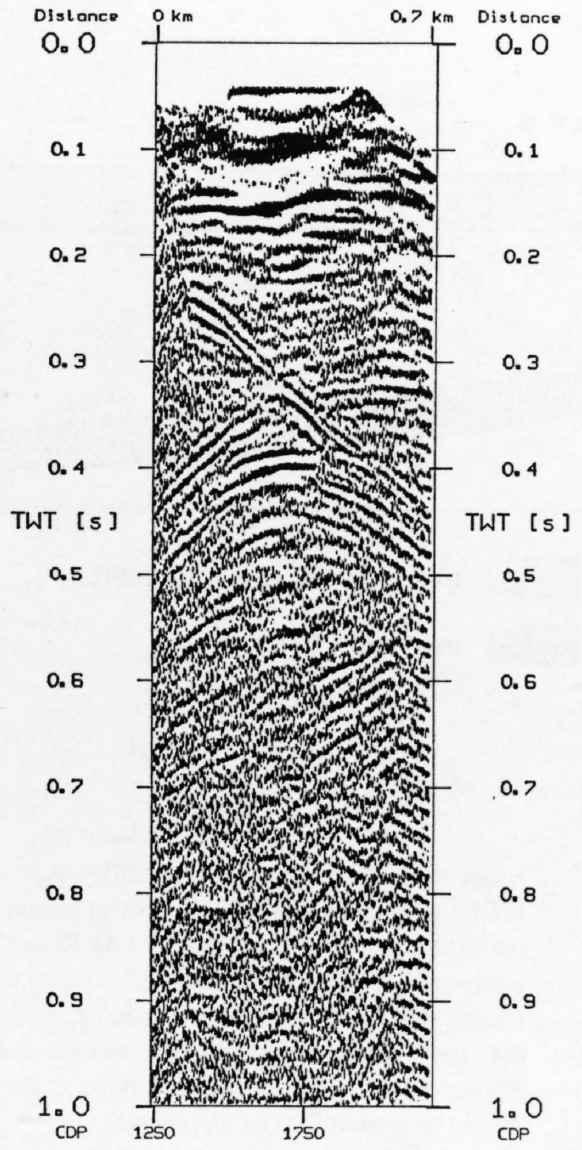

b)

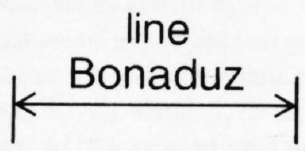

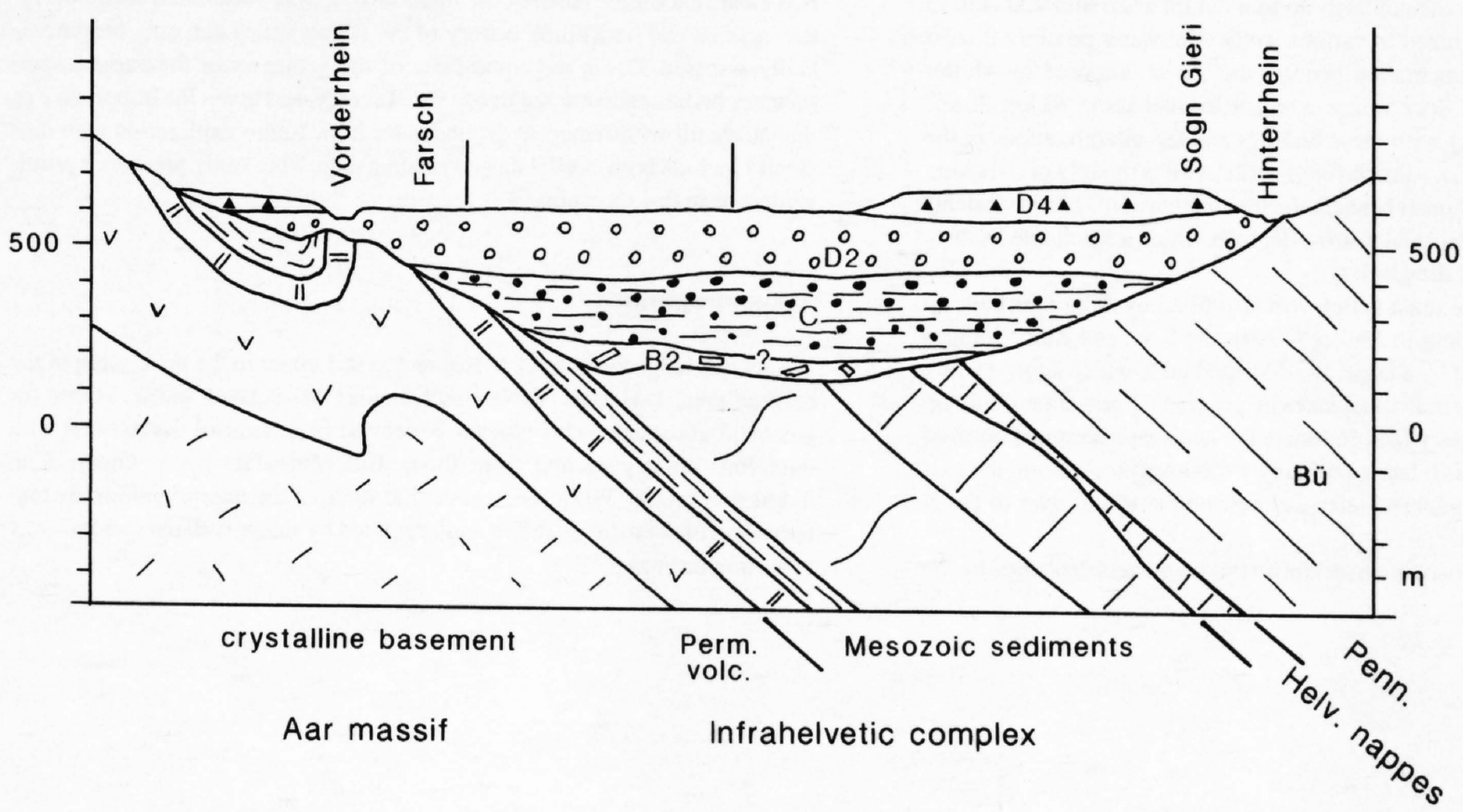

Figure 21.4-4
Line Bonaduz. a: Unmigrated final stack, b: geologic interpretation (horizontal equals vertical scale).
B2: Meltout and reworked till, C: Glacio-lacustrine deposits, D2: Fluviatile gravels, D4: Rockslide deposits. Bü: Penninic Bündnerschiefer (Tomül nappe).

TWT compare to the ones in line Chur and are thus also interpreted as fine grained glacio-lacustrine sediments. The bottom of the main valley as defined by the bow-tie structure, is at 450 msec TWT, which is equivalent to about 100 m above sea level. Similar to lines Chur and Ems a putative layer of meltout till is shown as oldest valley fill above the bedrock surface in Figure 21.4-4b.

21.4.3 Longitudinal section

Figure 21.4-5 is a longitudinal profile combining seismic, well and surface data. It demonstrates that the bed-rock bottom of the Rhine Valley drops from 100 m above sea level near Reichenau to about 100 m below sea level near Chur. This upper Rhine Valley thus is one of the classic overdeepened val-

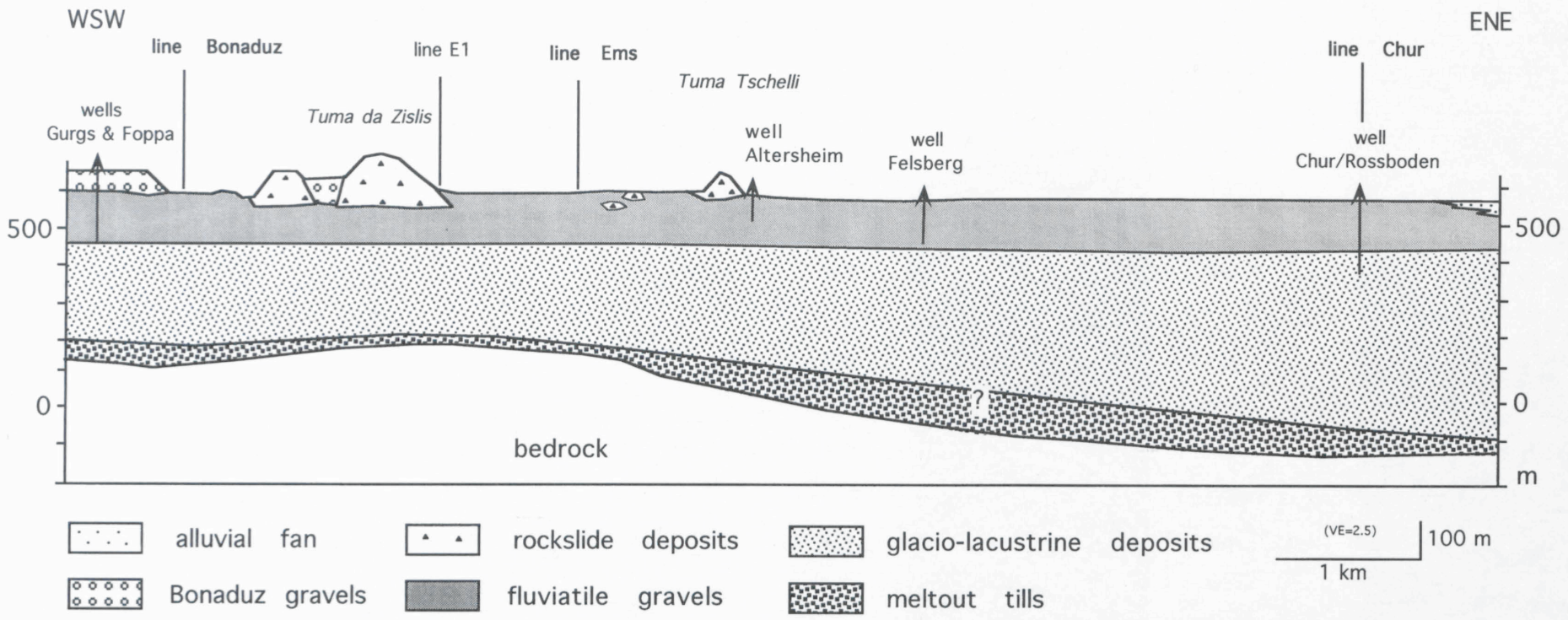

Figure 21.4-5
Longitudinal profile of the Rhine Valley.

leys, but the extent of this overdeepening up-stream (Vorderrhein/Rein anteriur in a westerly direction and Hinterrhein/Rein posteriur in a southerly direction) is not clear. It is to be expected that more overdeepening occurred at the confluences of large valley glaciers, such as the two Rhine glaciers near line Bonaduz, and Rhine glacier/Julia glacier near line Chur. To illustrate this effect, a slight rock barrier (a burried drumlin) is shown beneath line Ems in Figure 21.4-5.

The longitudinal profile also shows how the Rhine Valley was filled by a sequence of different processes. After overdeepening of the valley trough by the glaciers the valley remained probably filled by the melting ice for some time – inhibiting the tributaries to build up local fans and fill the valley right away. 25 km north of Chur, in well Balzers, the only well in the area reaching the bedrock surface, no lodgement till was recognized. Instead fine-grained glacio-lacustrine sediments apparently directly overly bedrock. These fine-grained clastic sediments accumulated up to a datum at around 400–450 m above sea level as reckognized in various wells. Meltwater possibly floated the glacier, allowing sedimentation beneath the ice as proposed by Müller (1994) in the case of the Seez valley, a valley located some 20 km downstream of Chur. In analogy with these findings and the interpretations in the Rhone Valley (section 21.2), a thin layer of meltout till is thought of as having accumulated as oldest sediment beneath the floating glacier. These sediments are then overlain by the glacio-lacustrine deposits which accumulated subsequently during melting of the glacier.

In this and later stages the main valley was also filled by delta fans built up by the tributaries. According to Müller (1994), the Seez and Rhine Valleys were at one time occupied by a large, fjord-shaped lake, which subsequently was dissected into smaller individual lakes by prograding gravel fans built up by tributaries. Large tributary fans dominate the landscape west and north of Chur. They were and are still being built up by tributary creeks from the easily erodable Penninic Bündnerschiefer and deviate the Rhine river to the N and E.

The glacio-lacustrine deposits are overlain by fluvial gravels deposited by the Rhine river along the axis of the valley. According to a groundwater survey (SGD/AGS document 18078) two prominent delta fans (Zizers and Untervaz) located on opposite sides of the Rhine 10 km downstream of Chur do not interfinger. They are interpreted as being separated by fluvial gravels containing silty layers in the upper part, i.e. at more than 430 m above sea level (i.e. above the fine-grained glacio-lacustrine deposits). The valley fill of the Rhine Valley is thus quite comparable to the one of the Rhone Valley discussed in section 21.2 of this chapter.

In the area between Reichenau and Chur, rockslide deposits form only the topmost tens of meters of the valley fill. They might represent remains of a rockslide that fell onto a late-stage glacier of the Last Ice Age, which melted off soon afterwards. Locally these rockslide debris are overlain by gravels of the Rhine river. These fluvial gravels make up much of the present valley floor, but have been incised by the Rhine river recently.

It is clear that on the basis of the three seismic lines discussed above alone, the incision and backfilling history of the Rhine Valley can only be superficially assessed. Given the complexity of the geometry of the various sedimentary bodies encountered in our small survey, and given the importance of the valley fill with regard to groundwater flow, future exploration activities should include both, well data and seismic data. This study presents a promising start in this direction.

Acknowledgements

We acknowledge the help of A. Roose and R. Lehner in the processing of the seismic data, I. Blaser, A. Neuenschwander, W. Schaad and R. Hänni for technical assistance. This chapter benefitted from fruitful discussions with numerous colleagues and from thoughtful comments by A. Green, Chr. Schlüchter and W. Wildi. We realize that some of the interpretations are tentative and likely to be modified and/or refined by future well data and seismic reflection profiling.